MEASUREMENT AND INTERPRETATION OF MOTIONAL ELECTRIC FIELDS IN THE SEA

by

THOMAS BAYES SANFORD

A.B., Oberlin College
(1962)

SUBMITTED IN PARTIAL FULFILLMENT
OF THE REQUIREMENTS FOR THE
DEGREE OF DOCTOR OF
PHILOSOPHY
at the
MASSACHUSETTS INSTITUTE OF
TECHNOLOGY
JUNE, 1967

Signature of Author _____
Department of Geology and Geophysics
May 1, 1967

Certified by _____
Thesis Supervisor

Accepted by _____
Chairman, Departmental Committee
on Graduate Students

ABSTRACT

MEASUREMENT AND INTERPRETATION

OF MOTIONAL ELECTRIC FIELDS IN THE SEA

by

T. B. Sanford

Submitted to the Department of Geology and Geophysics on May 1, 1967, in partial fulfillment of the requirement for the degree of Doctor of Philosophy.

The total motional electric current distribution is investigated for a quasi-steady, 3-dimensional ocean current. In order that electric currents associated with time variations in the induced magnetic field be negligible, a restriction is placed on the temporal and spacial variations of the flow. The quasi-static electric potential is calculated for a general flow and for a model of the Gulf Stream. The 3-dimensional solution for the electric potential is particularized for a 2-dimensional current which is broad compared with the ocean's depth. It is shown that for such a broad flow the electric current stream function is proportional to a transport function.

The surface expression and total structure of the electric current are calculated for several simple flows and for a cross section of the Gulf Stream. A detailed comparison of several GEK traverses across the Gulf Stream taken in conjunction with hydrographic sections reveals the presence of inertial period oscillations in the surface layers.

Presented and discussed are the results of several exploratory experiments to measure and interpret vertical potential differences in the sea. Although confirmations of the electric results by other methods are few, the evidence is strong that accurate determinations of magnetic east-west transport can be obtained from vertical potential measurements.

Thesis Supervisor: William S. von Arx
Title: Professor of Physical Oceanography

TABLE OF CONTENTS

Page

LIST OF FIGURES

Page

LIST OF TABLES

INTRODUCTION

Measurements of the induced electric fields and currents can provide detailed information about the velocity structure of an ocean current. During the past twenty years the measurement and interpretation of the surface electric current (GEK, von Arx, 1950) have provided valuable information about surface ocean currents. The observations of the electric fields and currents in the sea have been restricted to the measurements using electrodes towed at the surface (GEK) and electrodes fixed to the sea bottom. Other measurements have been proposed but few have been performed. Considering the recent development of free fall instruments, the operational status of moored buoys and the availability of electrical cables on oceanographic vessels, it is worthwhile to investigate new electrical measurements within ocean currents. This thesis is the result of an effort to understand and utilize the total electric current distribution within a 3-dimensional, quasi-steady ocean current.

The interpretation of the induced electric currents is based on the results of a theoretical study in Chapter 1 of the quasi-static electric potential induced within and near a laterally unbounded (free) ocean current. It is shown that electric fields and currents can be determined from the quasi-static scalar potential provided the horizontal scale of the time-dependent component of the flow is small compared to the electromagnetic penetration depth or skin depth. It is then possible to neglect electric

currents which are due to time variations in the induced magnetic field. In general and by example it is shown that the essential difference between a 2-dimensional stream and a 3-dimensional one having downstream velocity variations is that in the latter flow significant electric currents can exist in a horizontal plane. The analytic solution derived for the scalar potential is particularized for the case of a 2-dimensional, quasi-steady current which is broad compared with the ocean depth. The expressions derived are useful for the interpretation of the electrical measurements made on most natural streams. The electric current stream function is introduced and shown to be proportional to a transport function. In Chapter 2 the surface expression and total structure of the electric current are calculated for several simple flows and for a cross section of the Gulf Stream. Chapter 3 contains a detailed comparison of several GEK traverses across the Gulf Stream taken in conjunction with hydrographic sections. It is observed that inertial period oscillations were significantly influencing the surface layers. Chapter 4 presents and discusses the results of several exploratory experiments to measure and interpret the vertical potential differences in the sea. Comparisons of the electrical and direct determinations of volume transport per unit section are too few to firmly establish the operational utility of vertical measurements. Nevertheless, the evidence is strong that with improved technique accurate determinations of magnetic east-west transport can be obtained from vertical potential measurements.

Previous Investigations

Attention was first given to the induced field in the sea after Michael Faraday (1832) predicted such effects must be present in the English Channel. Faraday failed to confirm his prediction in an experiment on the Thames, but several decades later tidally induced potentials were observed on broken submarine cables. Further cable measurements and theoretical studies have been reported by Barber and Longuet-Higgins (1948), Barber (1948) and Longuet-Higgins (1947, 1949).

The existence of tidally induced electric currents in Dartmouth Harbor, England, was demonstrated by Young, Gerrard and Jevons (1920). They used both moored and towed electrode pairs. The investigations of Stommel (1948) and Longuet-Higgins (1949) presented the relevant theory, calculated the induced field arising from certain velocity fields and clarified the relationship between the electric current at the sea surface and the potential difference measured with towed electrodes. This information combined with the necessary operational technique established the method of towed electrodes, or GEK (von Arx, 1950).

Malkus and Stern (1952) published two important integral theorems. One of these theorems was used by Wertheim (1954) to relate the potential difference across the Florida Strait to the volume transport of the Florida Current. Wertheim's work is interesting in that it presents an instantaneous measure of the bulk motion of the stream and provides a time series of data extending over many

years (Stommel, 1957, 1959). Further measurements using submarine cables connecting Bermuda, Horta in the Azores and continental stations have been reported by Stommel (1954). Runcorn (1964) has used long submarine cables to study electric currents in the Pacific Ocean. On a smaller scale Morse et al (1958) have investigated the potential difference across small tidal streams which are less than 200 yards wide.

The paper by Longuet-Higgins, Stern and Stommel (1954), hereafter referred to as L-HSS, presents a systematic development of the theory of the induced potential. They outline the qualitative nature of the induced electric field from physical arguments and present detailed calculations for particular velocity distributions. This paper sets forth the proper procedure for interpreting GEK observations; unfortunately, their suggestions often are not followed in the routine analysis of GEK data.

More recently, theoretical studies of 2-dimensional, steady flows have been made by Tikhonov and Sveshnikov (1959) and Glasko and Sveshnikov (1961). Larsen (1966) in a thesis has computed the electric and magnetic fields associated with a model of the lunar semidiurnal tide along the California coast. This work, summarized by Larsen and Cox (1966), shows that the magnetic effects of the induced electric currents can be significant in the open ocean. In the present study the downstream variations of the tidal flow are shown also to play an important role in the generation of electric currents.

That a measurement of the vertical electric field should be an accurate index of the magnetic east-west velocity was pointed out by Malkus and Stern (1952). For this reason it is curious that the vertical electric field has received so little attention. Vertical potential measurements have been made (Ryzhkov, 1957; Mangelsdorf, 1962; Fonarev, 1963; Novysh and Fonarev, 1963; Fonarev, 1964; Fonarev and Novysh, 1964), but it seems that, excepting the work of Mangelsdorf, no attempt has been made to interpret the field oceanographically. The temperature, salinity and pressure differences between a vertically spaced pair of electrodes produce potential differences. This influence must be removed from the data to obtain the motionally induced electric field. By using a salt bridge, Mangelsdorf avoided these electrochemical differences of potential. In the case of the other measurements it is unclear what corrections, if any, were made (Solov'yev, 1960).

CHAPTER 1

THE SCALAR POTENTIAL FIELD WITHIN AN OCEAN CURRENT

In this chapter an expression is derived for the quasi-static scalar potential within and near a 3-dimensional, time-dependent ocean current. To avoid electric currents associated with the time variations of the induced magnetic field, a restriction is imposed on the scale and frequency of the time-dependent component of the flow. The spacial dependence of the potential gradient and electric current are discussed for a general flow, for a model of the Gulf Stream and for a flow which is broad compared with the ocean depth. As contrasted with a 2-dimensional, steady current, a 3-dimensional, nonsteady flow will induce in the ocean large-scale, horizontal electric currents influenced significantly by self-induction. The electric field, rather than being the gradient of a scalar potential, is now given as the solution of an electromagnetic problem dependent not only on the character of the flow but also on the electrical conductivity of the ionisphere, ocean and solid earth. Assuming a reasonable conductivity model, Larsen (1966) has calculated the electric and magnetic fields induced by the semidiurnal tide along the coast of California. His results show that self-induction can significantly contribute to the electric field in the ocean. Were it necessary that the self-induction in the sea be determined before electrical measurements could be interpreted, the oceanographic utility of such measurements

would be severely limited. Fortunately, the self-induced component of the electric currents will be small for flows narrow compared to the electromagnetic skin depth. The present discussion will be restricted to such flows.

The Problem

The ocean current is considered to be laterally unbounded but confined between the free surface and a uniformly conducting half space, the sea bottom. A right-hand rectangular coordinate system (x, y, z) is used with z measured positively upward. Let σ_1 and σ_2 represent the conductivity of the sea water and sea bed, respectively.

The motion is slow compared to the speed of light and the frequency of any oscillations small. Then free charges and displacement currents can be neglected; hence, Maxwell's equations (rationalized MKS) are

$$\nabla \times \underline{E} = -\frac{\partial \underline{B}}{\partial t} \qquad \nabla \cdot \underline{E} = 0$$

$$\nabla \times \underline{B} = \mu \underline{J} \qquad \nabla \cdot \underline{B} = 0$$

where $\underline{E}$ is the electric field, $\underline{B}$ the magnetic induction, $\underline{J}$ the electric current density and μ the permeability, assumed constant in each region. Ohm's Law for a medium moving with velocity $\underline{V}$ in the presence of a magnetic field requires that

$$\underline{J} = \sigma \{ \underline{E} + \underline{V} \times \underline{B} \} .$$

The relation

$$\underline{E} = -\frac{\partial \underline{A}}{\partial t} - \nabla \phi$$

is introduced with $\underline{A}$ the magnetic vector potential and ϕ the scalar electrostatic potential. The magnetic vector potential is defined, in accordance with the equation $\nabla \times \underline{E} = -\frac{\partial \underline{B}}{\partial t}$, as

$$\underline{B} = \nabla \times \underline{A}$$

with the restriction that

$$\nabla \cdot \underline{A} = 0 .$$

The equations can be greatly simplified provided the horizontal scale of the time-dependent component of the flow is small compared to the electromagnetic skin depth in the ocean (Appendix A). With this restriction we can neglect $\partial \underline{A}/\partial t$ compared with $\nabla \phi$. Moreover, the induced magnetic field can be neglected compared to the steady and uniform geomagnetic field $\underline{F}$. With the current density given by

$$\underline{J} = \sigma \{-\nabla \phi + \underline{v} \times \underline{B}\}$$

an equation for the scalar potential can be obtained by taking the divergence of the above equation:

$$\nabla \cdot \underline{J} = -\nabla^2 \phi + \underline{F} \cdot \nabla \times \underline{v} = 0$$

since $\nabla \times \underline{B} = \mu \underline{J}$.

The boundary conditions are that the normal component of the electric current density must vanish at the sea surface and that the potential and vertical current density are continuous at $z = -h$ and that the potential vanishes far

from the ocean current.

For the velocity field

$$\underline{V}(x,y,z,t) = (V_x, V_y, 0)$$

the governing equations and boundary conditions explicitly are:

$$\nabla^2\phi_1 = F_y \frac{\partial V_x}{\partial z} - F_x \frac{\partial V_y}{\partial z} + F_z\left(\frac{\partial V_y}{\partial x} - \frac{\partial V_x}{\partial y}\right) \qquad (0 \geq z \geq -h)$$

$$\nabla^2\phi_2 = 0 \qquad (-h \geq z > -\infty)$$

$$\frac{\partial \phi_1}{\partial z} = F_y V_x - F_x V_y \qquad z = 0$$

$$\phi_1 - \phi_2 = 0 \qquad z = -h$$

$$\sigma_1 \frac{\partial \phi_1}{\partial z} - \sigma_2 \frac{\partial \phi_2}{\partial z} = \sigma_1 (F_y V_x - F_x V_y) \qquad z = -h$$

$$\phi_2 \to 0 \qquad z \to -\infty$$

$$\phi_1 \text{ and } \phi_2 \to 0 \qquad (x^2+y^2)^{1/2} \to \infty .$$

Since the equations and boundary conditions are linear with constant coefficients, it is useful to introduce Fourier transforms. Any dependent variable $\psi(x,y,z,t)$ will be transformed as follows; provided that

$$\int_{-\infty}^{\infty}\int_{-\infty}^{\infty} |\psi|^2 dx\, dy < \infty ,$$

then

$$\hat{\psi}(\alpha,\beta,z,t) = \int_{-\infty}^{\infty}\int_{-\infty}^{\infty} \psi(x,y,z,t)\, e^{i(\alpha x+\beta y)}\, dx\, dy$$

and

$$\psi(x,y,z,t) = \frac{1}{4\pi^2}\int_{-\infty}^{\infty}\int_{-\infty}^{\infty} \hat{\psi}(\alpha,\beta,z,t)\, e^{-i(\alpha x+\beta y)}\, d\alpha\, d\beta .$$

Under this transformation the governing equations become

$$\frac{d^2\hat{\phi}_1}{dz^2} - \gamma^2\hat{\phi}_1 = F_y\frac{d\hat{V}_x}{dz} - F_x\frac{d\hat{V}_y}{dz} + iF_z(\alpha\hat{V}_y - \beta\hat{V}_x)$$

in the ocean and

$$\frac{d^2\phi_2}{dz^2} - \gamma^2\phi_2 = 0 \qquad \gamma^2 = \alpha^2+\beta^2$$

in the sea bed. The general solution to the above equations can be constructed readily by the method of variation of parameters (Jeffreys and Jeffreys, 1962) because the homogeneous solution is apparent. After the boundary conditions are satisfied the solution follows in a straight-forward manner:

$$\phi(x,y,z,t) =$$

$$\frac{1}{4\pi^2}\int_{-\infty}^{\infty}\int_{-\infty}^{\infty}\left\{\frac{\cosh\gamma(z+h) + \frac{\sigma_2}{\sigma_1}\operatorname{sgn}\gamma\sinh\gamma(z+h)}{\sinh\gamma h + \frac{\sigma_2}{\sigma_1}\operatorname{sgn}\gamma\cosh\gamma h}\int_{-h}^{0}\left[(F_y\hat{V}_x - F_x\hat{V}_y)\sinh\gamma\xi\right.\right.$$

$$\left. + iF_z(\alpha\hat{V}_y - \beta\hat{V}_x)\frac{\cosh\gamma\xi}{\gamma}\right]d\xi$$

$$\left.\left. + \int_{-h}^{z}\left[(F_y\hat{V}_x - F_x\hat{V}_y)\cosh\gamma(\xi-z) + iF_z(\alpha\hat{V}_y - \beta\hat{V}_x)\frac{\sinh\gamma(\xi-z)}{\gamma}\right]d\xi\right\}\cdot\right.$$

$$\cdot\, e^{-i(\alpha x+\beta y)}\, d\alpha\, d\beta$$

(1)

$$\phi_2(x,y,z,t) =$$

$$\frac{1}{4\pi^2}\int_{-\infty}^{\infty}\int_{-\infty}^{\infty}\frac{\int_{-h}^{0}\left[(F_y\hat{V}_x - F_x\hat{V}_y)\sinh\gamma\xi + iF_z(\alpha\hat{V}_y - \beta\hat{V}_x)\frac{\cosh\gamma\xi}{\gamma}\right]d\xi}{\sinh\gamma h + \frac{\sigma_z}{\sigma_s}\rho g\gamma\cosh\gamma h}$$

$$\cdot e^{|\gamma|(z+h)}\, e^{-i(\alpha x+\beta y)}\, d\alpha\, d\beta \,. \qquad (2)$$

Discussion of solution

The above solution has been used to examine the 3-dimensional analogs of the integral theorems of Malkus and Stern (Appendix B). Whereas in 2-dimensions several integral relations can be derived which involve the transport of an ocean current there seem to be no simple expressions in 3-dimensions. An approximate 3-dimensional theorem is derived.

Several general remarks can be made about the solution when the flow is broad compared with the depth. First, the principal contribution to the integral will be from low values of γ. Then the terms multiplied by F_z are dominant. Secondly, the electrical disturbances within a current are determined largely by the horizontal distribution of the vertically averaged velocity. To first order, a broad current can be modelled as a barotropic flow of velocity equal to the local vertically averaged velocity. Lastly, the electrical effects within a current are influenced by a weighting factor dependent on the horizontal length scales. Consider a barotropic current $\underline{V} = (V_x, 0, 0)$ which

has a typical width scale of W and a length scale of L, then the potential gradient in the y (width) direction is approximately

$$\frac{\partial \Phi_1}{\partial y} \doteq - \frac{F_z V_x}{1 + \frac{W^2}{L^2}}$$

Thus, the downstream scale has reduced the potential gradient, according to the factor $\left(1 + \frac{W^2}{L^2}\right)^{-1}$.

A free barotropic current

We will here consider the electrical effect of a small velocity perturbation to a mean flow. A current such as the Gulf Stream beyond Cape Hatteras can be considered a barotropic flow for purposes of computing its induced electric field. A reasonable model for the vertically averaged velocity of the Gulf Stream consisting of a steady 2-dimensional flow plus a progressive wave is

$$\underline{V} = \underline{1}_x V_0 \operatorname{sech} ly \left(1 + \epsilon e^{i(kx - \omega t)}\right) .$$

This model assumes that the wave has the same y dependence as the steady current. V_0 and l can be chosen so that the total volume transport and width of the stream are 100×10^6 m^3/sec and 100 km:

$$V_0 = .5 \text{ m/sec}$$

$$l = 2\pi/W \doteq 6.3 \times 10^{-5} \text{ m}^{-1}$$

for this scale, electromagnetic effects should be small for wave periods greater than 2 hours. Also, it is assumed that $\epsilon << 1$.

The Fourier transform of this current is

$$\hat{V}_x = \frac{2\pi^2}{\ell} V_0 \operatorname{sech} \frac{\pi\beta}{2\ell} \{\delta(\alpha) + \epsilon e^{-i\omega t}\delta(\alpha+k)\}$$

which when substituted into equation 1 yields (for $\sigma_2 = 0$):

$$\phi_1(x,y,z,t) = -\frac{F_z V_0}{\ell} \tan^{-1}(\sinh \ell y)$$

$$+ \frac{F_z V_0 \epsilon}{\ell} e^{i(kx-\omega t)} \frac{\partial}{\partial y} \int_{-\infty}^{\infty} \frac{\operatorname{sech} \frac{\pi\beta}{2\ell} e^{-i\beta y}}{\beta^2 + k^2} d\beta .$$

The integral above can be evaluated (Erdélyi, et al, 1954) with the result that

$$\phi_1(x,y,z,t) = -\frac{F_z V_0}{\ell} \left\{ \tan^{-1}(\sinh \ell y) \right.$$

$$\left. - 2 \operatorname{sgn} y \, \epsilon e^{i(kx-\omega t)} \sum_{n=0}^{\infty} (-1)^n \frac{(2n+1)\left\{e^{-k|y|} - e^{-(2n+1)\ell|y|}\right\}}{(2n+1)^2 - \frac{k^2}{\ell^2}} \right\} .$$

The y component of the potential gradient is

$$\frac{\partial \phi_1}{\partial y} = -F_z V_0 \operatorname{sech} \ell y \, (1 + \epsilon H(y; k, \ell) e^{i(kx-\omega t)})$$

where

$$H(y; k, \ell) = 1 - \frac{2k^2}{\ell^2} \cosh \ell y \sum_{n=0}^{\infty} (-1)^n \frac{(2n+1)\frac{\ell}{k} e^{-k|y|} - e^{-(2n+1)\ell|y|}}{(2n+1)^2 - \frac{k^2}{\ell^2}} .$$

Thus, the response of the cross-stream potential gradient to the given flow perturbation is determined by the function H. The response function H for y = 0 follows the approximate relation

$$H(0; k, \ell) \doteq e^{-\frac{k}{\ell}} .$$

Although the electric field due to the 2-dimensional mean current is undiminished, the wave component will be reduced significantly for almost all values of K. Circulating in the horizontal plane, large scale electric currents effectively short circuit the induction source.

A question arises as to the role downstream variations have in the generation of electric currents in flows adjacent to continental boundaries. Clearly, such boundaries of conductivity much less than that of sea water would reduce the electric currents and thus increase the potential gradient within the stream. Most of the electrical measurements using submarine cables were taken across flows confined to a strait or channel. Longuet-Higgins investigated the electric currents induced in a vertical plane by a 2-dimensional stream in an elliptical channel. Comparisons of the theoretical and observed potential differences across the English Channel indicated that electric currents reduced the generated emf by about 2/3. The electric currents induced in the horizontal plane were determined assuming a progressive Kelvin wave model of the semidiurnal tide. It can be shown (Appendix B) that the horizontal currents are small, reducing the potential gradient by less than 10%. In general, significant currents can develop in the horizontal plane only if the width of the stream is small compared to the breadth of the channel.

Although electric currents in the horizontal plane are generally small for streams confined within channels, these electric currents can be important for deep ocean motion. Stommel (1954) used submarine cables to study the potential differences between distant stations. The lunar semidiurnal potential differences between several stations were significantly less than expected from tidal theory. Stommel suggests that the tidal theory is inadequate while Larsen (1966) attributes the discrepancy to the presence of electric currents associated with time variations of the magnetic field. In addition, it is likely that the attenuation is also related to the 3-dimensional character of the tidal currents. The downstream scale of the motion as judged by the cotidal lines for the Atlantic (Defant, 1961) is often comparable and even less than the cross-stream scale.

Approximate 2-dimensional relations

In general, the Fourier inversion of equation 1 must be performed before the potential field can be obtained, but it is possible in some cases to derive approximate relations between the velocity field and the potential field. These relations are important because the potential field in an ocean current is of oceanographic interest mainly to the extent that it can be interpreted in terms of some aspect of the velocity field. The use of approximate relations greatly simplify this interpretation.

Equation 1 will be evaluated for a 2-dimensional current, having a breadth large compared with the ocean's

depth. A convenient method for approximating equation 1 is to expand the solution in a series of convolution integrals (Appendix D). The flow is described in a right-hand coordinate system (x, y, z) with the x axis aligned with the flow and z measured positively upward. The potential field together with the horizontal and vertical components of its gradient, valid when the flow is broad compared with the depth h but narrow compared to $\frac{\sigma_1}{\sigma_2} h$ and when y is not large $(0 \le |y| < \frac{\sigma_1}{\sigma_2} h)$, are:

$$\phi(y,z) = F_y \left\{ \int_{-h}^{z} V(y,\xi)\, d\xi + \int_{-h}^{0} \frac{\xi}{h} V(y,\xi)\, d\xi \right\}$$

$$- F_z \left\{ \frac{1}{2} \int_{-\infty}^{\infty} \tanh\left(\frac{\pi}{2} \frac{y-\lambda}{h}\right) \bar{V}(\lambda)\, d\lambda \right. \qquad (3)$$

$$- \frac{(z+h)^2}{z} \frac{d\bar{V}(y)}{dy} - \frac{1}{2h} \frac{d}{dy} \int_{-h}^{0} \xi^2 V(y,\xi)\, d\xi$$

$$\left. - \frac{\partial}{\partial y} \int_{-h}^{z} (\xi - z) V(y,\xi)\, d\xi \right\}$$

$$\frac{\partial \phi(y,z)}{\partial y} = F_y \frac{\partial}{\partial y} \left\{ \int_{-h}^{z} V(y,\xi)\, d\xi + \int_{-h}^{0} \frac{\xi}{h} V(y,\xi)\, d\xi \right\}$$

$$- F_z \bar{V}(y) \qquad (4)$$

$$\frac{\partial \phi(y,z)}{\partial z} = F_y V(y,z) + F_z \frac{\partial}{\partial y} \int_z^0 (V(y,\xi) - \bar{V}(y))\, d\xi \qquad (5)$$

with

$$\bar{V}(y) = \frac{1}{h} \int_{-h}^{0} V(y,\xi)\, d\xi .$$

Therefore, the vertical and horizontal electric current densities are

$$J_y = -\sigma \left\{ F_z (V(y,z) - \bar{V}(y)) + F_y \frac{\partial}{\partial y} \left(\int_{-h}^{z} V(y,\xi)\, d\xi + \int_{-h}^{0} \frac{\xi}{h} V(y,\xi)\, d\xi \right) \right\}$$

and

$$J_z = -\sigma F_z \frac{\partial}{\partial y} \int_z^0 (V(y,\xi) - \bar{V}(y))\, d\xi . \qquad (6)$$

L-HSS showed that

$$\left(J_y\right)_{z=-h}^{z=0} = -\sigma F_y h \frac{\partial \bar{V}(y)}{\partial y} ,$$

a condition satisfied by the present expression. Their estimate of the horizontal shear term was that it was of order $F_y h \frac{\partial \bar{V}}{\partial y}$; the term is given in more detail in the present expression. The expression for J_z is new and has several important consequences. First, it establishes the expected error in the interpretation of vertical potential measurements. Secondly, it can be seen that since the F_z term is generally much greater than the F_y term in the expression for J_y, the current density is given by the equations:

$$J_y = \sigma F_z \frac{\partial T^*}{\partial z} \quad \text{and} \quad J_z = -\sigma F_z \frac{\partial T^*}{\partial y} \qquad (7)$$

where T* is defined as

$$T^* \equiv \int_z^0 (V(y,\xi) - \bar{V}(y))\, d\xi$$

and will be called the excess transport. The expression $\sigma F_z T^*$ is the electric current stream function. Therefore, the electric current pattern is equivalent to that of the excess transport. A measurement of J_y as a function of depth, as by a freely falling pair of electrodes, would determine the $V(y,z) - \bar{V}(y)$, the excess velocity.

CHAPTER 2

COMPUTATIONS ON ANALYTIC AND HYDROGRAPHIC DATA

The Fourier transforms required in an evaluation of Equation 1 were performed numerically for several cases of 2-dimensional flow. The potential and current density at the sea surface were computed for analytic data and compared to the analytic solution. Also, the electrical disturbances were calculated for the velocity structure of the Gulf Stream as determined by a hydrographic survey.

Analytic data

The 2-dimensional flow

$$V(y,z) = \frac{V_0}{1+(\beta y)^2}$$

will induce at $z = 0$ the potential field

$$\phi(y,0) = \frac{F_y V_0 h}{2L(1+\beta^2 y^2)} - \frac{F_z V_0}{\beta} \tan^{-1}\beta y$$

where terms involving the conductivity of the sea bottom and terms of order $\beta^2 h^2$ have been neglected. Table 1 gives ϕ as a function of y evaluated for the given values of B_y, B_z, β, V_0 and h. Allowing a conducting sea floor, equation 1 was evaluated numerically for $\frac{\sigma_2}{\sigma_1} = 10^{-3}$ $\sigma_1 = .04$ mho km, $\beta = .02$ km^{-1}, $V_0 = 100$ cm/sec and $h = 4$ km on a grid $\Delta y = 10$ km and $\Delta z = 1$ km. Figures 1 and 2 present the results evaluated at the sea surface when the horizontal and vertical magnetic fields are treated separately. Electric currents develop in the presence of the conducting bottom and these act to reduce the potential differences generated. The horizontal electric current density in

TABLE 1

SURFACE POTENTIAL FOR ANALYTIC CASE

$$\phi(y,0) = \frac{B_y V_0 h}{2(1+\beta^2 y^2)} - \frac{B_z V_0}{\beta} \tan^{-1} \beta y$$

$V_0 = 100$ cm/sec , $\beta = .02$ km^{-1} , $h = 4$ km

y (km)	B_y=1, B_z=0	B_y=0, B_z=1	B_y=B_z=1
0	.20	0.0	0.20
-20	.17	1.90	2.07
-40	.12	3.37	3.50
-60	.08	4.38	4.46
-80	.06	5.06	5.12
-100	.04	5.54	5.58
-200	.01	6.63	6.64
-300	.005	7.03	7.03
-400	.003	7.23	7.23
-500	.002	7.36	7.36

Figure 1 Surface potential and electric current density for analytic case: $B_y = 0$, $B_z = 1$ gauss, four moving layers.

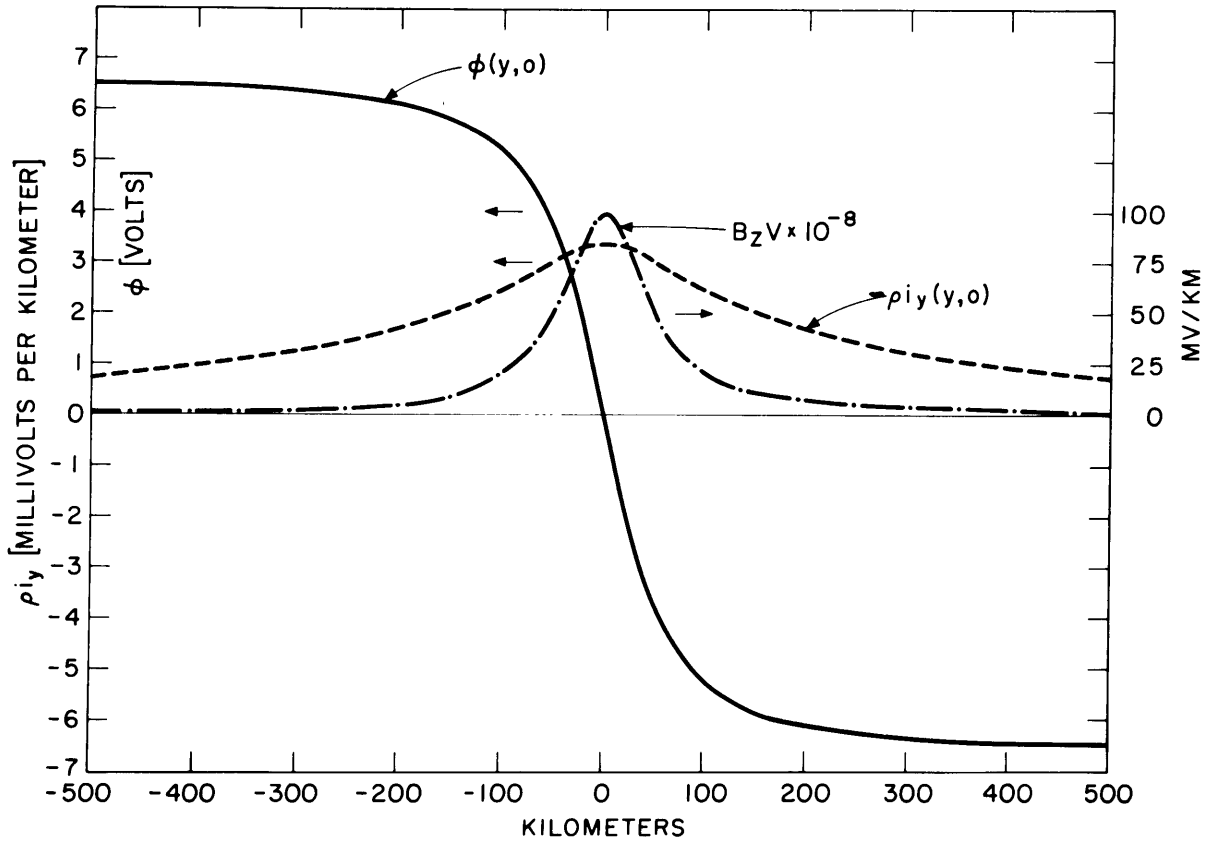
$\phi(y,o)$
$B_z V \times 10^{-8}$
$\rho i_y(y,o)$
ρi_y [MILLIVOLTS PER KILOMETER]
ϕ [VOLTS]
MV/KM
KILOMETERS
7
6
5
4
3
2
1
0
-1
-2
-3
-4
-5
-6
-7
100
75
50
25
0
-500
-400
-300
-200
-100
0
100
200
300
400
500

Figure 2 Surface potential and electric current density for analytic case: $B_y = 1$ gauss, $B_z = 0$, four moving layers.

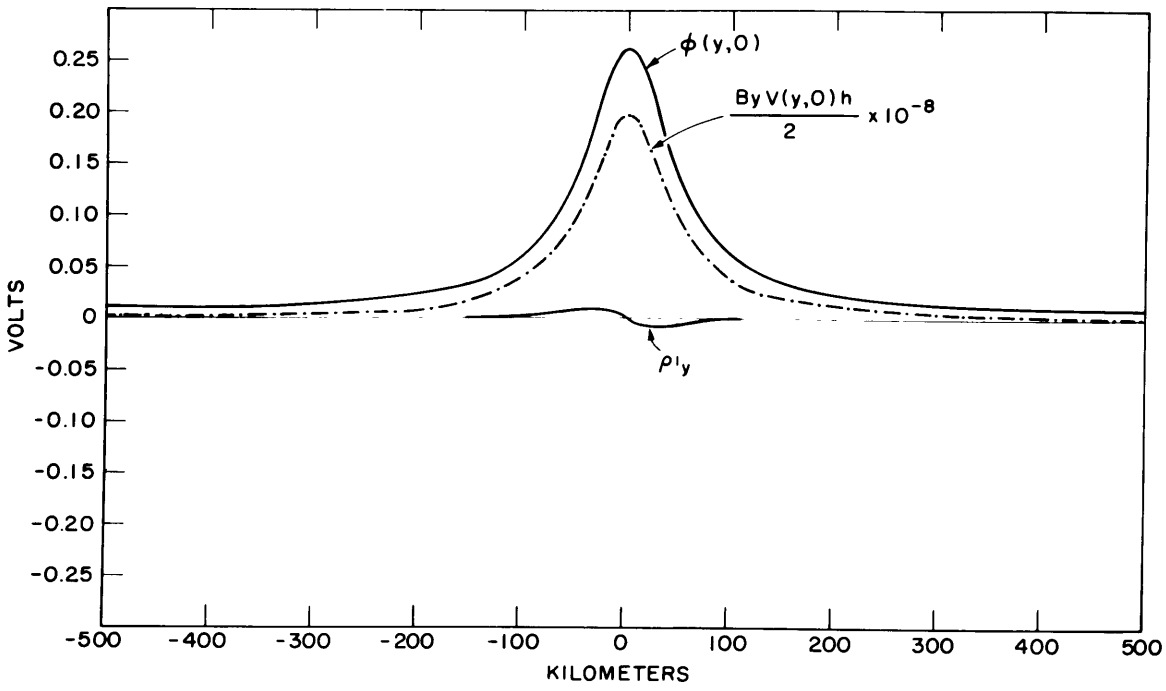
$\phi(y,0)$
$\frac{B_y V(y,0) h}{2} \times 10^{-8}$
ρl_y
VOLTS
0.25
0.20
0.15
0.10
0.05
0
-0.05
-0.10
-0.15
-0.20
-0.25
-500
-400
-300
-200
-100
0
100
200
300
400
500
KILOMETERS

Figure 1 never becomes very large, being less than 4% of the source term at y = 0, but its structure is very broad. The potential curve for $B_z \neq 0$ in Figure 1 has been reduced due to bottom conduction, but in Figure 2 we see that the contribution to the potential due to B_y has been increased.

A further example of a detailed calculation is illustrated in Figure 3. In this case the velocity field used previously, rides above a layer of stationary sea water. At any position, y, there are four layers moving at the same speed over three layers of motionless water. The resistivity ratio is again 10^{-3} and both magnetic components, each of unit value, are applied. The bottom water greatly reduces the potential field by permitting larger electric currents to flow. The main effect of B_y acting on the velocity field is to shift the center of the electrical effect slightly to the right.

Figure 3 is the surface expression of the current structure which exists throughout the stream. The stream function representing the electric current transport per unit (downstream) section is introduced as

$$i_y = \frac{\partial \psi}{\partial z} \quad \text{and} \quad i_z = -\frac{\partial \psi}{\partial y} .$$

As shown in the previous chapter, the stream function can be interpreted as

$$\psi(y,z) = \sigma B_z T^*$$

where

$$T^* = \int_z^0 (V(y,\xi) - \bar{V}(y))\, d\xi .$$

Figure 4 shows the streamlines of ψ computed for the same

Figure 3 The surface potential and electric current density for analytic case: B_y = 1 gauss, B_z = 1 gauss, four moving layers over three stationary layers.

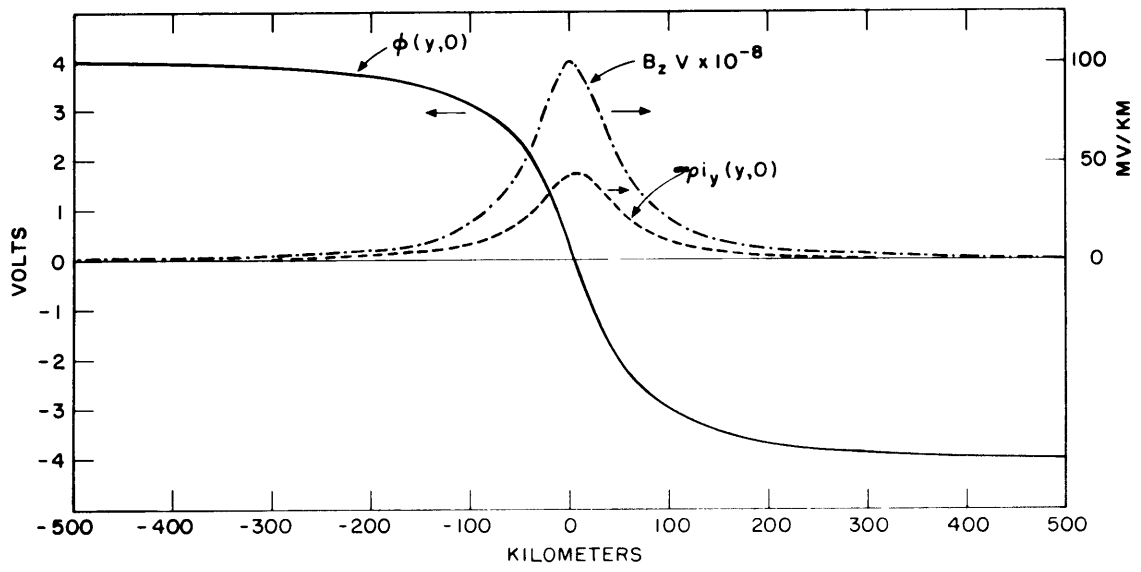
$\phi(y,0)$
B_z V x 10^{-8}
$pi_y(y,0)$
VOLTS
MV/KM
KILOMETERS
4
3
2
1
0
-1
-2
-3
-4
100
50
0
-500
-400
-300
-200
-100
0
100
200
300
400
500

Figure 4 The streamlines of electric current for flow as in Figure 3. Solid lines: ψ in units of ma/cm; dashed lines: isotachs of velocity.

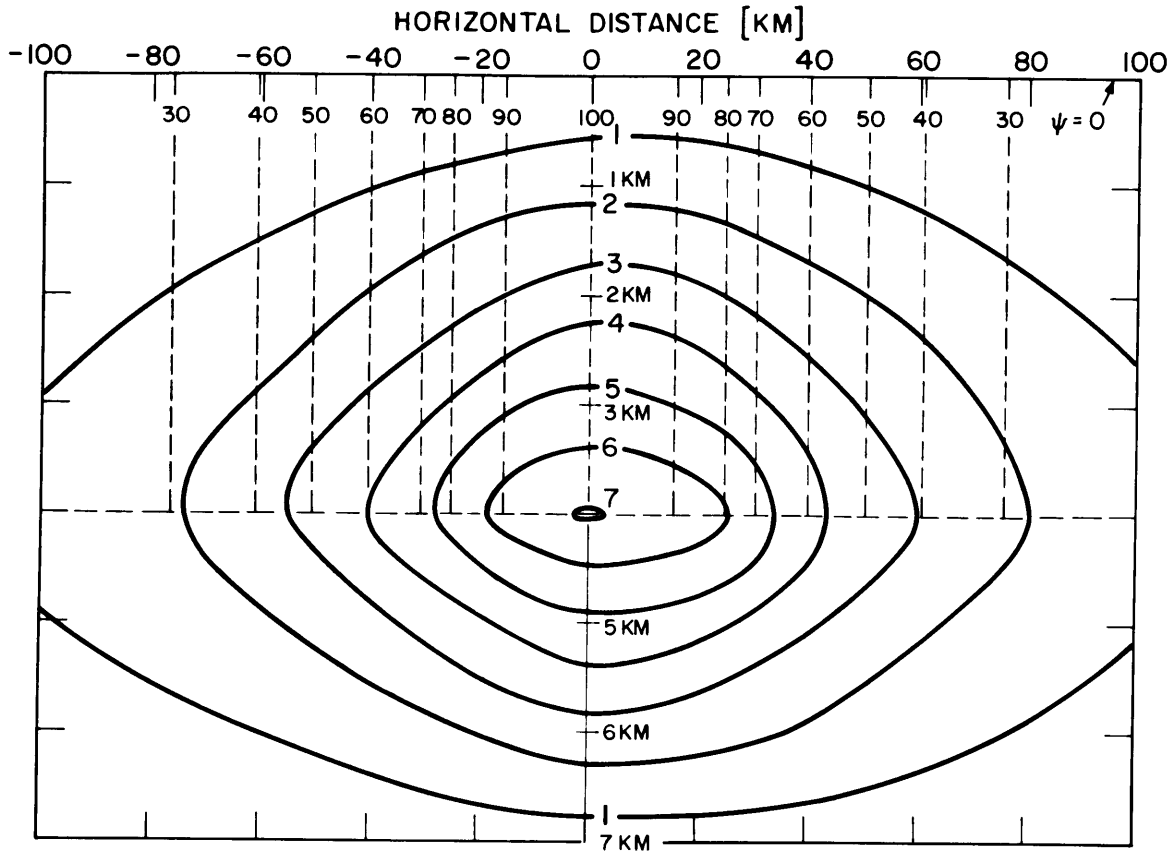
HORIZONTAL DISTANCE [KM]
-100
-80
-60
-40
-20
0
20
40
60
80
100
30
40
50
60
70
80
90
100
90
80
70
60
50
40
30
ψ = 0
1
2
3
4
5
6
7
1 KM
2 KM
3 KM
5 KM
6 KM
7 KM

flow as in Figure 3 on a grid $\Delta y = 10$ km and $\Delta z = 1$ km. In this example the pattern is almost symmetric, with some current penetration into the sea bottom.

Gulf Stream

The electric current density and stream function were computed for the much more complicated structure of the Gulf Stream illustrated in Figure 5. Calculations were made for the velocity distribution of the Stream determined by the method of dynamic sections (see also Figure 13). This information was kindly supplied by Mr. Joseph Barrett of Woods Hole Oceanographic Institution. Realistic value of the parameters were used on a grid with $\Delta y = 15$ km and $\Delta z = 400$ m. The bi-modal velocity structure and the counter-current region results in a rather complicated electric current structure. The current pattern in the region $|y| \geq 60$ km is distorted because the hydrographic data was available only for the range $-60 \leq y \leq 75$ km. The computations were carried out assuming a larger range but the velocity was assumed to be zero where no dynamic computations were available. The resulting artificially large shear zones at each end of the section produced strong electric currents as predicted by Equation 4. These edge effects could be eliminated only if some estimate is made of the velocity field outside the given range. Surface values for potential and ρL_y are shown in Figure 6. The character to the electric current is, of course, a consequence of the given velocity

Figure 5 The streamlines ψ of electric current for cross section of Gulf Stream. Solid lines: ψ in units of ma/cm; dashed lines: isotachs of velocity. $F_y = .176 \times 10^{-4}$ weber/m^2 $F_z = .525 \times 10^{-4}$ weber/m^2, $\frac{\sigma_1}{\sigma_i} = 10^{-3}$, $\sigma_i = 4$ mho/m $h^z = 4$ km.

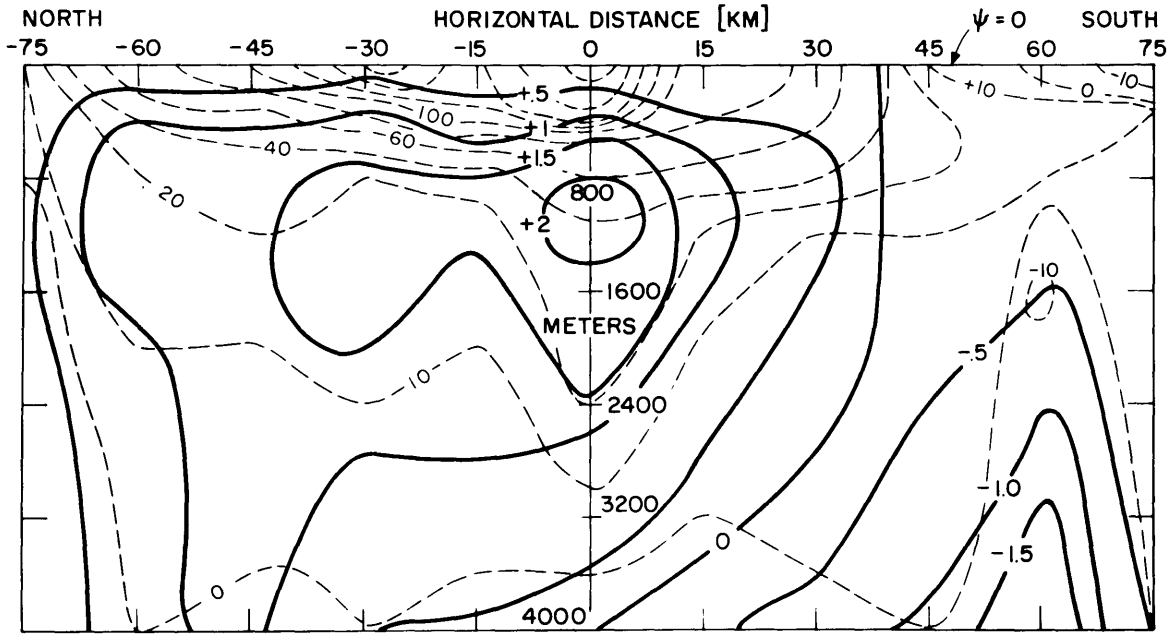
NORTH
HORIZONTAL DISTANCE [KM]
ψ = 0
SOUTH
-75
-60
-45
-30
-15
0
15
30
45
60
75
+.5
+1
+1.5
+2
100
60
40
20
10
0
800
1600
METERS
2400
3200
4000
+10
0
-10
-10
-5
-1.0
-1.5

Figure 6 The surface potential and electric current density for Gulf Stream: $F_y = .176 \times 10^{-4}$ weber/m^2; $F_z = .525 \times 10^{-4}$ weber/m^2, $\frac{\sigma_2}{\sigma_1} = 10^{-3}$ $\sigma_1 = 4$ mho/m.

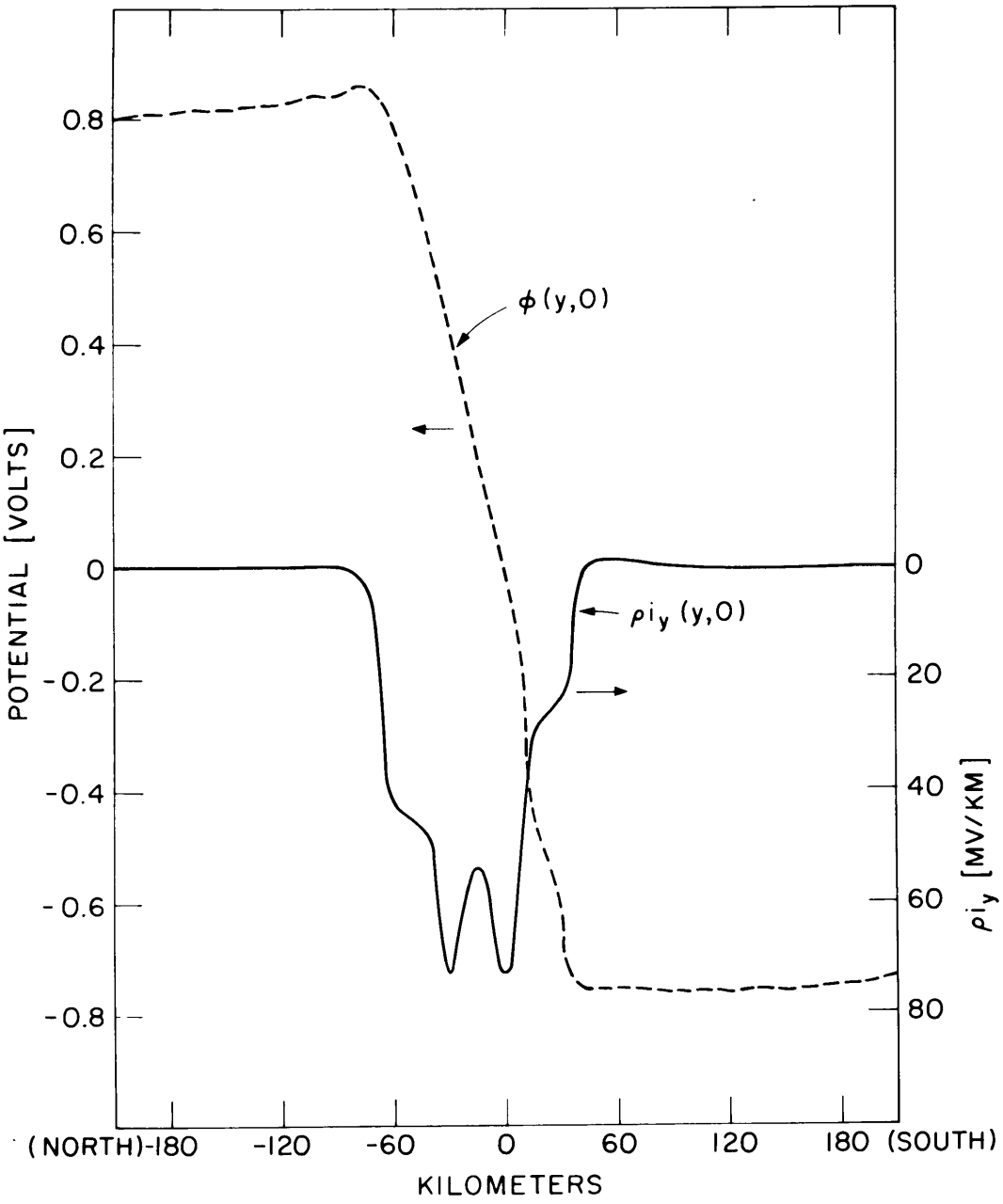
0.8
0.6
0.4
0.2
0
-0.2
-0.4
-0.6
-0.8
POTENTIAL [VOLTS]
φ(y,0)
ρi_y (y,0)
0
20
40
60
80
ρi_y [MV/KM]
(NORTH)-180
-120
-60
0
60
120
180 (SOUTH)
KILOMETERS

distribution. Whether or not the electric currents had this bi-modal feature in the Gulf Stream at that time is discussed in some detail in the next section.

CHAPTER 3

COMPARISONS OF GEK AND HYDROGRAPHIC DATA

There are small amounts of GEK data taken in conjunction with other oceanographic techniques. One instance, a coordinated GEK and hydrographic survey, serves as a good example of the method's utility when the horizontal GEK observations are interpreted correctly.

Equation 6 states that to first order the signal measured by a pair of towed electrodes is proportional to the difference between the surface velocity and the vertically averaged velocity. The same quantity can be obtained from the dynamic computations. Only on this basis is it appropriate to compare GEK and hydrographic data. But, it is important to emphasize several points about such a comparison. Both methods are similar in that they depend on the accurate measurement of the distribution of various quantities indirectly associated with a geophysical current. The methods are dissimilar in the procedures followed and the assumptions made in evaluating the measurements. The interpretation of electric measurements is purely kinematic since no assumptions are made about the cause of the velocity field. On the other hand, the dynamic computations make certain assumptions about the balance of forces within a flow. There has been much discussion about the degree to which the assumptions of the method of dynamic sections are valid. For example, LaFond (1965) discusses the effect of internal waves on the density structure and the resulting

fluctuations in the computed dynamic heights. Since it is appropriate to compare the two methods on the basis of their estimates of $V_s - \bar{V}$, it may be possible to gain insight into the dynamics of a flow.

Although there are many hydrographic sections of the Gulf Stream, there are few closely spaced sections taken in conjunction with detailed horizontal GEK measurements. Important exceptions are the three detailed cross sections of the Gulf Stream by Worthington (1954) and von Arx (1952) and some recent observations of the same type by Mangelsdorf and Barrett (unpublished). The location of these sections are indicated in Figure 7.

Observations of Worthington and von Arx

Worthington compares the surface currents inferred from hydrographic data using a reference level at 2000 meters, the GEK measurements corrected by a k factor of 1.2 and the difference between dead reckoned position and that determined from LORAN fixes. The dynamic computations indicated that the Gulf Stream was sharply banded at the surface and below into high and low velocity zones. The GEK values did not show this structure, but it was argued that the electric current probably would represent the average over the high and low velocity zones and hence, present a much smoother velocity picture.

Worthington and von Arx kindly supplied the original station and GEK data so that a detailed comparison of the two methods could be made. The analysis is quite simple.

Figure 7 Locations of experiments
A: ATLANTIS 165 Sections 1 and 2
B: ATLANTIS 165 Section 3
C: CRAWFORD 115
D: WHOI Station D
E: Northwest Providence Channel.

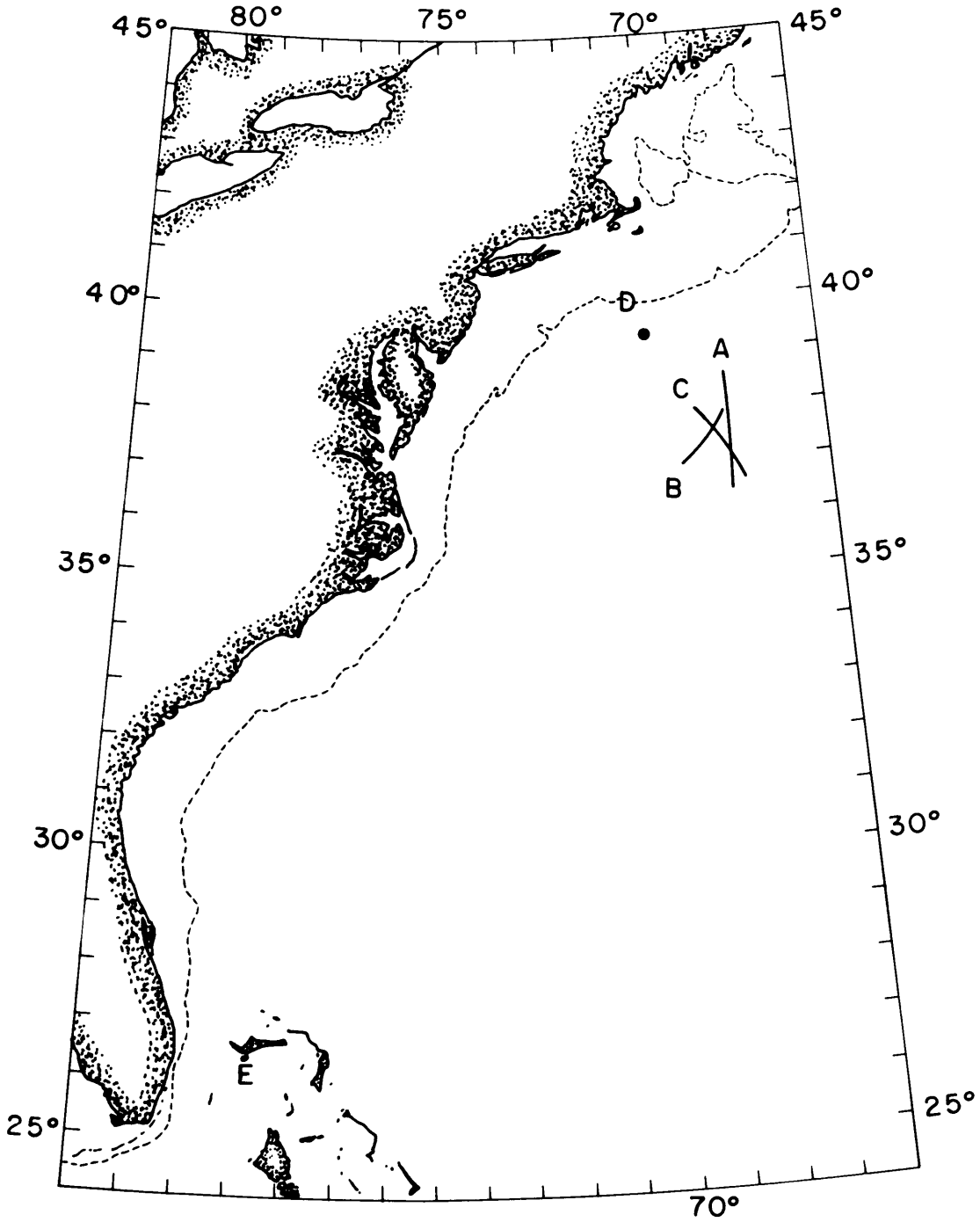
45°
80°
75°
70°
45°
40°
40°
D
A
C
B
35°
35°
30°
30°
E
25°
25°
70°

The k factor was removed from the GEK readings which already had been resolved into the component transverse to the section. The same horizontal length scale was made appropriate to both methods by averaging the GEK values, when several were available, between hydrographic stations. Even when calculated from the hydrographic data the second order term involving the lateral shear, thought possibly to be important by Worthington, was at most 5 percent of $V_s - \bar{V}$ and was not carried further in this work. For the same reason the average velocity was not corrected for vertical variations in the resistivity of the sea water or the presence of a conducting sea bottom. The GEK readings then determined $V_s - \bar{V}$ normal to the station section. The same quantity $V_s - \bar{V}$ was obtained immediately from the dynamic computations.

Results and discussion

Figures 8, 9 and 10 give the two estimates of $V_s - \bar{V}$ across the Gulf Stream for Worthington's three sections. The dynamic calculations still indicate sharp zones of comparatively fast and slow moving water, while the GEK values present a smoother velocity profile. The regularity is not a consequence of significant horizontal averaging. If the Gulf Stream had had the banded character as inferred from the dynamic calculations, the GEK measurements would have shown a similar nature. Stommel (1965) in a discussion of Worthington's section 2 states that the observed velocity structure probably involves the action on the density field

Figure 8 Comparison of surface minus average velocities for GEK and dynamic computations for ATLANTIS 165, section 1.

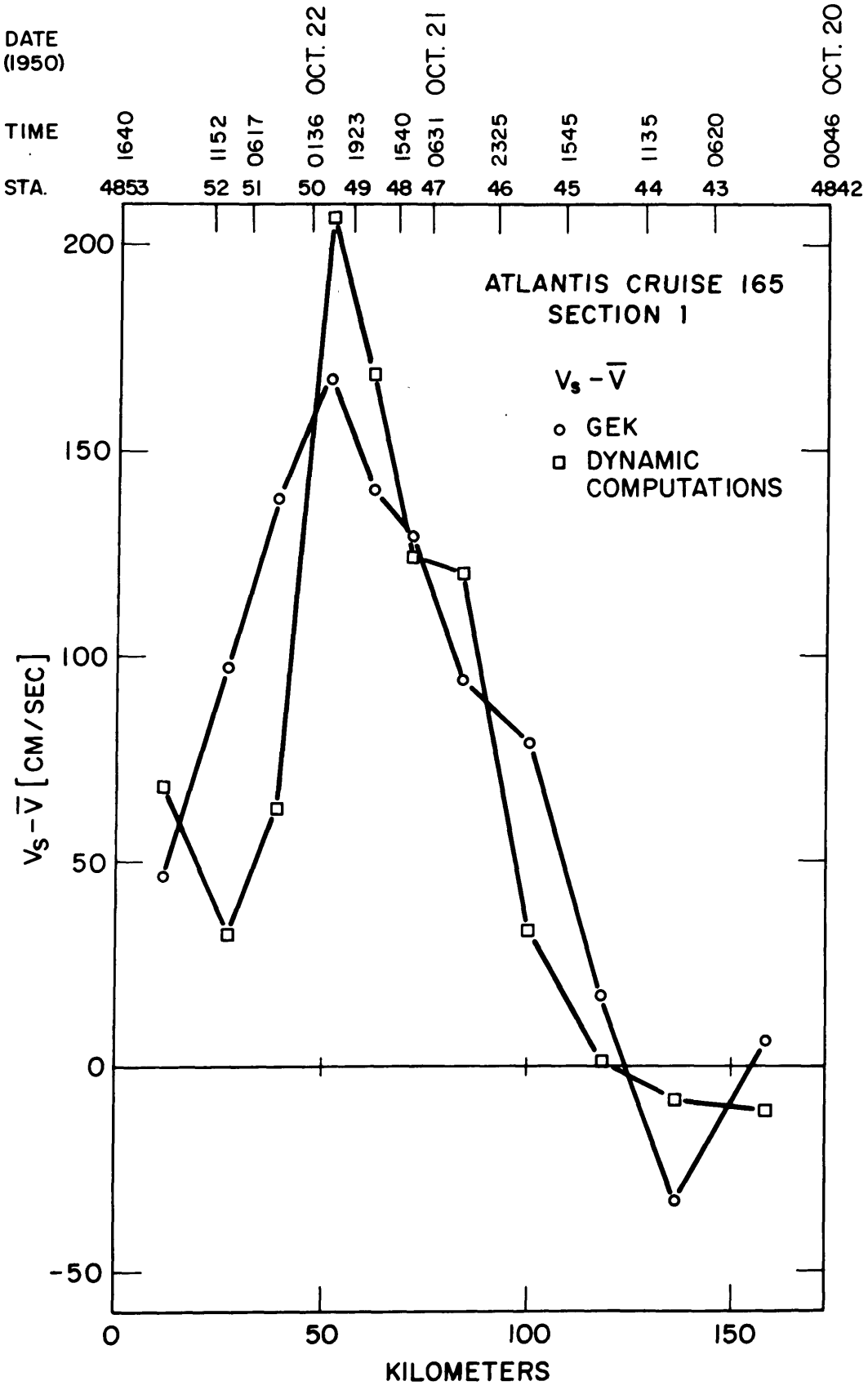
DATE (1950)
OCT. 20
OCT. 21
OCT. 22
TIME
1640
1152
0617
0136
1923
1540
0631
2325
1545
1135
0620
0046
STA.
4853
52
51
50
49
48
47
46
45
44
43
4842
ATLANTIS CRUISE 165
SECTION 1
$V_s - \bar{V}$
GEK
DYNAMIC COMPUTATIONS
$V_s - \bar{V}$ [CM/SEC]
200
150
100
50
0
-50
0
50
100
150
KILOMETERS

Figure 9 Comparison of surface minus average velocities for GEK and dynamic computations for ATLANTIS 165, section 2.

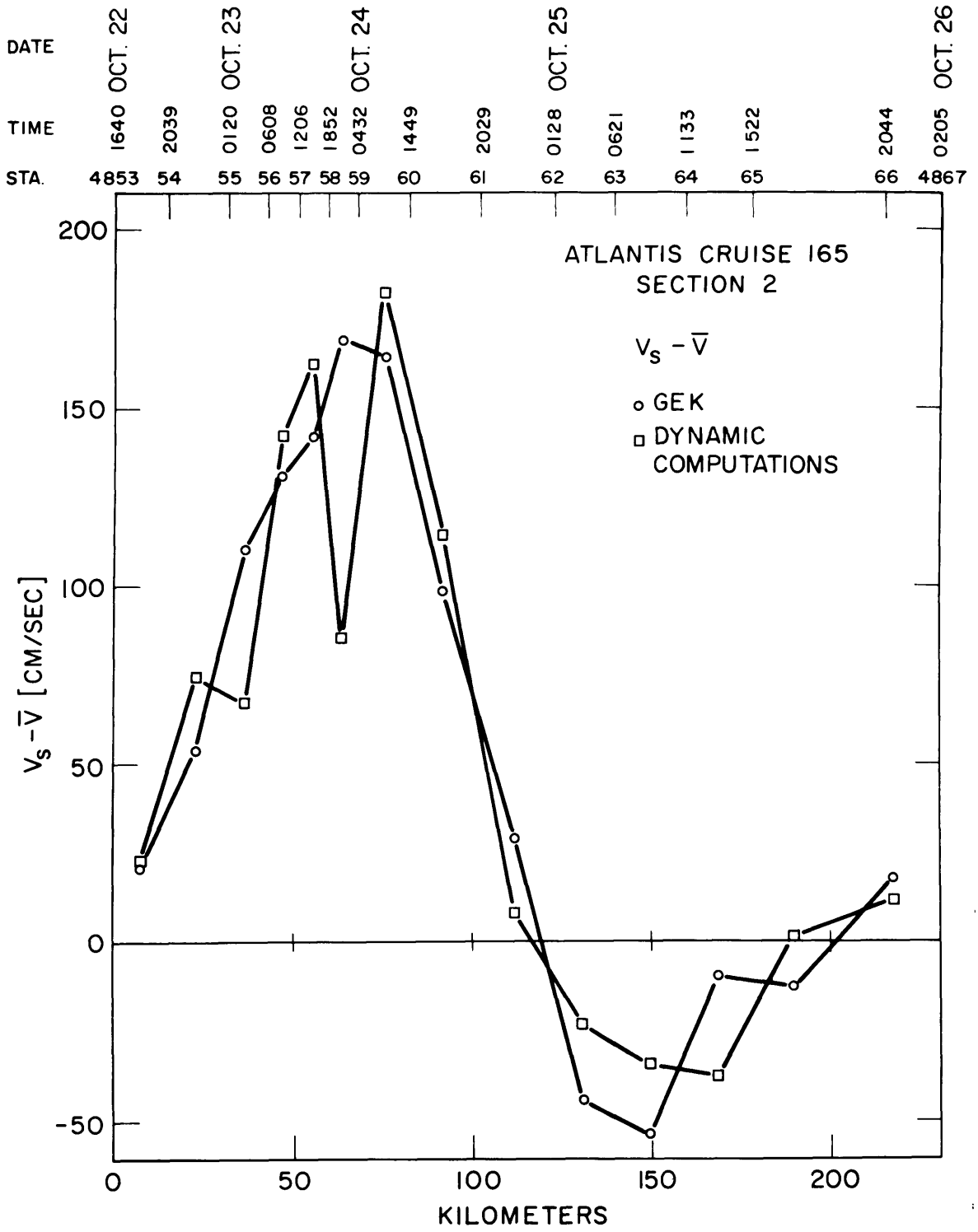
DATE
TIME
STA.
1640 OCT. 22
2039
0120 OCT. 23
0608
1206
1852
0432 OCT. 24
1449
2029
0128 OCT. 25
0621
1133
1522
2044
0205 OCT. 26
4853
54
55
56
57
58
59
60
61
62
63
64
65
66
4867
ATLANTIS CRUISE 165
SECTION 2
$V_S - \overline{V}$
o GEK
□ DYNAMIC COMPUTATIONS
$V_S - \overline{V}$ [CM/SEC]
200
150
100
50
0
-50
0
50
100
150
200
KILOMETERS

Figure 10 Comparison of surface minus average velocities for GEK and dynamic computations for ATLANTIS 165, section 3.

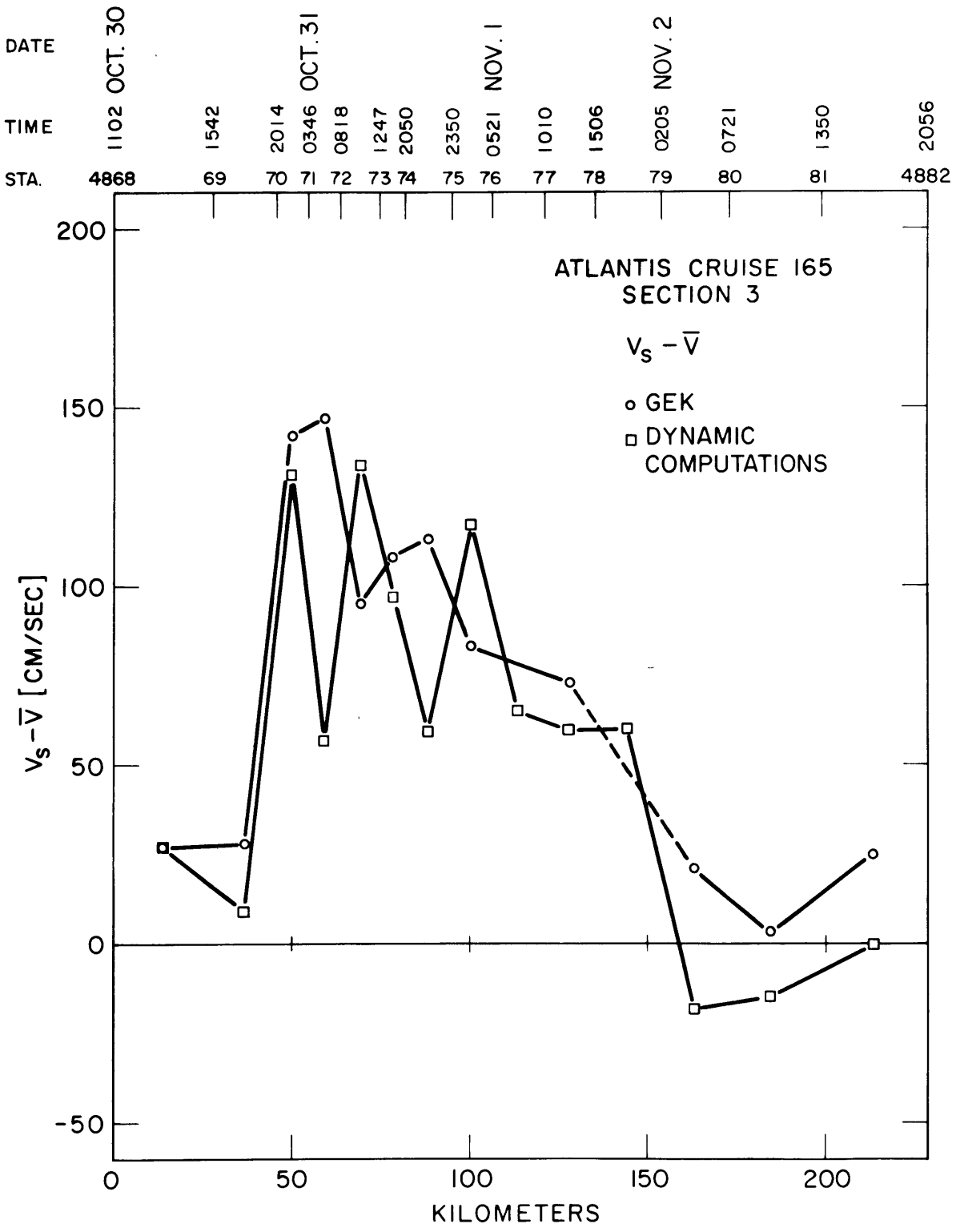
DATE
TIME
STA.
1102 OCT. 30
1542
2014
0346 OCT. 31
0818
1247
2050
2350
0521 NOV. 1
1010
1506
0205 NOV. 2
0721
1350
2056
4868
69
70
71
72
73
74
75
76
77
78
79
80
81
4882
ATLANTIS CRUISE 165
SECTION 3
$V_S - \bar{V}$
o GEK
□ DYNAMIC COMPUTATIONS
$V_S - \bar{V}$ [CM/SEC]
200
150
100
50
0
-50
0
50
100
150
200
KILOMETERS

of a nongeostrophic process such as internal inertial gravity or tidal waves.

In Figure 11 the differences between the two estimates of $V_s - \bar{V}$ are plotted versus the mean time between station pairs. The differences oscillate about zero with some regularity. There is good correspondence between the estimated period of these oscillations and the local inertial period which varies over the section from 19.2 to 20.2 hours. The conclusion that the observed differences are related to inertial oscillations in the Gulf Stream is probably justified, but it must be realized that these data have been inferred from two indirect methods each possessing unestimated experimental errors. The six days of observations in sections 1 and 2 comprise about 8 cycles and argue rather strongly that the differences are periodic. In order that any periodicity be recognizable in the presence of the mean motion of the Gulf Stream, it is necessary that the disturbances be in phase over a large time-space domain.

A histogram of the time differences between the 25 station pairs of sections 1 and 2 is shown in Figure 12. Section 3, made four days after section 2, was made across a Gulf Stream meander. Because of the 4 days delay and the more complicated nature of the Stream at this section, the data have not been included in the histogram. The stations are distributed in time such that the inertial period can be isolated since almost all of the station pairs are separated by less than half an inertial period. On the other hand, the record is probably aliased by contributions from

Figure 11 Differences between GEK and dynamic computations versus mean time between stations for ATLANTIS 165, sections 1, 2 and 3.

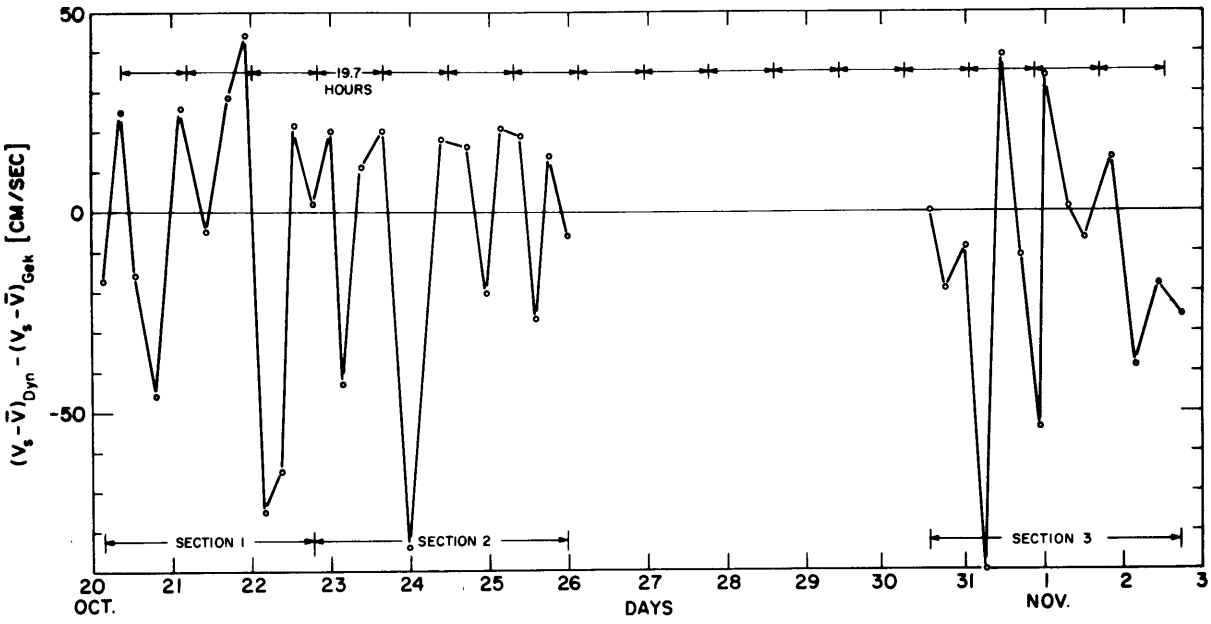
50
0
-50
19.7
HOURS
SECTION 1
SECTION 2
SECTION 3
20
OCT.
21
22
23
24
25
26
27
28
29
30
31
1
NOV.
2
3
DAYS
$(V_s-\bar{V})_{Dyn}-(V_s-\bar{V})_{Gek}$ [CM/SEC]

Figure 12 Histogram of time differences between hydrographic stations for ATLANTIS 165, sections 1 and 2.

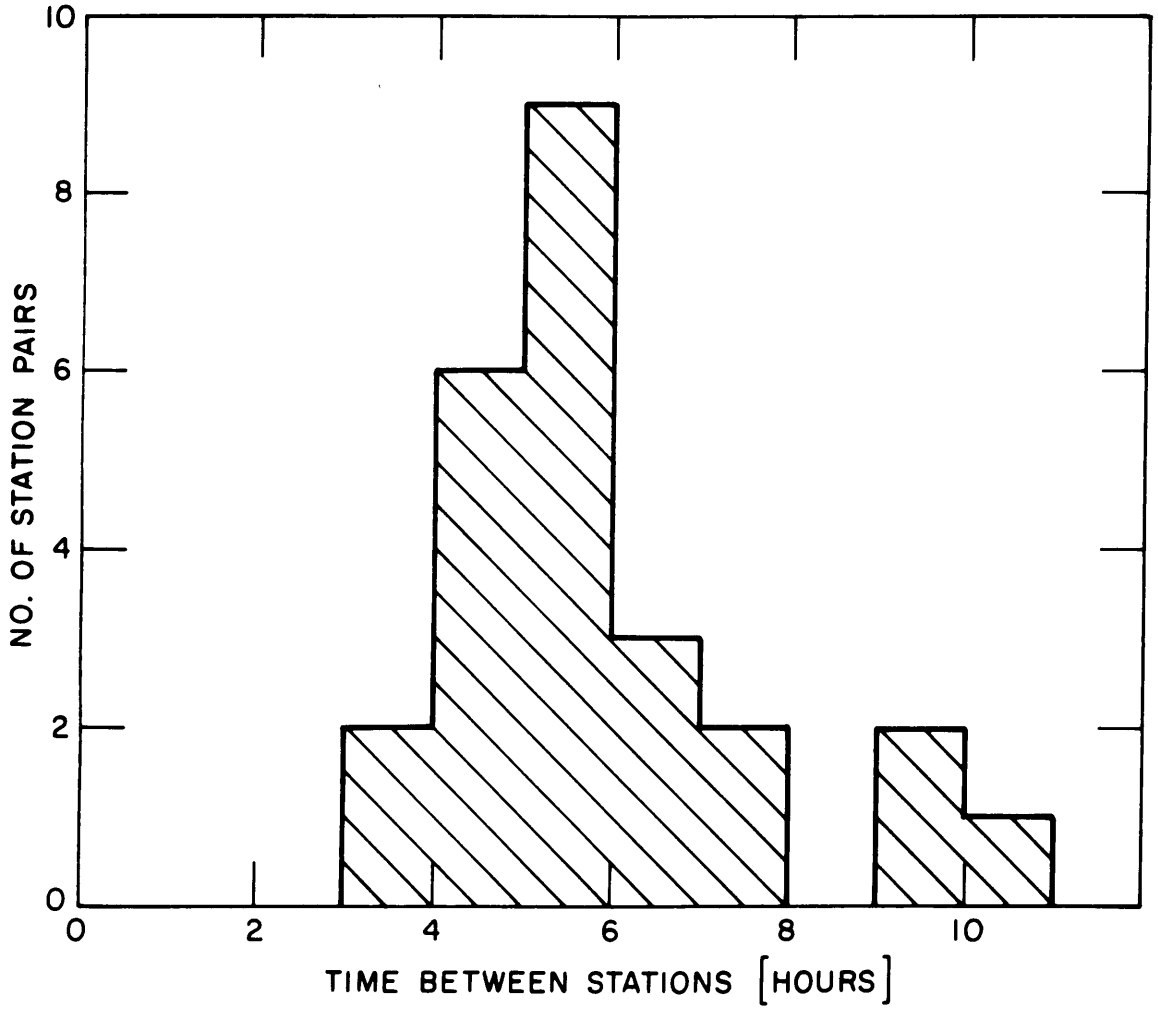
10
8
6
4
2
0
NO. OF STATION PAIRS
0
2
4
6
8
10
TIME BETWEEN STATIONS [HOURS]

higher frequency processes, such as the semi-diurnal tidal component.

If there were inertial currents present, it would be expected that their speed of flow would be in the order of 10 cm/sec. The GEK values can be assumed to have such a component. The dynamic computations, as pointed out in Worthington's paper, are very sensitive to small errors in position which may result in erroneous estimates of the slopes of the isobaric surfaces. Worthington asserts that an error of 1 km in station position could result in a scatter of $\pm$50 cm/sec in the dynamic calculations. The observed differences between GEK and dynamic computations were thought to be due in part to uncertainty in station position as determined by LORAN. One can apply the same argument to the case when the Gulf Stream or some part of it, such as the surface layers, has moved laterally the order of 1 km in the period between stations. Whereas the errors in the geographic position of stations would tend to be random, the errors due to the transverse movement of the current should reflect the periodicity of the movement. Moreover, it is possible that the amplitude, but not the period of the oscillations in Figure 11, is affected by the non-simultaneity of the shallow and deep hydrographic casts.

Newton (1965) has predicted the existence of semi-inertial velocity variations along the axis of the Gulf Stream. Newton finds that the period, Ta, of the type of motion he studied should be

$$T_a = \frac{T_{inertial}}{1 - n}$$

He asserts that $n = \frac{1}{2}$. These oscillations, having a period of twice the inertial period or a full pendulum day, if present in the record are not dominant. The largest (locally) negative differences in Figure 11 for sections 1 and 2 are about two inertial periods apart. A similar conclusion cannot be drawn from the positive differences.

Webster (1963) found a strong inertial peak in the energy density spectrum obtained from the records of moored current meters placed on both sides of the Gulf Stream. Day and Webster (1965) compared the data from current meters on the same and different moorings in the Sargasso Sea near Bermuda. Coherence between current meters was not found at the inertial frequency. The present results require strong coherence between current meters at the same depth. The observations of Hunkins (1967) of the inertial motion of an ice island indicates that the ice pack as a whole exhibits this circular motion.

As far as the energy source for the motion is concerned, all that is known is that the weather during this cruise was poor. Rough seas and strong, variable winds were experienced.

Conclusions

On the basis of these observations, the speculation is made that the Gulf Stream, particularly the surface layers,

was being perturbed by inertial oscillations. Because the method of dynamic sections was more disturbed by this occurrence than the method of towed electrodes, a comparison of the methods revealed this disturbance. The inertial disturbance seemed to have little space dependence of phase either across the section or in the region upstream which was later advected through the section. A large region of the Gulf Stream appeared to have been in synchronous motion at or near the inertial frequency.

Observations of Mangelsdorf and Barrett

Another example of a coordinated GEK and hydrographic survey is available in the recent work of Mangelsdorf who has kindly supplied unpublished observations obtained with his salt bridge GEK apparatus (Mangelsdorf, 1965). The hydrographic data were taken by Mr. Joseph Barrett. In this case, average GEK values were determined over five minutes of record with 10 or more such values obtained between stations. Mangelsdorf applied a correction to the average GEK values between stations to account for the variation of sea water conductivity with depth. Hence, the GEK values are in terms of $V_s - \bar{V}_\sigma$ where $\bar{V}_\sigma$ is the conductivity averaged velocity (see Appendix E). This correction is small. The GEK values and dynamic computations are indicated in Figure 13. Again the banded structure of the Stream is apparent in the dynamic sections but not in the GEK values.

Figure 13 Comparison of surface minus average velocities for GEK and dynamic computations for CRAWFORD 115.

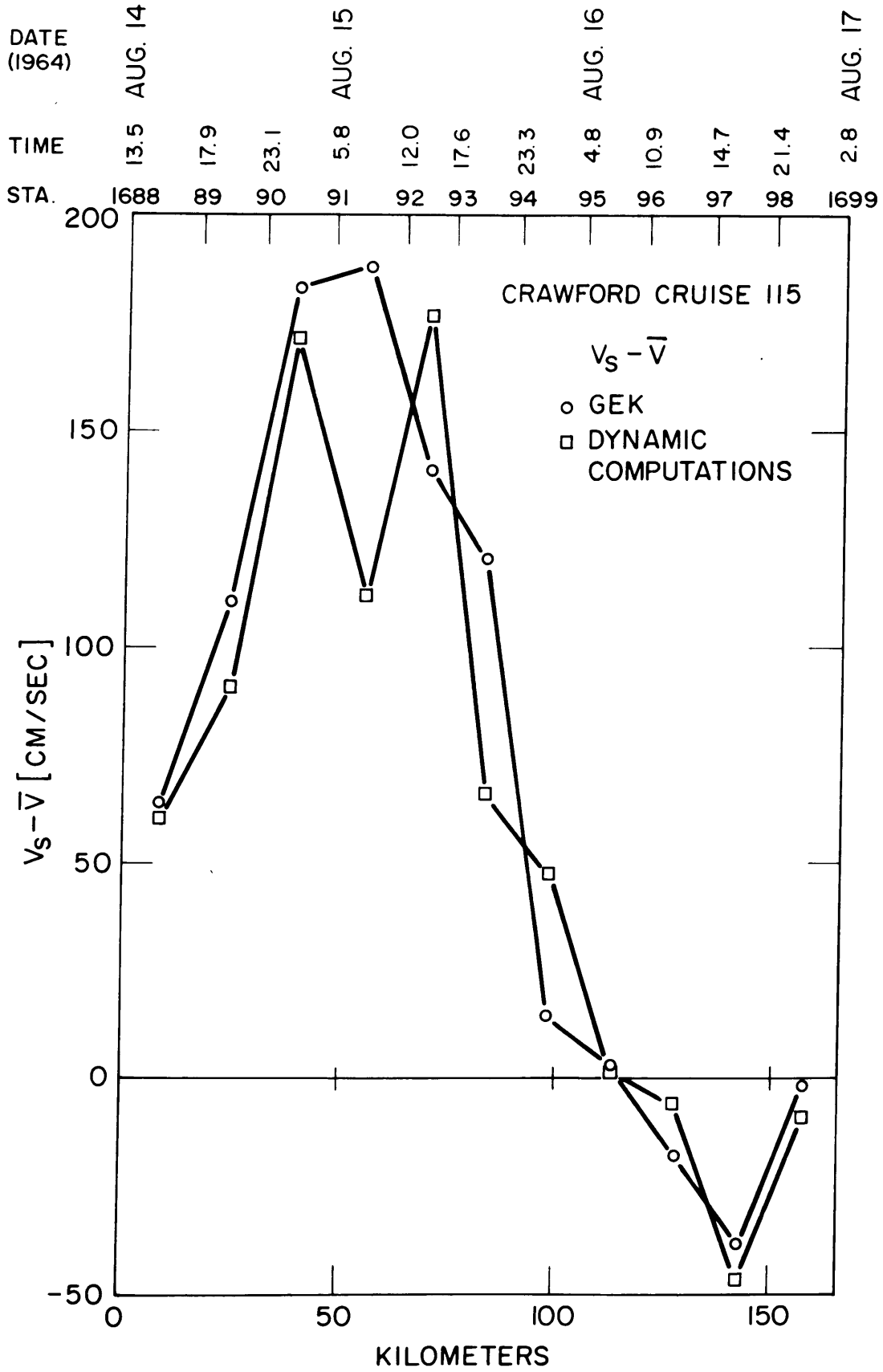
DATE (1964)
AUG. 14
AUG. 15
AUG. 16
AUG. 17
TIME
13.5
17.9
23.1
5.8
12.0
17.6
23.3
4.8
10.9
14.7
21.4
2.8
STA.
1688
89
90
91
92
93
94
95
96
97
98
1699
CRAWFORD CRUISE 115
$V_S - \bar{V}$
o GEK
□ DYNAMIC COMPUTATIONS
$V_S - \bar{V}$ [CM/SEC]
200
150
100
50
0
-50
0
50
100
150
KILOMETERS

Results and discussion

The differences between the two results are plotted versus the mean time between stations in Figure 14. The data in this small sample do not show strong variations in the inertial frequency range, but are suggestive of semidiurnal tidal oscillations. The correspondence of the peaks to the semidiurnal period, M_2(12.42 hours), may be an artiface of the sampling scheme which was inappropriate to define this frequency.

The velocity profiles for the three station pairs in the middle of the Gulf Stream are presented in Figure 15. Above about 400 meters, the middle station pair gives a velocity profile which differs from that of the adjacent stations. It is probable that the surface waters have undergone transverse movement relative to the axis of the Stream.

Upon considering together the observations of Worthington and Mangelsdorf it is not surprising that the periods of oscillation appear to be different. Moored current meters indicate the presence of both inertial and tidal variations in the ocean. Those records near the Gulf Stream often indicate that inertial currents are dominant for a period and then are followed by a succession of tidal motions (Webster, 1966).

Figure 14 Differences between GEK and dynamic computations versus mean time between stations for CRAWFORD 115.

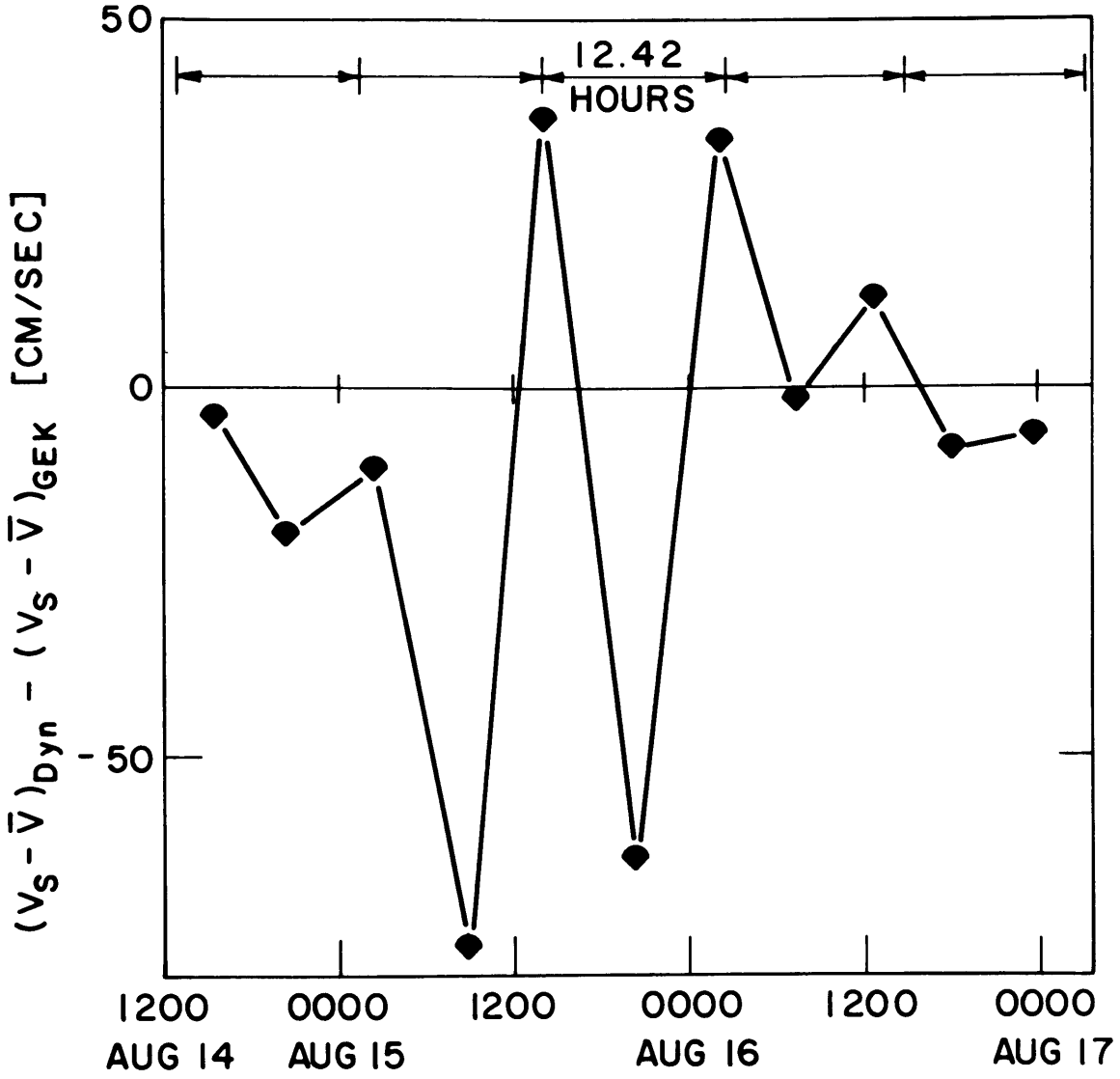
50
0
-50
12.42
HOURS
$(V_S - \bar{V})_{Dyn} - (V_S - \bar{V})_{GEK}$ [CM/SEC]
1200
AUG 14
0000
AUG 15
1200
0000
AUG 16
1200
0000
AUG 17

Figure 15 Three station pairs from CRAWFORD 115 in core of Gulf Stream showing reduced surface velocities for middle station pair.

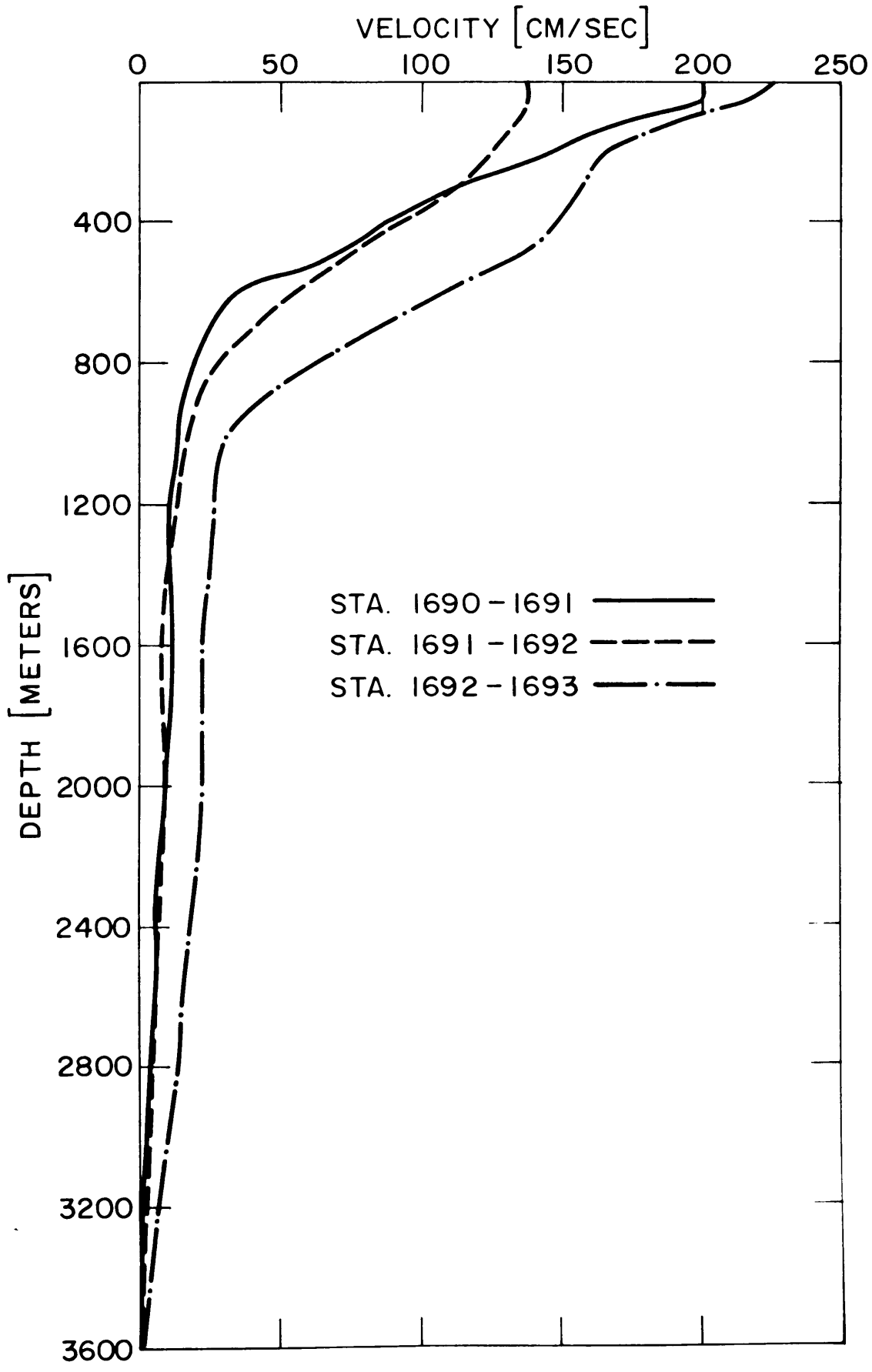
VELOCITY [CM/SEC]
0
50
100
150
200
250
400
800
1200
1600
2000
2400
2800
3200
3600
DEPTH [METERS]
STA. 1690 - 1691
STA. 1691 - 1692
STA. 1692 - 1693

CHAPTER 4

EXPERIMENTS

Four deep water experiments were attempted with the assistance of the personnel of the Buoy Lab of Woods Hole Oceanographic Institution. Limited success was achieved in the first of the series with the results reported here. In other attempts to measure the vertical potential differences in the sea using moored buoys, one buoy failed to be deployed and had to be immediately recovered; in another the instrumented cable failed. The fourth experiment to observe the potential as a function of depth was from a drifting ship.

Several other experiments were performed in the Northwest Providence Channel with the assistance of the personnel of the Physical Oceanography Lab of Nova University. Here again a moored buoy failed to provide useful information. In this case, it seems likely that one of the electrodes was contaminated. Two vertical potential profiles were made and will be discussed in this section.

The interpretation of the potential measurements is based on equation 5 :

$$\frac{\partial \phi}{\partial z} = F_y V(y,z) + F_z \frac{\partial}{\partial y} \int_z^0 (V(y,\xi) - \bar{V}(y))\, d\xi$$

The second term on the right side is at most of order h/L, the ratio of the vertical and horizontal scales and generally can be neglected. The vertical potential gradient can be written as $\frac{\partial \phi}{\partial z} = H V \sin\Theta$

since $F_y = H \sin\Theta$ where H is the horizontal component of the total geomagnetic field $\underline{F}$ and Θ the flow direction measured clockwise from magnetic north. The flow direction is usually not available when vertical measurements are made so it is convenient to replace V sin Θ by V_E, the magnetic east component of the velocity. Then we obtain

$$\frac{\partial \phi}{\partial z} = H V_E$$

Integration of this expression produces

$$T_E(y, z_2 - z_1) = H^{-1}[\phi(y, z_2) - \phi(y, z_1)] \quad m^2/sec$$

when H is given in weber/m^2 and ϕ in volts.

Electrodes

The measurements reported here were made with silver-silver chloride electrodes fabricated as suggested by von Arx (1950, 1962). An attempt was made to improve electrode stability, but the results were generally inconclusive; though, it was found that electrodes of this manufacture should be fused for 20 minutes, rather than 15 minutes as previously thought, at 460° C in order to convert all the silver oxide into elemental silver.

Vertical GEK from Drifting Ship near Buoy Station D

To examine the difficulties in making a potential profile from a drifting vessel, a cruise was made aboard the R.V. Crawford of Woods Hole Oceanographic Institution. The principal work of deploying and retrieving moored buoys unfortunately permitted only one vertical profile to be

made. The lowering was made at station D located as shown in Figure 7. It was realized that this experiment would not provide reliable quantitative information about the magnetic east-west transport since neither T-S nor drift corrections would be accurately known. But, it did serve as a test of procedures and gear and did provide potential information of some interest.

Equipment

The basic equipment consisted of a 1500 meter length of single conductor, double-armored wire wound on a hydraulic winch. One silver-silver chloride electrode, in a protective case, was attached to the free end of the cable, while the other electrode was let overboard on another unarmored cable. Attached below the end of the armored wire was a depth-time recorder, a film recording current meter and a hydro-weight. The depth recorder was used to determine pressure depth as a check against the metered amount of cable. The current meter was to supply the relative velocity information required to define the absolute velocity field.

Results and discussion

The winch was stopped at a particular depth for several minutes while the potential difference was recorded. The average readings at each depth are presented in Figure 16. Averaging was necessary because the readings contained surface wave-induced components. The numbers beside the points indicate the elapsed time in minutes since the start

Figure 16 Vertical potential differences obtained on CRAWFORD 140 while ship drifting at station D.

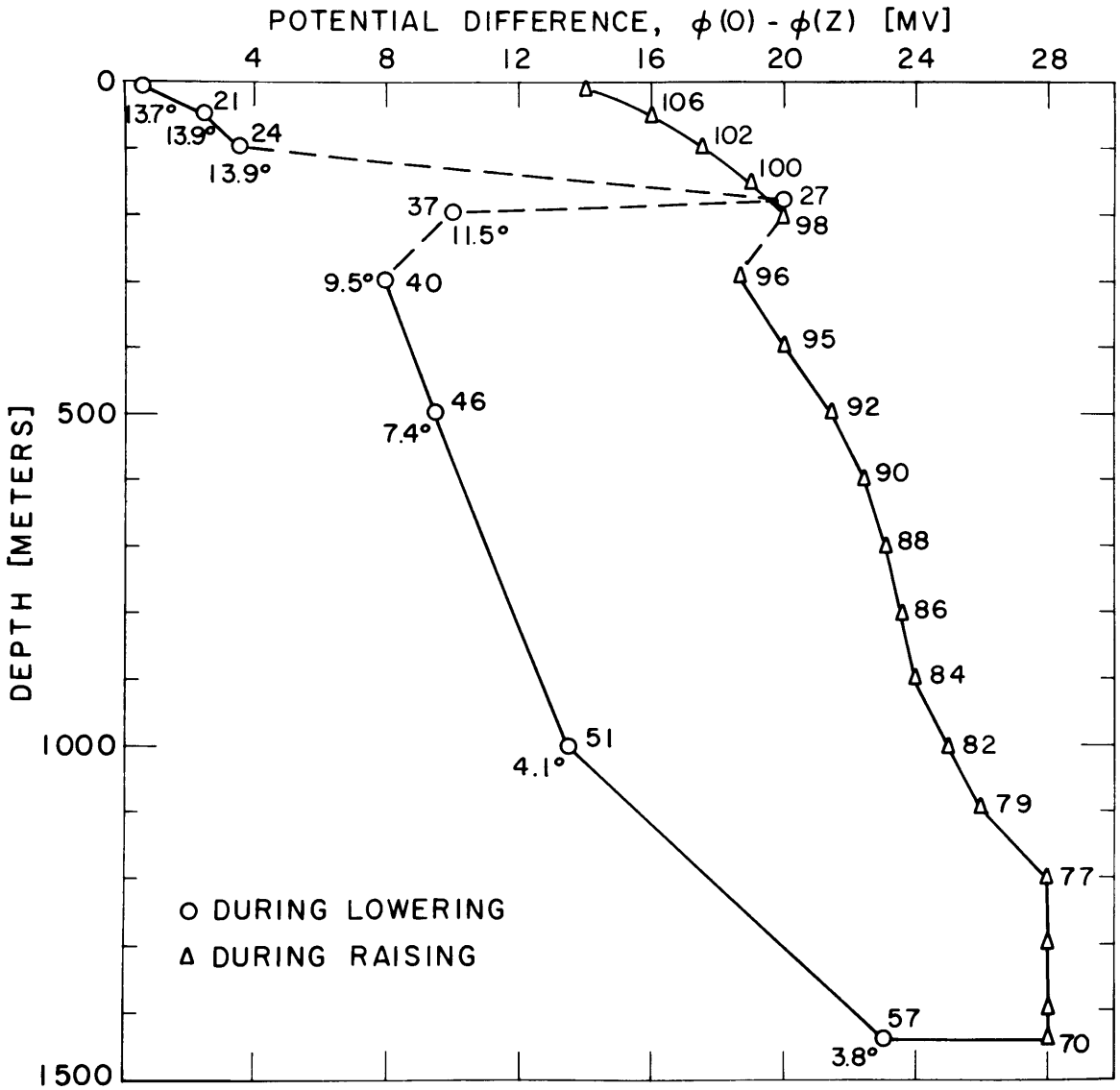
POTENTIAL DIFFERENCE, $\phi(0) - \phi(Z)$ [MV]
4
8
12
16
20
24
28
0
500
1000
1500
DEPTH [METERS]
13.7°
21
13.9°
24
13.9°
106
102
100
27
98
37
11.5°
9.5°
40
96
95
92
46
7.4°
90
88
86
84
82
51
4.1°
79
77
57
3.8°
70
O DURING LOWERING
Δ DURING RAISING

of the experiment and the estimated temperature at each depth.

The potential profile exhibits strong hysteresis. This behavior is consistent with the expected electrochemical effects, but is several times greater than can be accounted for by the results of Appendix F. It must be noted that a lag was introduced in the construction of the electrode cases (see von Arx, 1950) requiring from 10-30 minutes for the electrode to approach equilibrium in each new environment. Allowing for this, it still appears that some other process must be responsible for the excessive hysteresis.

This process might be identified from the record. Firstly, the interelectrode potentials at the surface, where the drift is unimportant, differ by 14 millivolts. Immediately after the experiment, the electrode cases with the electrode inside were disconnected from their cables and placed together in a plastic bucket of sea water. The potential difference was only 1.2 mv. Although it is possible that the electrode bias potential could have changed after leaving the sea, it seems more likely that the potential difference observed at the surface is due to other causes. The next point is that peculiar changes occurred in the region 170-200 meters on both curves. These points are definitely related to cable handling difficulties. After 150 meters of cable had been released, the cable developed several large, loose loops which produced a tangled spool. The steps taken to free the spool left several sharp bends in the cable at 173 meters. The observed high voltages,

both on release and return, seem related to cable damage at that point.

If damage to the cable is the source of the hysteresis, then it is not entirely possible to remove the resulting error, yet it is interesting to make the following crude adjustment. If we require that the data satisfy two physical requirements; namely, that $\Delta\phi = 0$ at the surface and that the slope of $\Delta\phi$ versus depth be continuous, we obtain values as shown in Figure 17. It may be fortuitous that this procedure should give such a reasonable profile. Below 300 m the profile closely parallels the line drawn on the basis of the observed drift rate of the ship, assuming that the water had little motion below this depth.

Ordinarily, the next step in the analysis of the data would be to remove the contributions due to the drift of the ship and the temperature and salinity effects. But, considering the observed hysteresis, the lack of TS values at each level, and the variations in ship drift, there was little use in carrying the analysis further. The experiment failed, but it served to indicate the operational difficulties involved in such measurements.

Conclusions

These experiences suggested that the next attempt at vertical measurements from a drifting vessel be made where the flow is strongly east-west, where frequent and accurate fixes could be obtained along with temperature and salinity at each level during the experiment. It would also be

Figure 17 Vertical potential differences obtained on CRAWFORD 140 while ship drifting at station D - after data adjustments, see text.

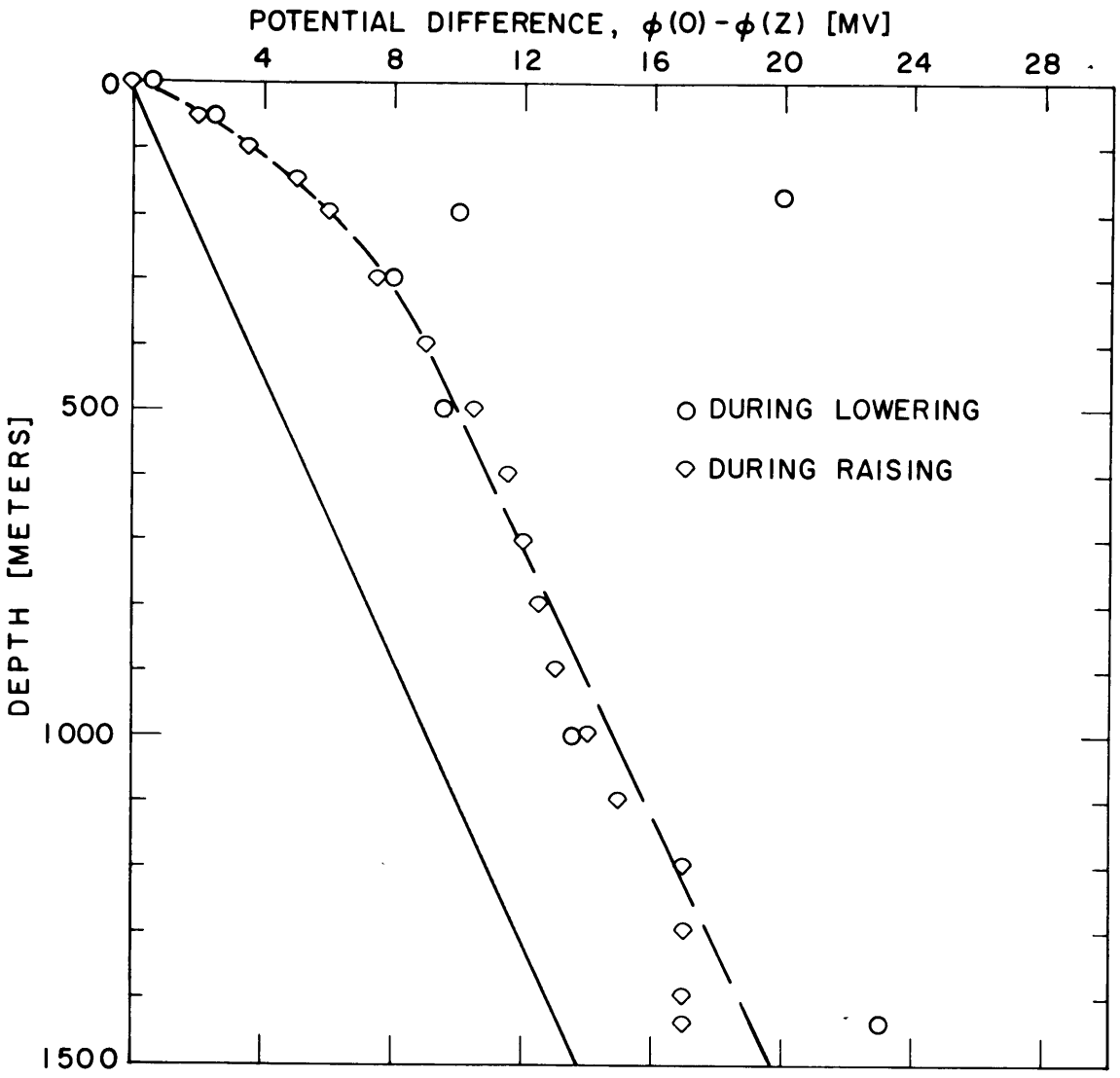
POTENTIAL DIFFERENCE, $\phi(0)-\phi(Z)$ [MV]
4
8
12
16
20
24
28
0
500
1000
1500
DEPTH [METERS]
DURING LOWERING
DURING RAISING

valuable to have independent measurements of the flow for comparison.

Vertical GEK from Drifting Ship in Northwest Providence Channel

Incorporating the improvements suggested by the previous experiments, vertical potential gradient observations were made in conjunction with precision navigation and an independent transport measurement. The vertical potential measurements from a drifting ship were obtained with the generous assistance of the personnel and facilities of the Physical Oceanography Lab of Nova University.

The observations (Richardson and Finlen, in press) in the Northwest Providence Channel indicated that there was easterly flow on the southern side of the channel and westerly flow on the northern side. Their results showed that the second order term involving the shear of the excess transport was negligible. It was decided to occupy their station #2 where the flow was expected to be strong and westerly. The volume transport per unit section was determined from measurements of the run time, depth and horizontal deflection of a freely falling body. This technique described by Richardson and Schmitz (1965) also provided the temperature as a function of depth. The drift of the ship was determined by the Hi-Fix system (see Richardson and Schmitz, 1965) with slave stations located at Virginia Key and Boca Raton, Florida.

Equipment and procedure

Potential measurements were made with silver-silver chloride electrodes attached to a small, double-armored, single conductor cable (Amergraph 1-H-100). The cable was wound on the large drum of a crank-operated winch. The free end of the cable passed around a thimble (3 inch diameter) and extended back up the cable for about 10 meters. For 10 meters on either side of this point, at which an electrode connector was installed, the cable was covered with plastic tubing. The tubing shielded the electrode from electrical effects due to cable corrosion. Attached to the thimble was a line containing a depth-time recorder and a timed weight release. The latter supported two 23Kg sash weights which were jettisoned prior to the retrieval of the cable to reduce the nevertheless exhausting task of spooling in almost 700 meters of the wire with a hand-cranked winch.

A surface electrode was installed on another section of the same type cable. The electrode was placed at a depth of about 10 meters. A sash weight was attached 10 meters below this point, and the cable was jacketted in plastic tubing as before.

The equipment was installed aboard the Gulfstream, a small high speed ship, outfitted with the Hi-Fix master station.

With the ship hove to, the deep electrode was lowered in steps of about 50 meters. The potential differences were measured at each level using a Keithly 148 millivoltmeter. The amplified output of this instrument was passed

through an electronic low pass filter having a cutoff frequency of 0.1 cps and an attenuation of 40 db per decade. The filtered signal was recorded on a Leeds and Northrup, Model H stripchart recorder. This yielded a record in which the wave-induced variations were greatly reduced.

Throughout the experiment the ship's position as indicated on the Hi-Fix counters and time were recorded photographically at regular intervals.

Results and discussion

Two lowerings were made, one each on December 19 and 20, 1966. In both cases the procedure was the same. Figure 18 presents the measured potential differences found on the 19th averaged over one minute, the cable drift correction and the combination of the two curves. The potential difference due to ship drift was computed as

$$\Delta\phi = - H V_{CE} z$$

where H is the horizontal component ($.25 \times 10^{-4}$ weber/m^2) of the geomagnetic field, V_{CB} the magnetic east component of the cable (ship) drift and z the depth, measured positively upward. The drift of the ship was quite small during all but the deepest section of the first lowering. The values found on the following day, during which the ship's drift was much larger, are shown in Figure 19. Some of the observed scatter in the potential reading is probably related to variation in the speed of the ship's drift. After the extra weight was released in preparation for raising the cable, the potential difference changed markedly on both days. The sign and magnitude of this change is

Figure 18 Vertical potential differences obtained aboard the GULFSTREAM in Northwest Providence Channel on December 19, 1966. Shown are the potential differences as measured, the potential contribution due to ship's drift and the drift corrected differences.

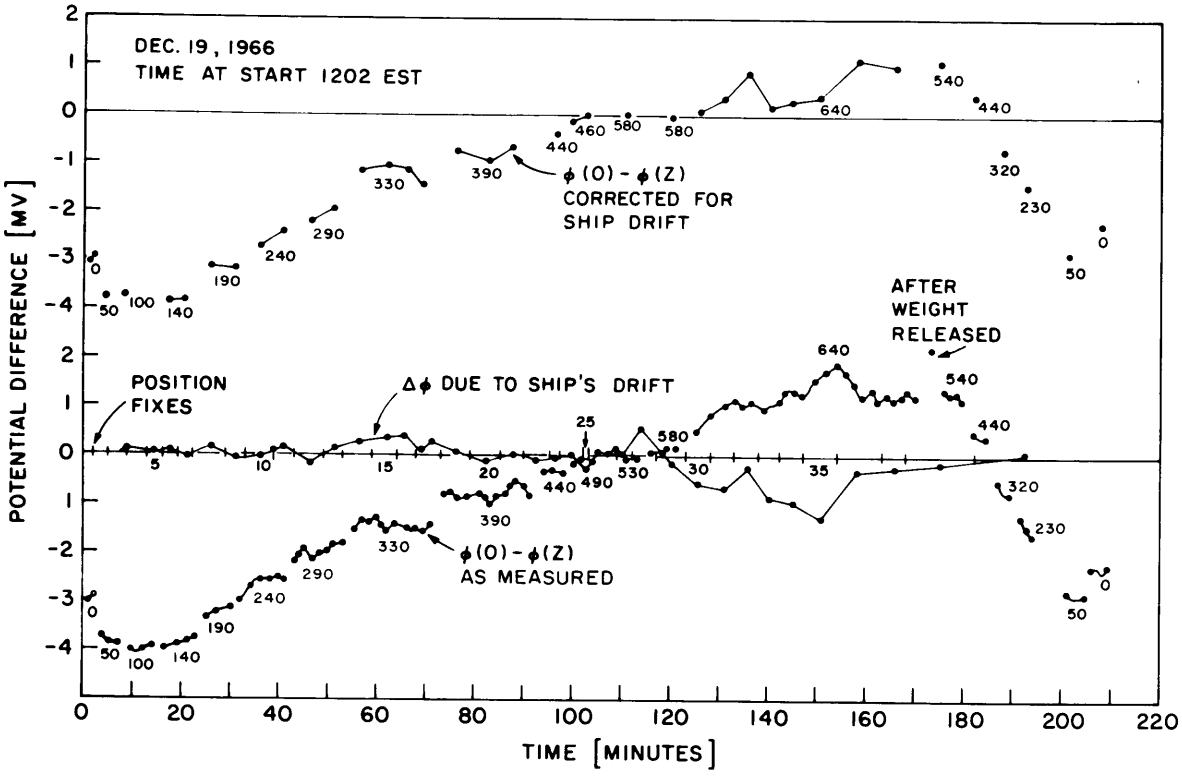
DEC. 19, 1966
TIME AT START 1202 EST
φ(0) - φ(Z)
CORRECTED FOR
SHIP DRIFT
AFTER
WEIGHT
RELEASED
POSITION
FIXES
Δφ DUE TO SHIP'S DRIFT
φ(0) - φ(Z)
AS MEASURED
POTENTIAL DIFFERENCE [MV]
TIME [MINUTES]

Figure 19 Vertical potential differences obtained aboard the GULFSTREAM in Northwest Providence Channel on December 20, 1966. Shown are the potential differences as measured, the potential contribution due to ship's drift and the drift corrected differences.

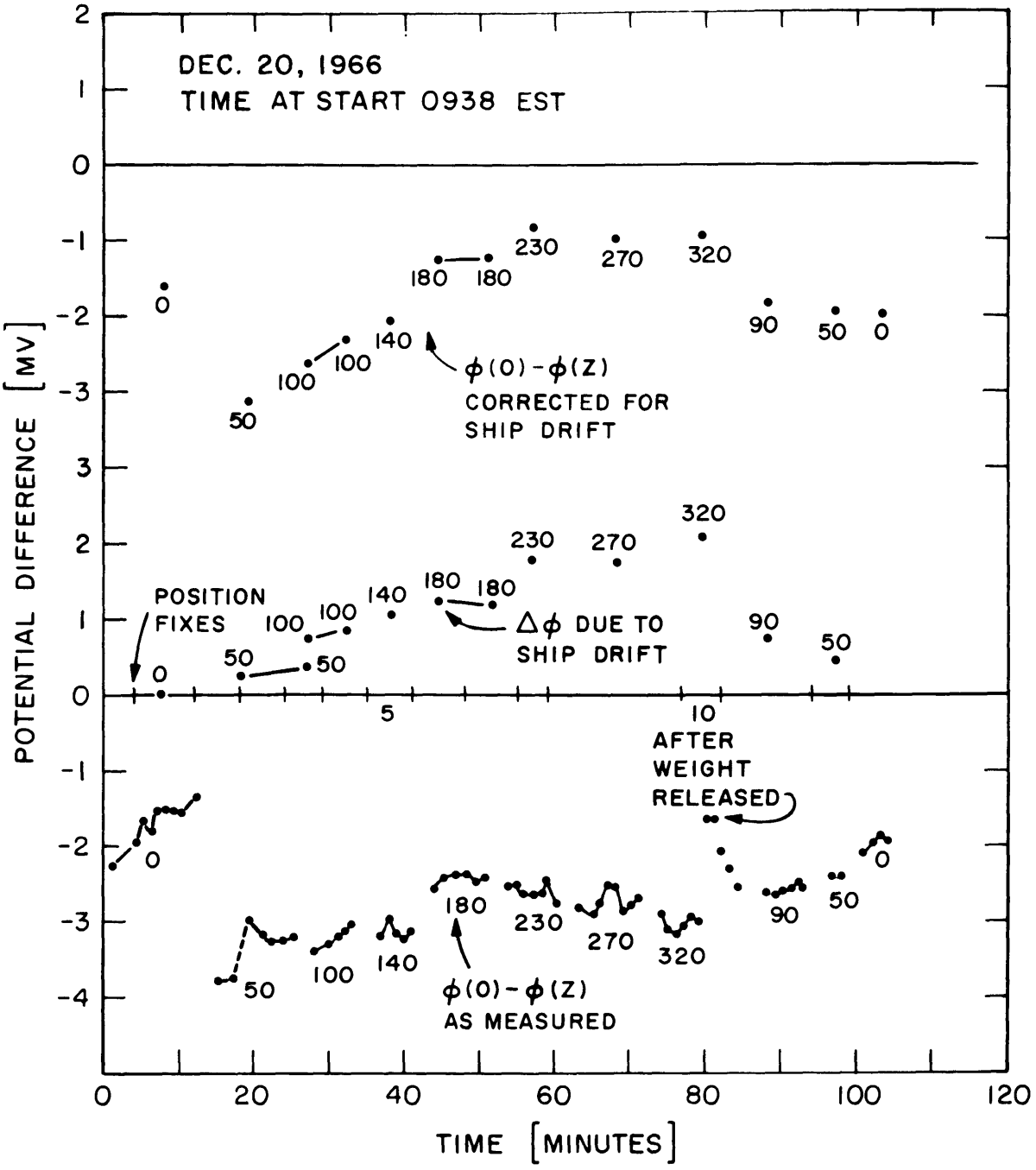
DEC. 20, 1966
TIME AT START 0938 EST
POTENTIAL DIFFERENCE [MV]
TIME [MINUTES]
φ(0)-φ(Z)
CORRECTED FOR
SHIP DRIFT
POSITION
FIXES
Δφ DUE TO
SHIP DRIFT
AFTER
WEIGHT
RELEASED
φ(0)-φ(Z)
AS MEASURED

consistent with the expected induction due to the cable moving under reduced tension into a new equilibrium profile.

The transport instrument provided temperature as a function of depth which, through prior knowledge of the T-S correlation for these waters, also provided the salinity. A T-S diagram, Figure 20, was constructed from data published by the Institute of Marine Sciences of the University of Miami (1962, 1963). The TS effects were computed by the relation

$$\Delta\phi_{TS} = \mathcal{E}_S\,(S(0) - S(z)) + \mathcal{E}_T\,(T(0) - T(z))$$

where E_T and E_S are the temperature and salinity coefficients determined in Appendix F.

The potential values before and after the weight was released are considered separately. There is a physical constraint to be applied to the data, namely, that $\phi(0) - \phi(z)$ is to be zero at $z = 0$. For clarity this constraint is applied in two steps. First, the data as the electrode is raised are adjusted so that at $z = 0$, about 10 meters below the surface, the potential difference is the same as that found at the start of the experiment. Later, this common value is set equal to zero. The drift corrected potentials are compared to the calculated electrochemical effects in Figures 21 and 22. The horizontal bars about each of the data points indicate the extremes of the measurement at each depth. Both figures exhibit a tendency for the measured signal to follow the TS effects closely. This illustrates

Figure 20 T-S diagram for waters of Northwest Providence Channel.

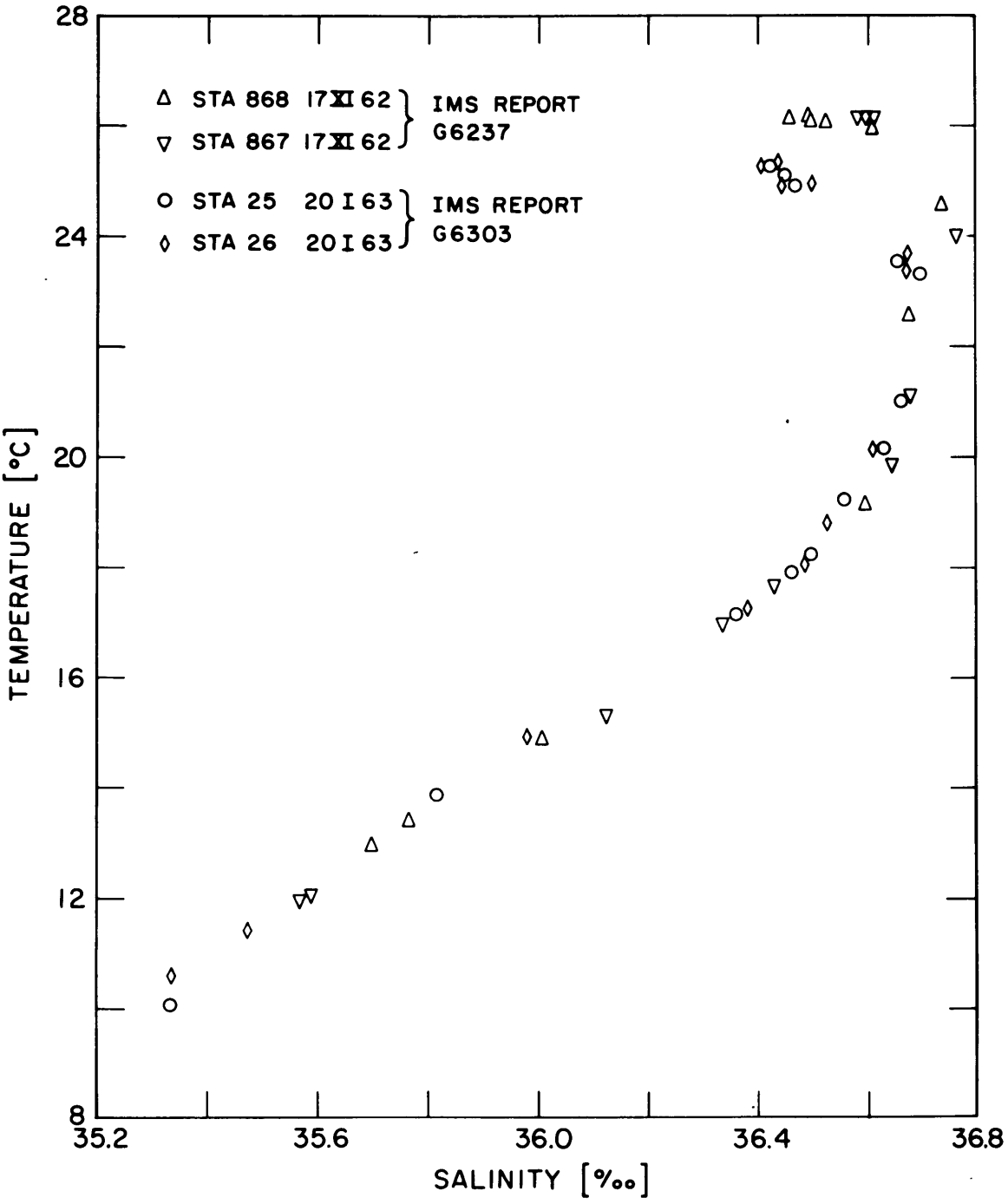
STA 868 17XI 62
STA 867 17XI 62
IMS REPORT G6237
STA 25 20 I 63
STA 26 20 I 63
IMS REPORT G6303
TEMPERATURE [°C]
SALINITY [‰]
28
24
20
16
12
8
35.2
35.6
36.0
36.4
36.8

Figure 21 Drift corrected potential differences and T-S potential contribution versus depth for December 19th. Circles: $\phi(o) - \phi(E)$ as measured during recovery (see text).

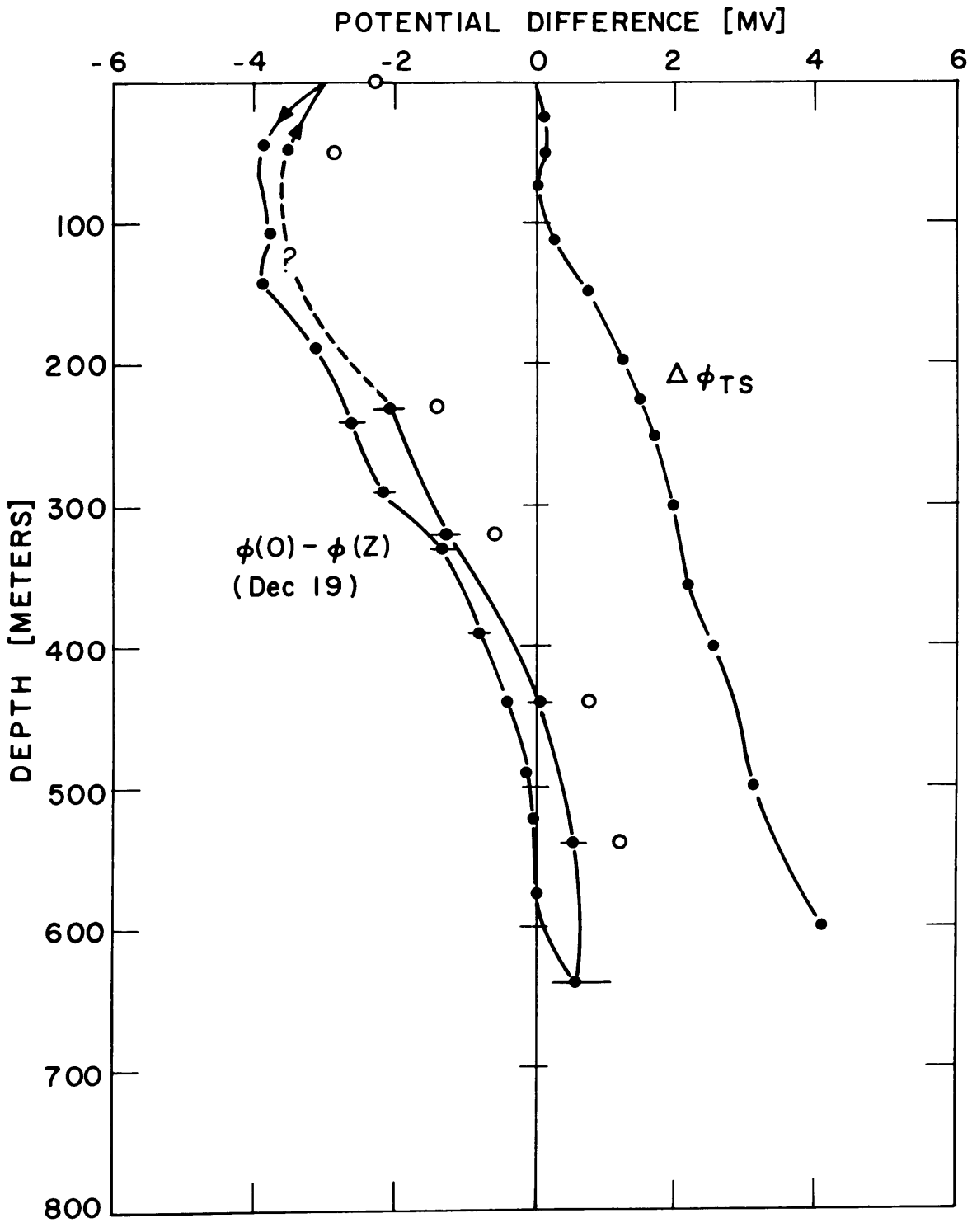
POTENTIAL DIFFERENCE [MV]
-6
-4
-2
0
2
4
6
100
200
300
400
500
600
700
800
DEPTH [METERS]
?
$\phi(0) - \phi(Z)$
(Dec 19)
$\Delta\phi_{TS}$

Figure 22 Drift corrected potential differences and T-S potential contribution versus depth for December 20th. Circles: $\phi(0) - \phi(z)$ as measured during recovery (see text).

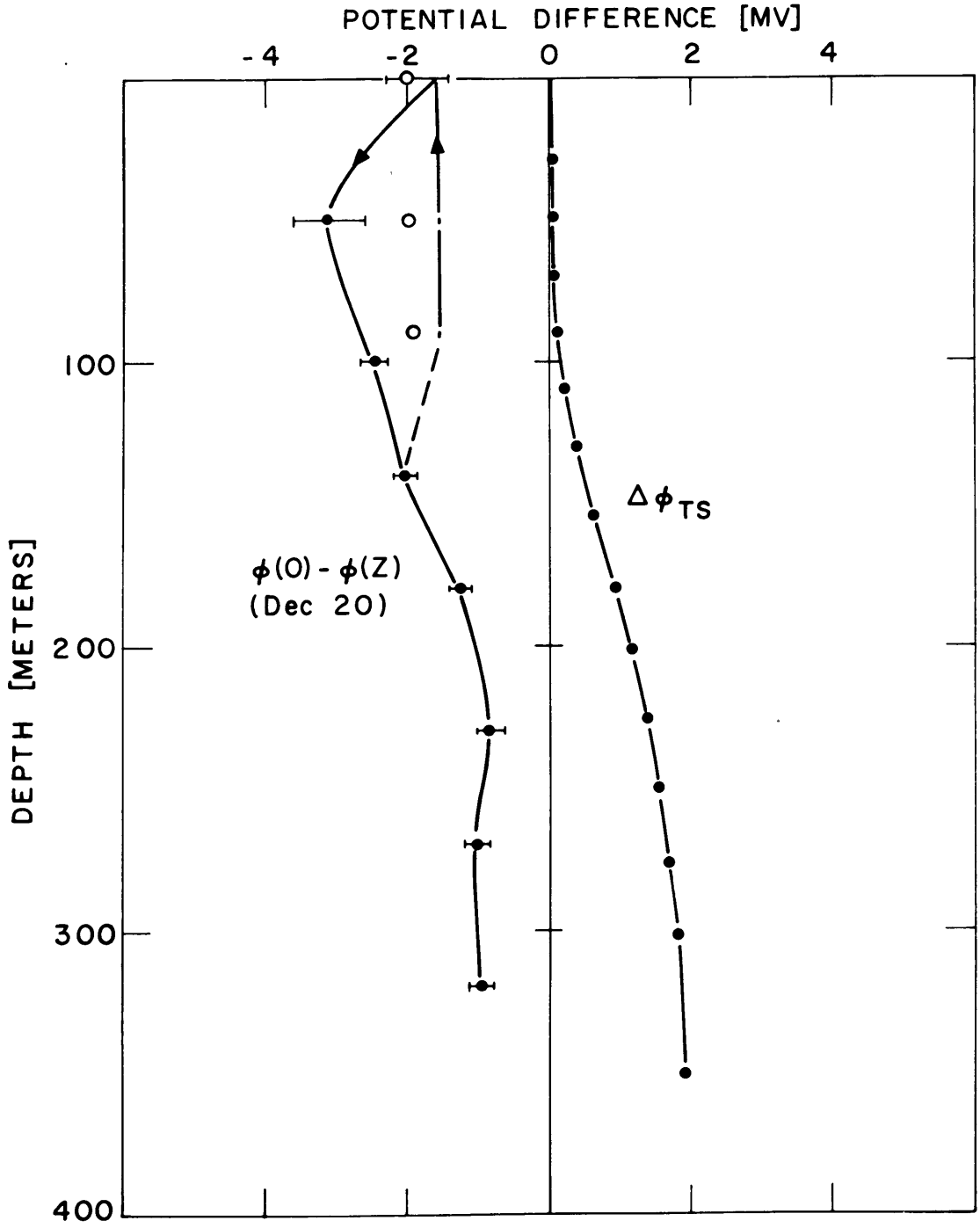
POTENTIAL DIFFERENCE [MV]
-4
-2
0
2
4
100
200
300
400
DEPTH [METERS]
$\phi(0) - \phi(Z)$
(Dec 20)
$\Delta\phi_{TS}$

the dominant influence the temperature and salinity variations have over these measurements. This set of measurements exhibit little of the strong hysteresis found in the previous experiment (see Figure 16).

The difference between the two curves in each figure should represent the magnetic east-west transport. Setting $\phi(0) - \phi(z)$ equal to zero at z = 0, the induced field is presented in Figure 23 as are the east-west components of the transports as determined by Richardson using his instrument. The latter measurements were made just after the electrode lowering was recovered on each day.

The potential versus depth curves exhibit some strange behavior. An interpretation of the data presented in Figure is that $\phi(0) - \phi(z)$ becomes more negative as the lower electrode (at z) passes through a region of westerly flow. The measurement indicates that the flow was not westerly throughout the water column. A comparison with the true transport to 138, 368, and 780 meters indicates that the electric measurements do not represent the true character of the flow.

The data taken on the next day also suggest layers of easterly flow, but in this case the data are consistent with the magnetic east-west transport as directly measured. There was good agreement between the two determinations of transports to 138 and 372 meters. The lower electrode was not extended beyond 320 meters nor was the value of the total transport available. Actually, the correspondence at 372 meters exists only to the extent that a projection of

Figure 23 Transports as determined by electric and Richardson-Schmitz (X) methods.

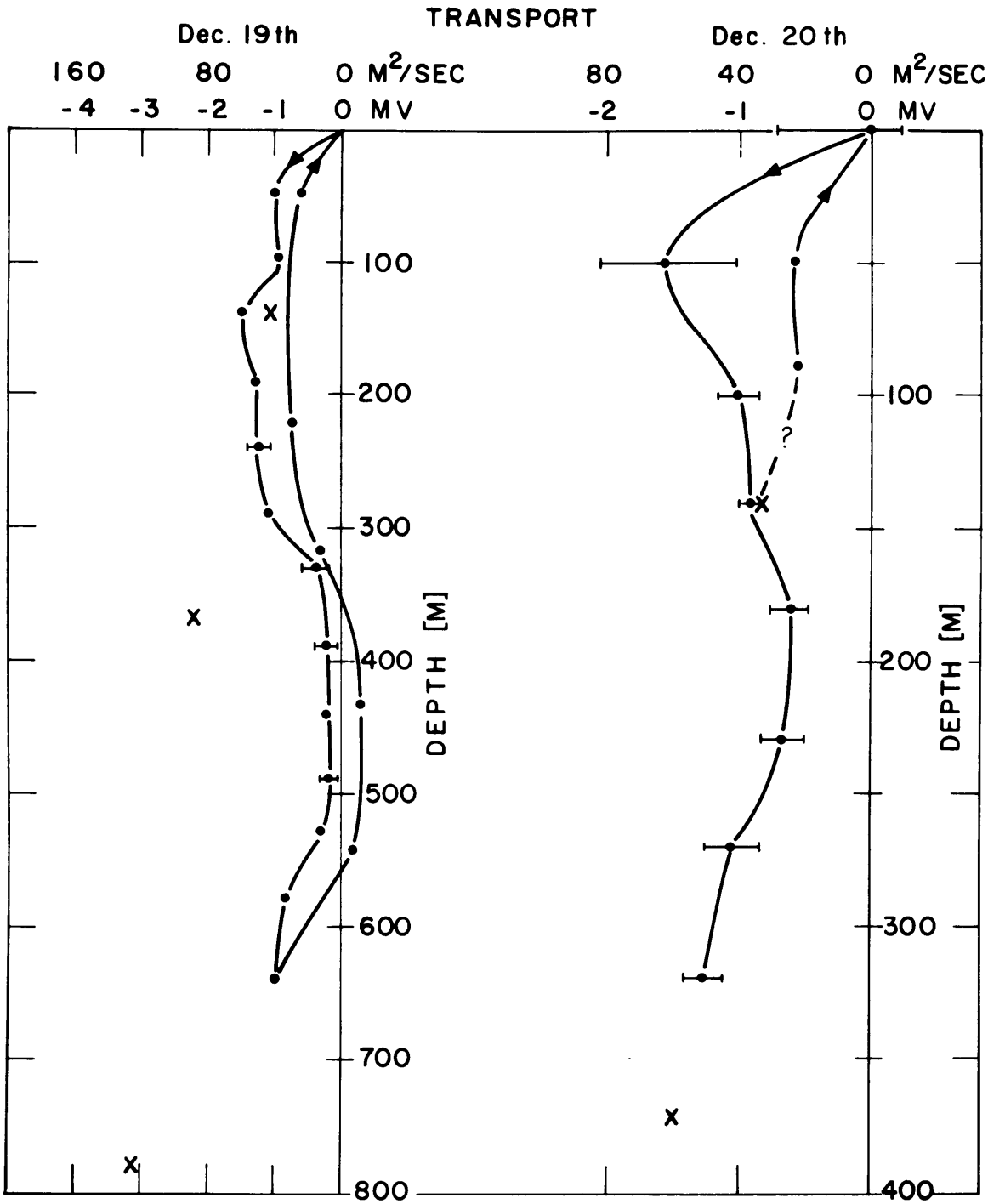
TRANSPORT
Dec. 19th
160
80
0 M²/SEC
-4
-3
-2
-1
0 MV
Dec. 20th
80
40
0 M²/SEC
-2
-1
0 MV
100
200
300
400
500
600
700
800
DEPTH [M]
?

the curve beyond 320 meters would intersect the directly measured value at 372 meters. There is a considerable difference between the lowered and raised values at 50 and 100 meters. The surface current was 35 cm/sec on the 19th but only 5 cm/sec on the 20th. If this low speed on the 20th is representative of much of the surface layer, say the upper 50-100 meters, then the actual transport profile would resemble that found while raising the electrode.

Richardson and Finlen found at their station #2 that on one day the total transport (through 800 meters) was the same as the transport to 300 meters. This observation requires an average flow speed of 50 cm/sec in the upper 300 meters and zero below. Probably the region below 300 meters consists of regions of easterly and westerly flow which contribute no net transport. The present measurements seem to indicate somewhat more detail of this layered flow.

No reason has been found to explain the difference between the two experiments. There is the possibility that due to differences in the ship's drift on the two days the inter-electrode length was tilted in the cross stream (north-south) direction. Such a condition would contribute a potential difference due to the vertical magnetic field acting on the current and yield a horizontal GEK signal. It is also possible that the electrodes behaved quite differently on the two days, even though the same electrodes were used in the same configuration both times.

A vertical potential difference measurement may be biased by the ship's galvanic field. This effect is most

important when the upper electrode is very close to the vessel. This field behaves somewhat as a dipole field so the electrode should be at least a vessel-length below the surface.

Conclusions

A method such as this might be used to advantage in many situations of oceanographic interest. It should complement the existing techniques available for studying the Equatorial Countercurrents. The speed of the ship's drift being estimated by the apparent change in transport as the electrode is extended into the less active waters below the currents. The Gulf Stream sections discussed in Chapter 3 suggest a situation in which a vertical GEK could have been used. The observed transports per unit section were as high as 1000 m^2/sec toward the east. In which case the electrochemical effects would be almost an order of magnitude less than the induced field. The measurements would, of course, be relative unless the drift of the vessel were accurately determined.

These pilot experiments have confirmed expectations in regard to the electrochemical contribution. As can be seen in Figure 21 this effect exceeds the value of the motionally-induced potential. That any correspondence between the direct and indirect transport measurements was possible is probably a reasonable test of the corrections made. With improved technique it can be expected that a vertical measurement from a ship can provide useful transport information, at least in strong east-west currents.

Vertical GEK from Moored Buoy

In order to obtain potential differences at sea for an extended period, a deep water moored instrument was set at buoy station D (see Figure 7) during Crawford cruise 140 in April, 1966. A large toroidal surface buoy supported the recording equipment and the mooring. The potential difference between a surface and two lower electrodes was to be monitored for two months. The mooring cable, in addition to supporting the electrode cables, contained three self-recording current meters.

Another mooring containing recording equipment, cables and electrodes was to be set within one-half mile of the other. This subsurface mooring with the recording gear enclosed in a glass sphere was not successfully deployed and had to be recovered immediately.

In addition to these two moorings, an instrumented mooring was set in this same general area (WHOI Station D) on Atlantis II cruise 25 in August, 1966. This experiment provided no useful data. It was determined that the lower electrode was torn from its case by drag forces as the anchor descended.

This chronicle dramatizes the general difficulty in obtaining reliable oceanographic information. The meagre data obtained, compared to that expected, leads one to marvel that any are available at all. Somewhat more than four months of record were expected but only one day of data was obtained.

The instruments aboard the first mooring were designed as a balance among several system requirements. First, since the RV Crawford would return to the buoy site several days after deployment, it was decided to recover the early record. In order to minimize the polarization of electrodes, an amplifier was needed before the recorders. The measurement cycle was chosen to conserve battery power, monitor amplifier performance and produce a readable record of potential difference against an accurate time base. Finally, it was decided to deploy three electrodes; one near the surface and two at greater depths.

Equipment

The voltages were recorded on a pair of recording galvanometers (Rustrak Model 88), one of which could be readily removed from the rest of the instrument. Driving the parallel recorders was a unity gain, high-input-impedance amplifier. Good small-signal performance was obtained when the operational amplifier module was operated at $\pm$ 6 VDC instead of the recommended $\pm$15 VDC. The lower operating voltages not only reduced the power requirements, but permitted the use of a common power supply for both the amplifier and recorder motors. A signal scanner was made to monitor the potential differences between electrodes and the performance of the amplifier. The gear train of the two month recorder motor ($\frac{1}{2}$ RPM) was disassembled and an output shaft extension was installed. This shaft drove a cam and a multipole rotary switch. Electrically, the rotor of the switch was connected

to the amplifier input, while the twelve positions, or contacts, of the stator were divided among four signal sources. A measurement cycle consisted of a calibration voltage of 23.2 mv (lasting 15 seconds), an electrode potential difference (40 seconds), zero voltage or system ground (10 seconds) the other electrode voltage and ended with the calibration signal (15 seconds) again. The cycle was not immediately repeated but was initiated by a chronometric sequence timer which applied power to the recorder. A cycle once started by the timer was maintained and finally ended by a parallel switch activated by the cam on the output shaft extension. Obviously, this arrangement requires that the sequence timer switch be closed for a period less than the cycle time, about two minutes. A choice of star wheels for the timer permitted repetition intervals to be varied from five minutes to one hour. In this way battery power was conserved, and the rate of advance of the chart was accurately controlled.

A cycle was initiated every five minutes for the experiment reported here. The short-term removable recorder was set to advance its chart paper about one-half inch per cycle, while the other recorder moved at one-sixth this rate.

Figure 24 is a diagram of the amplifier and scanner circuits. The completed instrument is illustrated in Figure 25.

The amplifier-recorder was enclosed in a PVC battery case attached to the instrument platform of the toroidal buoy. Fastened by hose clamps to the outside of the case were eight magnesium cells (size no. 6) which provided instrument power. Three signal leads, enclosed in rubber

Figure 24 Schematic diagram of recorder system.

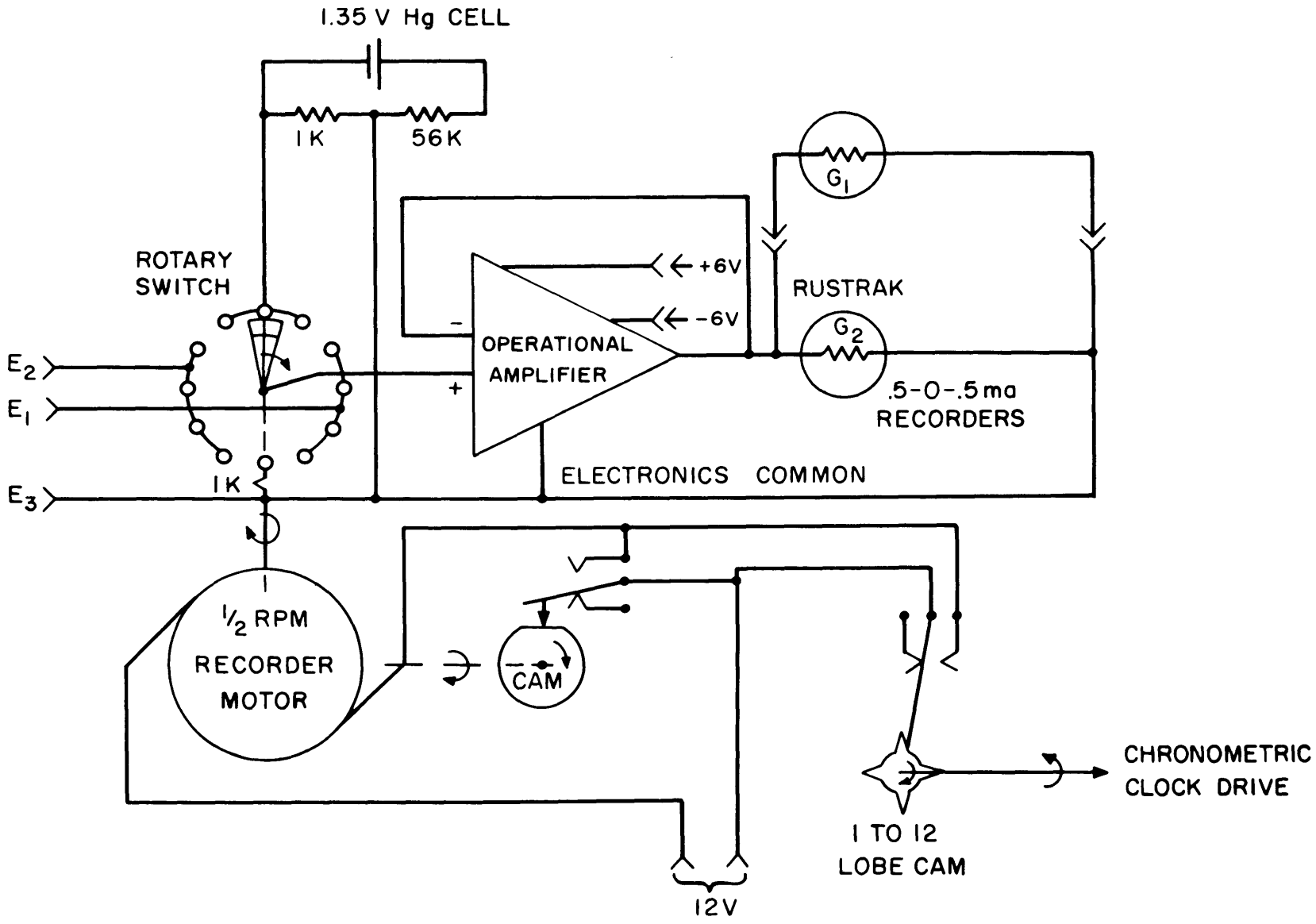
1.35 V Hg CELL
1K
56K
ROTARY SWITCH
E2
E1
E3
1K
+6V
-6V
OPERATIONAL AMPLIFIER
G1
RUSTRAK
G2
.5-0-.5 ma RECORDERS
ELECTRONICS COMMON
1/2 RPM RECORDER MOTOR
CAM
CHRONOMETRIC CLOCK DRIVE
1 TO 12 LOBE CAM
12V

Figure 25 Recorder system.

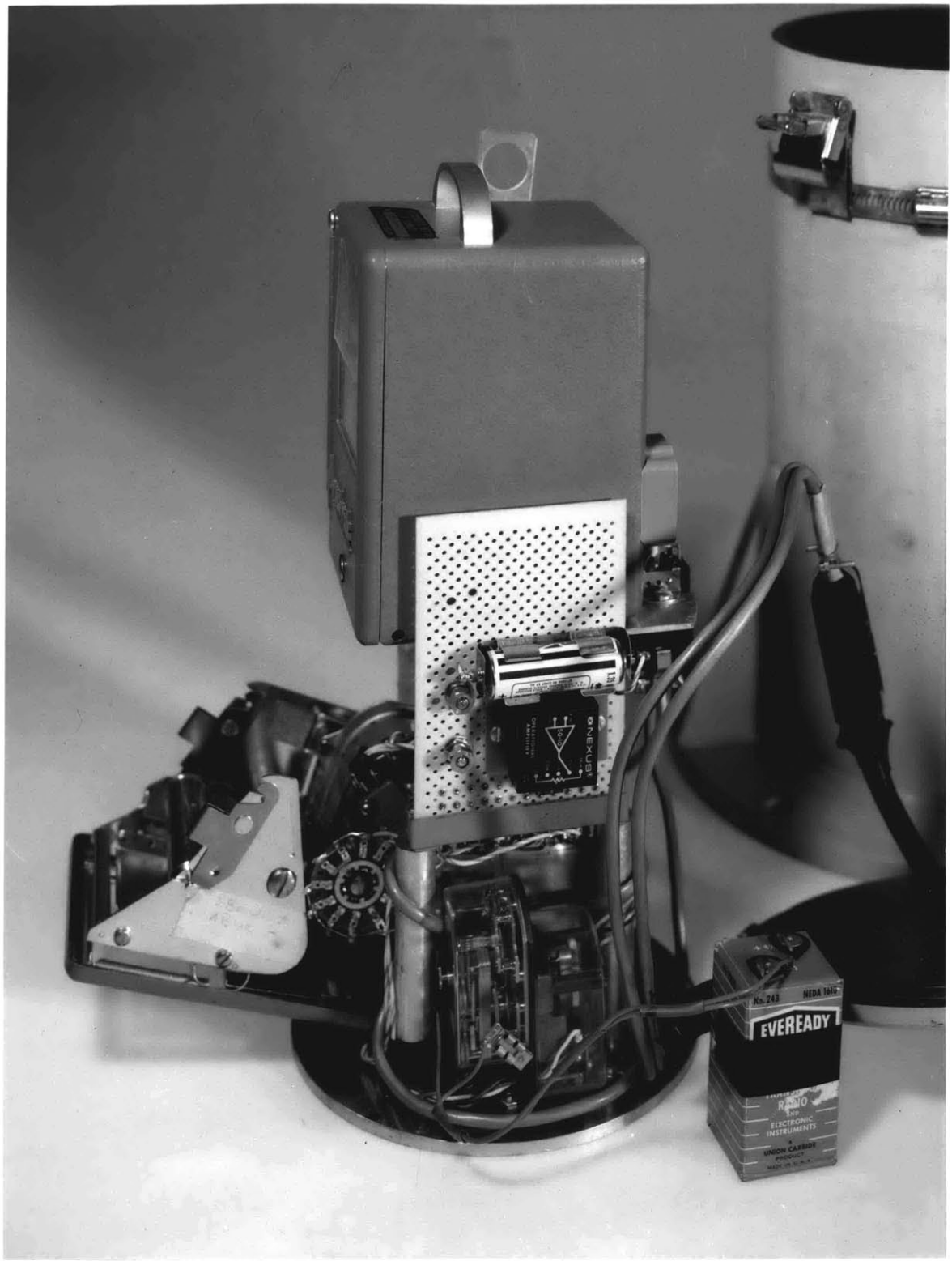
NEXUS
No. 243
NEDA 1610
EVEREADY
ELECTRONIC
INSTRUMENTS
UNION CARBIDE

hose for protection and terminated with waterproof connectors, extended from the platform to the end of the bridle and chain. One electrode was connected just below that point, about five meters below the surface. Extending from the end of the chain into the deep water were two insulated but unarmored wires (no. 12 copper with 3/16 inch polyethylene insulation) taped at intervals to the support member, an eighth inch steel, neoprene jacketted tow cable. One lead terminated in an electrode at 1100 meters, while the other was connected to an electrode at 1700 meters. All three electrodes were enclosed in cases.

Three self-recording current meters were installed in the buoy cable; one at a depth of about 7 meters and the other two at 100 and 1000 meters, respectively. The buoy and instruments were deployed at buoy station D at 1600 on April 20, 1966. This station is identified by WHOI as buoy station number 198 at 39° 22.5'N and 69° 58.0 W. The water depth there is approximately 2600 meters.

Results and discussion

The RV Crawford returned to this station on April 23rd and one recorder was removed. The record showed that the electrode signals were off scale, greater than 50 mv, until 1800 on April 20th. The calibration and zero marks on the record indicated that the recording system was operating correctly. Hence, the large voltages must have been due to processes affecting the cables and the electrodes. This might be related to the fact that difficulties were encountered

deploying this buoy. After the 100 meter deep current meter was in the line, a temporary line connecting two sections of two cables parted. An attempt was made to recover the free end of the tow cable by reeling in the electrode cable which parted under the strain of raising the current meter. The buoy had to be recovered and set again. Besides the repair of the break several more junctions had to be made in order to permit the redeployment of the equipment. That added splices had to be made was unfortunate because with a high impedance recording system it is vitally important to prevent leaks. Whether these leaks occurred or drag forces damaged the cable or electrodes is not known.

After 1800 on the 20th, the record was read for each cycle, and the two electrode differences were assigned the time at the start of the cycle. Often there were large changes in value from one cycle to another, but the record showed that the amplifier was stable. From 1930 on April 21st to 1200 on the 22nd the record was again off scale. Once the signal returned it was much more irregular. The loss of data and the erratic behavior later suggests that the data after the first day are even less reliable.

The average voltages over six cycles, or one half hour, are presented in Figure 26. During the twenty-five hours of available record, the signals followed a nearly sinusoidal oscillation. Both of the measured potential differences have excursions of plus or minus five millivolts about their means. The form of the scatter for both is very similar. This indicates that much of the scatter is related to the

Figure 26 Vertical potential differences obtained from moored buoy at Station D.

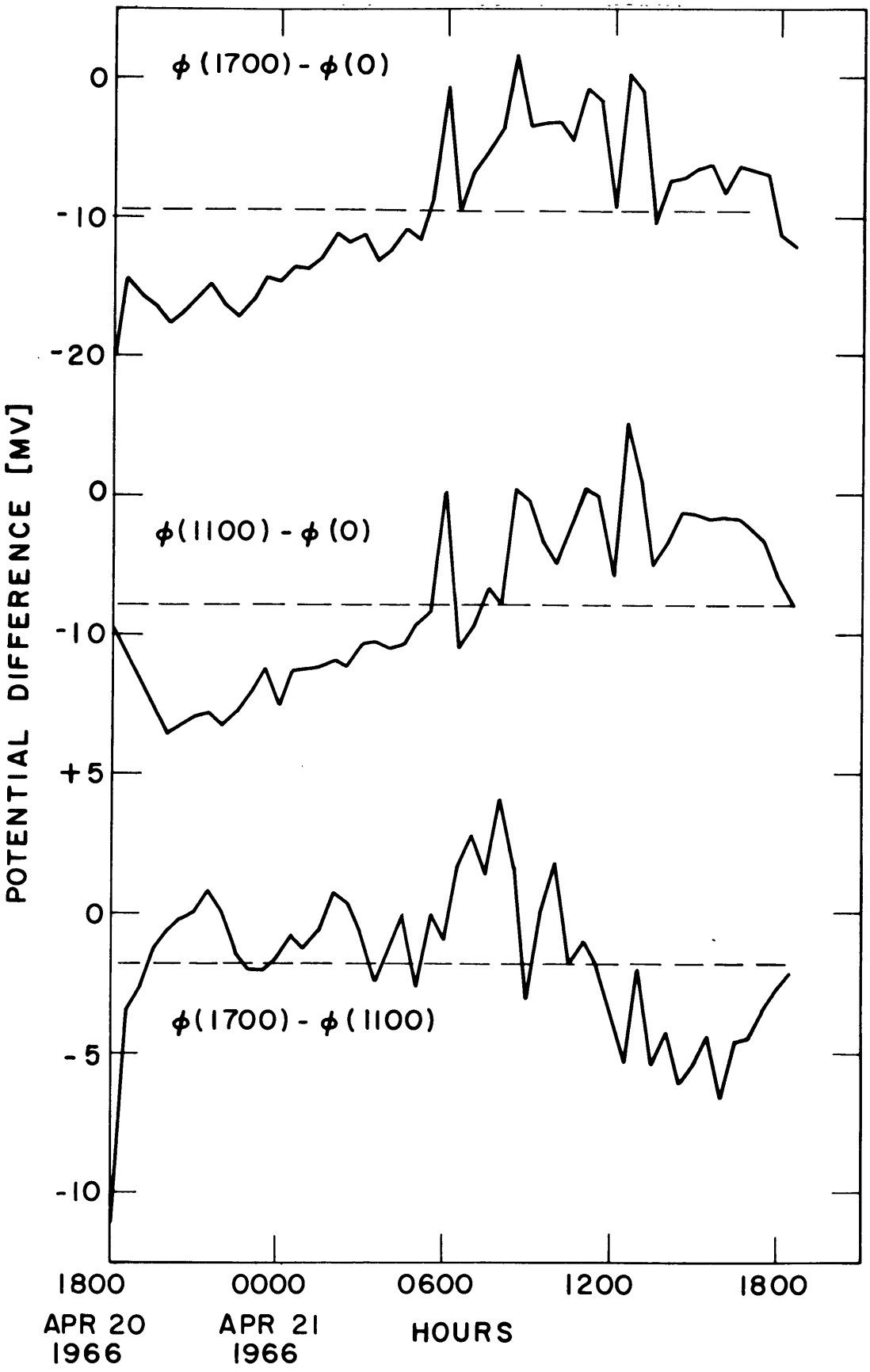
φ (1700) - φ (0)
φ (1100) - φ (0)
φ (1700) - φ (1100)
0
-10
-20
0
-10
+5
0
-5
-10
POTENTIAL DIFFERENCE [MV]
1800
APR 20
1966
0000
APR 21
1966
0600
1200
1800
HOURS

behavior of the surface electrode and cable. Figure 26 also presents the potential difference between 1700 and 1100 meters. In looking at the difference between the two voltages, it must be realized that the two measurements are not quite simultaneous.

Whether or not the sinusoidal character of the potential differences is real is not known. The average flow in the upper 1000 m required to induce 5 mv potential difference is about 25 cm/sec. Any possibility of comparing the electric and current meter estimates of transport was lost with the two deep meters when the mooring line parted several weeks after deployment. The buoy, the electrical equipment and the surface current meter were recovered adrift by a commercial vessel on route to Italy. The current meter was eventually returned and the film read. Typical of the difficulties encountered in this experiment, the rotor of the current meter was stuck until early in the morning of April 22nd, a time several hours after the end of electric data.

Conclusions

The results of this exploratory experiment using a moored buoy seem of doubtful reliability. No definite cause is known for the large voltage fluctuations. Nevertheless, the method is expected to provide useful magnetic east-west transport information. Used in conjunction with conventional current meters the vertical potential differences provide integrated velocity data not available from the current meters alone.

Further experiments should be made with improved technique.

I am reminded of Michael Faraday's (1832) remarks about his experiments to measure tidally induced potential differences in the Thames:

> I made experiments therefore (by favour) at Waterloo Bridge, extending a copper wire nine hundred and sixty feet in length upon the parapet of the bridge, and dropping from its extremities other wires with extensive plates of metal attached to them to complete contact with the water. The wire therefore and the water made one conducting circuit; and as the water ebbed or flowed with the tide, I hoped to obtain currents analogous to those of the brass ball.
>
> I constantly obtained deflections at the galvanometer, but they were very irregular, and were in succession referred to other causes than that sought for. The different condition of the water as to purity on the two sides of the river; the difference in temperature; slight differences in the plates, in the solder used, in the more or less perfect contact made by twisting or otherwise; all produced effects in turn: and though I experimented on the water passing through the middle arches only; used platina plates instead of copper; and took every other precaution, I could not after three days obtain any satisfactory results.

REFERENCES

Barber, N.F., The Magnetic Field Produced by Earth Currents Flowing in an Estuary or Sea Channel, Mon. Not. Roy. Astr. Soc., Geophys. Suppl., 5(7), 258-269, 1948.

Barber, N.F. and M.S. Longuet-Higgins, Water Movements and Earth Currents: Electrical and Magnetic Effects, Nature 161, 192-193, 1948.

Day, C. Godfrey and T. Ferris Webster, Some Current Measurements in the Sargasso Sea, Deep Sea Res. 12, 805-814, 1965.

Defant, Albert, Physical Oceanography, Vol. II, Pergamon Press, 1961.

Erdélyi, A. Ed. Tables of Integral Transforms, Vol. 1, McGraw-Hill, New York, 1954.

Faraday, M., Bakerian Lecture- Experimental Researches in Electricity, Phil. Trans. Roy. Soc., London, Part 1, 163-177, 1832.

Fonarev, G.A., Vertical electric currents in the sea, Geomag. and Aeron., 3, 636-637, 1963.

Fonarev, G.A. and V.V. Novysh, Some results of telluric current measurements at station North Pole-10 in 1963, Academy of Sciences of the USSR, Doklady, Earth Science Section 160, 1-2, 1965.

Fonarev, G.A., Distribution of electromagnetic variations with depth in the sea, Geomag. and Aeron. 4, 881-882, 1964.

Glasko, V.B. and A.G. Sveshnikov, On electric fields in ocean currents caused by the earth's magnetic field, Geomag. and Aeron.1, 68-75, 1961.

Hunkins, Kenneth, Inertial Oscillations of Fletcher's Ice Island (T-3), J. Geophys. Res., 72(4), 1165-1174, 1967.

Jeffreys, H. and B.S. Jeffreys, Methods of Mathematical Physics, Cambridge, 1962.

La Fond, E.C., Internal waves (Part I), The Sea ed. M.N. Hill, Vol 1, Interscience, New York-London, 1962.

Larsen, J.C. Thesis, Scripps Institution of Oceanography, 1966.

Larsen, J.C. and C. Cox, Lunar and solar daily variation in the magnetotelluric field beneath the ocean, J. Geophys. Res. 71 (18), 4441-4445, 1966.

Longuet-Higgins, M.S., The Electric Field Induced in a Channel of Moving Water, Admiralty Research Laboratory, Teddington Report ARL/R.2/102.22/W.(mimeographed report), 1947.

Longuet-Higgins, M.S., The Electrical and Magnetic Effects of Tidal Streams, Mon. Not. Roy. Astr. Soc., Geophys. Suppl. 5 (8), 297-307, 1949.

Longuet-Higgins, M.S., M.E. Stern and H. Stommel, The electrical field induced by ocean currents and waves, with applications to the method of towed electrodes, Pap. Phys. Oceanogr. Meteor. XIII (1), 1-37, 1954.

Malkus, W.V.R. and M.E. Stern, Determination of ocean transports and velocities by electromagnetic effects, J. Mar. Res. 11 (2), 97-105, 1952.

Mangelsdorf, P.C. Jr., The worlds longest salt bridge, Marine Sciences Instrumentation Vol 1, Plenum Press, New York, 1962.

Morse, R.M., M. Rattray, Jr., R.G. Paquetle and C.A. Barnes, The measurement of transports and currents in small tidal streams by an electromagnetic method, Technical Report No. 57, Dept. of Oceanography. U. of Washington, 1-70, 1958.

Newton, Chester W., Semi-inertial velocity variations along the Gulf Stream axis, Deep Sea Res. 12, 893-897, 1965.

Novysh, V.V. and G.A. Fonarev, Telluric currents in the Arctic Ocean, Geomag. and Aeron. 3, 919-921, 1963.

Richardson, W.S. and W.J. Schmitz, Jr., A technique for the direct measurement of transport with application to the Straits of Florida, J. Mar. Res. 23(2), 172-185, 1965.

Richardson, W.S. and J.R. Finlen, The transport of Northwest Providence Channel. J. Mar. Res. (in press).

Runcorn, S. Measurements of planetary electric currents, Nature, 202, 10-13, 1964.

Ryzhkov, Yu.G., Measurement of electric current in the ocean, Doklady Akademii Nank SSSR. CXIII(4) 787-790, 1957. (Trans. Office of Tech. Serv. U.S. Dept. of Commerce, Wash., D.C. PB 141218T, JPRS (DC) L-542.)

Stommel, H., The theory of the electric field induced in deep ocean currents, J. Mar. Res. 7 (3), 386-392, 1948.

Stommel, H., Exploratory measurements of electric potential differences between widely spaced points in the North Atlantic Ocean, Archiv fur Meteorologie, Geophysik und Bioklimatologie, 7, Ser. A, 292-304, 1954.

Stommel, H., Florida Straits transports, 1952-1956, Bul. Mar. Sc. Gulf Carib. 7 (3), 252-254, 1957.

Stommel, H., Florida Straits transports: June 1956-July 1958, Bul. Mar. Sc. Gulf Carib. 9(2), 222,223, 1959.

Stommel, H., The Gulf Stream, Univ. of Calif. Press, Berkeley, 1965.

Tikhonov, A.N. and A.G. Sveshnikov, On the slow motion of conducting medium in a stationary magnetic field, Izv. Acad. of Sc. USSR, Geophysics Ser. 30-34, 1959.

von Arx, W.S., An Electromagnetic Method for Measuring the Velocities of Ocean Currents from a Ship Under Way, Pap. Phys. Oceanogr. Meteorol. II(3), 1-62, 1950.

von Arx, W.S., Notes on the surface velocity profile and horizontal shear across the width of the Gulf Stream, Tellus 4(3), 211-214, 1952.

von Arx, W.S., An Introduction to Physical Oceanography, Addison-Wesley, Reading, Mass., 1962.

Webster, T. Ferris, A preliminary analysis of some Richardson current meter records, Deep Sea Res. 10, 389-396, 1963.

Webster, T. Ferris, On the representativeness of direct current measurements, Trans. SCOR Sympos. on Oceanic Variability, Rome, 1966.

Wertheim, G.K., Studies of the electrical potential between Key West, Florida, and Havana, Cuba, Trans. Amer. Geophys. Un. 35(6), 872-882, 1954.

Worthington, L.V., Three detailed cross-sections of the Gulf Stream, Tellus 6, 116-123, 1954.

Young, F.B. H. Gerrard and W. Jevons, On Electrical Disturbances due to Tides and Waves, Phil. Mag. Ser. 6, 40, 149-159, 1920.

ACKNOWLEDGEMENTS

The writer wishes to thank Professor William S. von Arx, who suggested the problem, for his encouragement and guidance throughout this investigation.

The cooperation of the Staff of Woods Hole Oceanographic Institution is appreciated. The observations of Worthington and von Arx were supplied, in a form most suitable for reanalysis, by L. V. Worthington. Professor Mangelsdorf kindly supplied unpublished GEK and hydrographic data. The Buoy Lab under Dr. N. Fofonoff assisted in the preparation and deployment of the moored buoy experiments. In this regard particular credit is due Robert Heinmiller for his help.

Special gratitude is extended to the Physical Oceanography Lab of Nova University and particularly to its director, Professor William S. Richardson. Very much appreciated are the efforts of Professor Richardson, Professor P. Niiler, Bruce Pitcairn, Fredrick White and Henry White for manning the crank operated winch.

For stimulating discussions and ideas I wish to thank Professor H. Stommel, Professor P. Mangelsdorf and Dr. C. Wing. The efforts of fellow graduate student, Ortwin von Zweck are appreciated in preparing for and assisting in the Northwest Providence Channel experiment.

In addition to Professor von Arx, appreciation is expressed to Professors D. E. Carrett, E. L. Mollo-Christensen,

M. E. Stern and T. F. Webster for their critical reading of the manuscript.

The research was supported by the Office of Naval Research under contract Nonr 1841 (74).

Computational work was done in part at the Computation Center at M. I. T.

BIOGRAPHICAL NOTE

The author, Thomas Bayes Sanford, was born in Toledo, Ohio on April 22, 1940. He completed his high school education in 1958 at Vermilion High School, Vermilion, Ohio. That fall he entered Oberlin College and received in June, 1962, the degree of Bachelor of Arts in physics. While at Oberlin he held a Four Year Scholarship. From June, 1962, to September, 1963, he was employed by the National Aeronautics and Space Administration working in cryophysics and the generation of intense magnetic fields at Lewis Research Center in Cleveland, Ohio. Under an educational assistance program he completed two graduate courses in the Physics Department at Case Institute of Technology.

The author entered the Department of Geology and Geophysics at M. I. T., where he held a junior staff appointment as Research Assistant. During the academic year 1966-67 he held an appointment as Instructor of Oceanography. While at M. I. T. he was elected to associate then to full membership in the Society of the Sigma Xi.

He was married in 1962 to Marilyn Wilmore of Indianapolis, Indiana. They have two children, James C. and Cynthia L.

APPENDICES

APPENDIX A

THE ROLE OF ELECTRIC CURRENTS ASSOCIATED WITH INDUCED MAGNETIC VARIATIONS

In this section we determine the criterion governing when the time variations of the magnetic field and the associated electric currents can be neglected. Maxwell's equations, neglecting free charges and displacement currents are:

$$\nabla \times \underline{E} = -\frac{\partial \underline{B}}{\partial t} \qquad \nabla \cdot \underline{E} = 0$$

$$\nabla \times \underline{B} = \mu \underline{J} \qquad \nabla \cdot \underline{B} = 0$$

The equation $\underline{J} = \sigma \{ \underline{E} + \underline{V} \times \underline{B} \}$ together with the two curl equations above yields

$$\frac{\partial \underline{B}}{\partial t} = \nabla \times \underline{V} \times \underline{B} + \frac{1}{\mu\sigma} \nabla^2 \underline{B} \qquad \text{A.1}$$

We let $\underline{B} = \underline{F} + \underline{B}'$ where $\underline{F}$ is the steady, uniform geomagnetic field and $\underline{B}$ the magnetic variation. Moreover, assume $\underline{V}$ and $\underline{B}'$ are of the form

$$V = V_o e^{i(\underline{k} \cdot \underline{x} - \omega t)}$$

$$B' = B'_o e^{i(\underline{k}' \cdot \underline{x} - \omega t)}$$

Then equation A.1 states approximately that

$$C\left(1 - \frac{V_o}{C} + \frac{i k'^2}{\mu\sigma\omega}\right) B'_o = -F V_o$$

where $C = \frac{\omega}{k}$. Since $\frac{V_o}{C} \ll 1$ we can neglect the time variations in the magnetic field provided:

$$\frac{i k'^2}{\mu \sigma \omega} \gg 1$$

The wave number k' is complex but its modulus should be of order k, the source wave number. Noting that $\mu \sigma \omega = \frac{2}{\delta^2}$ where δ is the skin depth for electromagnetic wave penetration in a conducting medium, the above equation becomes

$$k\delta > \sqrt{2}$$

For a stream with time dependent velocity variation satisfying the above relation it is expected that the effects due to a time varying magnetic field are of secondary importance.

Electrical measurements on a narrow current such as the Gulf Stream should not be significantly influenced by $\frac{\partial \underline{B}}{\partial t}$ effects arising from velocity variations of periods greater than several hours.

APPENDIX B

THE 3-DIMENSIONAL ANALOGS OF THE INTEGRAL THEOREMS OF MALKUS AND STERN

The first theorem is that which in 2-dimensions relates the horizontally integrated potential difference between the surface and some depth to the total volume transport through the enclosed surface. In terms of the potential function, equation 1, the integral is

$$\int_{-\infty}^{\infty} [\phi(x,y,0) - \phi(x,y,z)]\, dy$$

$$= \frac{1}{4\pi^2} \int_{-\infty}^{\infty} dy \int_{-\infty}^{\infty}\int_{-\infty}^{\infty} [\hat{\phi}(\alpha,\beta,0) - \hat{\phi}(\alpha,\beta,z)]\, e^{-i(\alpha x + \beta y)}\, d\alpha\, d\beta .$$

If the order of integration is reversed, and it is noted that

$$\int_{-\infty}^{\infty} e^{-i\beta y}\, dy \equiv 2\pi\, \delta(\beta)$$

where $\delta(\beta)$ is the Dirac delta function, then it follows that

$$\int_{-\infty}^{\infty} [\phi(x,y,0) - \phi(x,y,z)]\, dy$$

$$= \frac{1}{2\pi} \int_{-\infty}^{\infty} \left\{ \frac{1 - \cosh\alpha z}{\sinh\alpha h + \frac{\sigma_2}{\sigma_1} \operatorname{sgn}\alpha \cosh\alpha h} \int_{-h}^{0} \left\{ (F_y \tilde{V}_x - F_x \tilde{V}_y)(\sinh\alpha(\xi+h) \right.\right.$$

$$\left. + \frac{\sigma_2}{\sigma_1} \operatorname{sgn}\alpha \cosh\alpha(\xi+h)) \right.$$

$$\left.\left. + i F_z \tilde{V}_y (\cosh\alpha(\xi+h) + \frac{\sigma_2}{\sigma_1} \operatorname{sgn}\alpha \sinh\alpha(\xi+h)) \right\} d\xi \right.$$

$$+\int_z^0 \left\{ (F_y \tilde{V}_x - F_x \tilde{V}_y)\cosh\alpha(\xi - z) + i F_z \tilde{V}_y \sinh\alpha(\xi - z) \right\} d\xi \Bigg\}$$

$$\cdot e^{-i\alpha x} d\alpha$$

where $\tilde{V} = \hat{V}(\alpha, \beta = 0, \xi) = \int_{-\infty}^{\infty} dy \int_{-\infty}^{\infty} V(x, y, \xi)\, e^{-i\alpha x} dx$

Thus, no simple general expression exists analogous to the 2-dimensional theorem. This is because the integral

$$\int_{-\infty}^{\infty} dy \int_z^0 \rho i_z d\xi \neq 0 \quad ;$$

that is, the net vertical electric current into the section ($-\infty < y < \infty$, $z < \xi < 0$) is not zero. Conservation of electric current is maintained by electric currents flowing in the horizontal plane (x, y).

If we assume that the velocity variations are small in a distance x, which is large compared with h, then the most significant contributions to the integrals over α will be for small α . Expanding the hyperbolic functions in powers of α , then for $\frac{\sigma_2}{\sigma_1} = 0$ an approximate theorem results:

$$\int_{-\infty}^{\infty} [\phi(x, y, 0) - \phi(x, y, z)]\, dy$$

$$= \int_{-\infty}^{\infty} dy \left\{ \int_z^0 (F_y V_x - F_x V_y)\, d\xi + \frac{z^2}{2} \frac{\partial^2}{\partial x^2} \int_{-h}^{0} (F_y V_x - F_x V_y)\left(1 + \frac{\xi}{h}\right) d\xi \right.$$

$$\left. - F_z \frac{\partial}{\partial x} \int_z^0 (\xi - z)(V_y - \bar{V}_y)\, d\xi \right\} .$$

The second theorem relates the potential difference across a stream to the transport of the current. Consider the integral:

$$\phi(x,Y,0) - \phi(x,-Y,0)$$

$$= \frac{1}{4\pi^2} \int_{-\infty}^{\infty} \int_{-\infty}^{\infty} \frac{e^{-i\alpha x}\{e^{-i\beta Y} - e^{i\beta Y}\}}{\sinh\gamma h + \frac{\sigma_2}{\sigma_1}\operatorname{sgn}\gamma \cosh\gamma h} d\alpha d\beta \int_{-h}^{0} \{(F_y \hat{V}_x - F_x \hat{V}_y)$$

$$\cdot (\sinh\gamma(\xi+h) + \frac{\sigma_2}{\sigma_1}\operatorname{sgn}\gamma \cosh\gamma(\xi+h))$$

$$+ iF_z \frac{(\alpha \hat{V}_y - \beta \hat{V}_x)}{\gamma} (\cosh\gamma(\xi+h) + \frac{\sigma_2}{\sigma_1}\operatorname{sgn}\gamma \sinh\gamma(\xi+h))\} d\xi.$$

In the limit as $Y \to \infty$ we find that

$$\lim_{Y\to\infty} \{e^{-i\beta Y} - e^{i\beta Y}\} = -2\pi i \beta \delta(\beta).$$

Since we have assumed that $\hat{V}_x$ and $\hat{V}_y$ exist (i.e., are finite for all α, β), it can be shown that

$$\phi(x,\infty,0) - \phi(x,-\infty,0) = 0.$$

In 2-dimensions the theorem can have two forms depending on whether or not $\frac{\sigma_2}{\sigma_1} = 0$. With the coordinate system aligned so that $V = V_x$ we find that

$$\phi(\infty, 0) - \phi(-\infty, 0) = \begin{cases} -\frac{F_z T}{h} & \frac{\sigma_z}{\sigma_1} = 0 \\ 0 & \frac{\sigma_z}{\sigma_1} \neq 0 \end{cases}$$

where T is the total volume transport of the stream. A useful expression when Y is finite follows from equation

$$\phi(a) - \phi(b) = -F_z \int_a^b \bar{V}(y)\, dy .$$

APPENDIX C

ELECTRIC CURRENTS WITHIN A KELVIN WAVE IN A CHANNEL AND ALONG A COAST

The electric currents induced in a horizontal plane are investigated here for a barotropic Kelvin tidal flow laterally confined (1) within a narrow insulating channel and (2) in the semi-infinite region off an insulating coast. The coordinate system (x, y, z) is right-handed with z measured positively upward. The depth of the water is constant in both cases.

(1) Kelvin wave in insulating channel

Consider an infinite rectangular channel ($-\infty < x < \infty$, $0 \le y \le a$, $0 \ge z \ge -h$) in which flows a progressive wave of the form

$$V_x = V_0 e^{-\frac{f}{c}y} e^{i(kx-\omega t)}$$

in the presence of a vertical magnetic field F_z. We introduce the transformation for any dependent variable:

$$\psi_n(\alpha,t) = \int_{-\infty}^{\infty} e^{i\alpha x}\,dx \int_0^a \psi(x,y,t)\cos\frac{n\pi y}{a}\,dy$$

and

$$\psi(x,y,t) = \frac{1}{2\pi}\int_{-\infty}^{\infty}\left\{\frac{\hat{\psi}_0}{a} + \frac{2}{a}\sum_{n=1}^{\infty}\hat{\psi}_n\cos\frac{n\pi y}{a}\right\}e^{-i\alpha x}\,d\alpha$$

Thus,

$$\hat{V}_n(\alpha,t) = -\frac{2\pi V_0 \frac{f}{c}\left((-1)^n e^{-\frac{f}{c}a} - 1\right)\delta(\alpha+k)}{\left(\frac{f}{c}\right)^2 + \left(\frac{n\pi}{a}\right)^2}$$

The governing equation is

$$\nabla^2 \phi = F_z V_o \frac{f}{c} e^{-\frac{f}{c} y} e^{i(kx-\omega t)}$$

with the boundary conditions

$$\frac{\partial \phi}{\partial y} = \begin{cases} -F_z V_o e^{i(kx-\omega t)} & y = 0 \\ -F_z V_o e^{-\frac{f}{c} a} e^{i(kx-\omega t)} & y = a \end{cases}$$

$$\frac{\partial \phi}{\partial z} = 0 \qquad z = 0, -h .$$

The solution is

$$\phi = \frac{-2F_z V_o}{a} e^{i(kx-\omega t)} \sum_{n=1}^{\infty} \frac{((-1)^n e^{-\frac{f}{c} a} - 1)(\frac{n\pi}{a})^2}{(k^2 + (\frac{n\pi}{a})^2)((\frac{f}{c})^2 + (\frac{n\pi}{a})^2)} .$$

In the English Channel $(n\pi)^2 >> k\frac{f}{c}a^2$ for the semidiurnal tide, thus the potential difference across the channel is $\phi(x,a,t) - \phi(x,0,t) =$

$$-\frac{F_z V_o e^{i(kx-\omega t)} (1 + e^{-\frac{f}{c} a})}{\sqrt{k^2 + (\frac{f}{c})^2}} \tanh \frac{a\sqrt{k^2 + (\frac{f}{c})^2}}{2}$$

(2) Kelvin wave in semi-infinite channel

In the region $(-\infty < x < \infty , 0 \le y < \infty , 0 \ge z \ge -h)$ a Kelvin wave progresses along a coast. The formal solution, equation 1, gives the particular solution to this problem. The zero normal electric current boundary condition at $y = 0$ required is satisfied by an image flow in the region $y < 0$. Thus, we assume a flow of the form

$$V_x = V_o \operatorname{sgn} y \, e^{-\frac{f}{c} y} e^{i(kx-\omega t)}$$

which has a transform of

$$\hat{V}_x = \frac{4\pi i V_0 \beta}{\beta^2 + (\frac{f}{c})^2} \delta(\alpha + k) e^{-i\omega t}.$$

Substitution of the above expression for V_x into equation 1 yields

$$\phi(x,y,t) = \frac{V_0 F_z e^{i(kx-\omega t)}}{\pi} \int_{-\infty}^{\infty} \frac{\beta^2 e^{-i\beta y} d\beta}{(\beta^2+k^2)(\beta^2+(\frac{f}{c})^2)}$$

The integral can be evaluated for $y > 0$ along a contour enclosing the simple poles at $\beta = -ik$ and $\beta = -i\frac{f}{c}$ The result is

$$\phi(x,y,t) = \frac{V_0 F_z e^{i(kx-\omega t)}}{k^2-(\frac{f}{c})^2} \left(k e^{-ky} - \frac{f}{c} e^{-\frac{f}{c}y}\right) \quad y>0.$$

Discussion of the two cases

The reduction of the potential difference due to the flow of electric current can be estimated for the English Channel: let $a = 10^5$ m, $\frac{f}{c} = \frac{1}{3} \times 10^{-5}$ m^{-1} and $k = 1.5 \times 10^{-5}$ m^{-1}:

(1) Channel

$$\phi(a) - \phi(0) = -.78 F_z V_0 \times 10^5 \text{ volt}$$

compared with

$$\phi(a) - \phi(0) = -.85 F_z V_0 \times 10^5 \text{ volt}$$

when k = 0.

(2) Coast . .

$$\phi(a) - \phi(0) = -.50 F_z V_0 \times 10^5 \text{ volt}.$$

The electric currents in a horizontal plane reduce the cross-channel potential difference less than 10% These currents are negligible compared to the electric currents in a vertical plane discussed by Longuet-Higgins (1949).

Larsen (1966) computed the electric and magnetic field for case (2) appropriate for a wave along the California coast. A comparison of the present analytic solution with the results of Larsen's computations indicates that significant electric currents arise from magnetic variations. Such a comparison serves to emphasize the necessity of including self-induction in extremely broad flows such as the deep ocean tides.

APPENDIX D

APPROXIMATE EXPRESSIONS FOR THE SCALAR ELECTRIC POTENTIAL AND ITS GRADIENT FOR A BROAD, 2-DIMENSIONAL CURRENT

In this appendix are derived expressions for the scalar potential and its gradients valid within a broad 2-dimensional ocean current.

In the case of 2-dimensional flow it is convenient to use a coordinate system (x, y, z) with the x axis aligned with the flow and z measured positively upward. Equation 1 is the same except that $\hat{V}_y = 0$ and

$$\hat{V}_x(\alpha, \beta, z) = 2\pi \delta(\alpha) \hat{V}_x(\beta, z).$$

The first term of equation 1 is now of the form

$$\frac{1}{2\pi} \int_{-\infty}^{\infty} G(\beta, z) L(\beta) e^{-i\beta y} d\beta \qquad \text{D.1}$$

where

$$G(\beta, z) = \frac{\cosh \beta(z+h) + \frac{\rho_1}{\rho_2} \operatorname{sgn}\beta \sinh \beta(z+h)}{\sinh \beta h + \frac{\rho_1}{\rho_2} \operatorname{sgn}\beta \cosh \beta h} \qquad \text{D.2}$$

and

$$L(\beta) = \int_{-h}^{0} (B_y \sinh \beta\xi - i F_z \cosh \beta\xi) \hat{V}(\beta, \xi) d\xi$$

Equation D.1 can be expressed in terms of a convolution integral:

$$\int_{-\infty}^{\infty} g(y-\lambda) l(\lambda) d\lambda$$

where g and l are the transforms of G and L. The transform of L is straight forward but that of G is more difficult.

To obtain g we first consider the integral

$$I(y,z;h,\tfrac{\rho_1}{\rho_2}) = \frac{1}{2\pi}\int_{-\infty}^{\infty} \frac{\cosh\beta(z+h)\, e^{-i\beta y}\, d\beta}{\sinh\beta h + \tfrac{\rho_1}{\rho_2}\operatorname{sgn}\beta \cosh\beta h}$$

for $z<o$. Let $\beta = p + iq$, p, q real, then $\beta = |\beta| e^{i\theta}$ where $|\beta| = +\sqrt{p^2+q^2}$ and $\theta = \tan^{-1} q/p$. With this definition the discontinuity function, $\operatorname{sgn}\beta$, equals $e^{-i\theta}$. The zeros of the function

$$\sinh\beta h + \tfrac{\rho_1}{\rho_2}\operatorname{sgn}\beta \cosh\beta h$$

occur at

$$\beta_n = \pm \frac{i}{h}\left(\tan^{-1}\tfrac{\rho_1}{\rho_2} + n\pi\right) \qquad n = o, 1, 2, \cdots$$

In addition, there may be a pole of some order at $\beta = 0$. There is a question about the most suitable method for dealing with this point. There is a difficulty owing to the presence of the nonanalytic function sgn which is commonly defined as zero for zero argument. The evaluation of this pole presents difficulties which have not been resolved. These mathematical points, though have little relevence to the physical problem under consideration. The residue of the pole will only add a constant to the total integral. The sum of the other poles can be evaluated within this constant. Under the physical condition that ρ_1/ρ_2 is small we require that

$$\lim_{\rho_1/\rho_2 \to 0} I(y,z;h,\tfrac{\rho_1}{\rho_2}) = I(y,z;h)$$

a relation which serves to determine the constant.

For $y<0$ and $z<0$, consider the contour, C , for the

integral I:

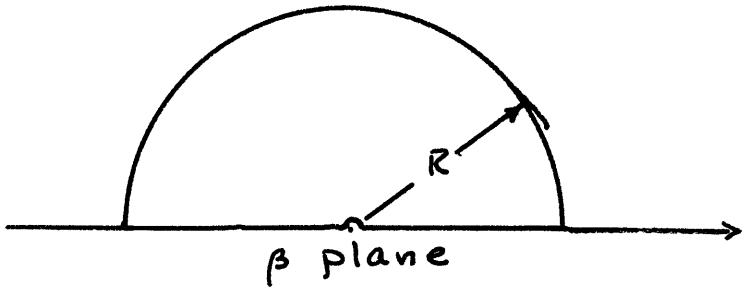

As R becomes infinite, the contribution to I over the arc vanishes, hence

$$I_1(y,z;h,\rho_1/\rho_2) = i\sum_{n=0}^{\infty} \text{Res}(\beta_n)$$

$$= \frac{i}{2\pi}\left\{C + \frac{e^{(\frac{\rho_1}{\rho_2}-\frac{\pi}{2})(\frac{y+i(z+h)}{h})}}{2\cosh\frac{\pi}{2h}(y+i(z+h))} + \frac{e^{(\frac{\rho_1}{\rho_2}-\frac{\pi}{2})(\frac{y-i(z+h)}{h})}}{2\cosh\frac{\pi}{2h}(y-i(z+h))}\right\}$$

where the approximations $\tan^{-1}\frac{\rho_1}{\rho_2} \doteq \frac{\rho_1}{\rho_2}$ and $(1+(\frac{\rho_1}{\rho_2})^2) \doteq \cos\frac{\rho_1}{\rho_2} \doteq 1$ have been used.

By the same method, it is easy to show for $\rho_1/\rho_2 = 0$, $y<0$ and $z<0$ that

$$I_1(y,z;h) = \frac{-i}{4h}\left\{\tanh\frac{\pi}{2h}(y+i(z+h)) + \tanh\frac{\pi}{2h}(y-i(z+h))\right\}.$$

The limit as $\frac{\rho_1}{\rho_2} \to 0$ requires that C = -1, hence

$$I_1(y,z;h,\rho_1/\rho_2)$$

$$= \frac{i}{2h}\left\{-1 + \frac{e^{(\frac{\rho_1}{\rho_2}-\frac{\pi}{2})(\frac{y+i(z+h)}{h})}}{2\cosh\frac{\pi}{2h}(y+i(z+h))} + \frac{e^{(\frac{\rho_1}{\rho_2}-\frac{\pi}{2})(\frac{y-i(z+h)}{h})}}{2\cosh\frac{\pi}{2h}(y-i(z+h))}\right\}$$

The evaluation of I for $y > 0$ produces a similar result as found above. Then I, after some manipulations becomes

$$= \frac{\pm i}{2h}\left\{1 - e^{\mp \beta_1 \frac{y}{h}}\left(\frac{\cos(\beta_1 - \frac{\pi}{2})\frac{z+h}{h} + e^{\pm \pi \frac{y}{h}}\cos \beta_2 \frac{z+h}{h}}{\cosh \frac{\pi y}{h} + \cos \frac{\pi}{h}(z+h)}\right)\right\} \quad \text{D.3}$$

where choice of the sign depends on the sign of y. The upper sign is taken for $y > 0$ and the lower for $y < 0$.

The second term in the numerator of equation D.2 for $G(\beta, z)$ could be evaluated similarly. The convolution of g and 1 might be a more suitable means of computing for analytic than that followed in Chapter 2. For the present purposes the expressions for $G(\beta, z)$ are cumbersome and when used in the convolution integral provide results which are not readily susceptible to physical interpretation. An alternative procedure is to consider only the denominator of G and express the numerator as a power series in β. Evaluation of this function alone, or more simply, letting $z + h = 0$ in equation D.3 produces

$$\frac{1}{2\pi}\int_{-\infty}^{\infty} \frac{e^{-i\beta y}\, d\beta}{\sinh \beta h + \beta_1 \beta_2 \beta \cosh \beta h} = \frac{\pm i}{2h}\left\{1 - \frac{e^{\mp (\beta_1 - \frac{\pi}{2})\frac{y}{h}}}{\cosh \frac{\pi}{2}\frac{y}{h}}\right\} \quad \text{D.4}$$

The other factor in the convolution integral will consist of a series of terms such as

$$i P_2 \cosh \beta (z+h) \int_{-h}^{0} \hat{V}(\beta, \xi) \cosh \beta \xi \, d\xi \, .$$

Expanding the hyperbolic functions in a power series in β and taking the Fourier inversion of this series yields

$$i F_z \left\{ h \bar{V}(y) - \frac{(z+w)^2}{2} h \frac{\partial^2}{\partial y^2} \bar{V}(y) - \frac{\partial^2}{\partial y^2} \int_{-h}^{0} \frac{\xi^2}{2} V(y,\xi) d\xi_{D.5} \cdots \right\}$$

The above series is then convolved with the function on the right of equation D.4. The convolution integral can be greatly simplified in the case of greatest geophysical interest. We will assume that the motion is broad compared to the depth (i.e $h/L \ll 1$), that $\frac{\rho_1}{\rho_2} \frac{L}{h} < 1$ and restrict y such that $\frac{\rho_1}{\rho_2} \frac{|y|}{h} < 1$. The latter two restrictions are made so that effects due to a conducting bottom are small. Then the substitution

$$\pm \frac{i}{2h} \left\{ 1 - \frac{e^{\mp(\rho_1/\rho_2 - \frac{\pi}{2}) \frac{y-\lambda}{h}}}{\cosh \frac{\pi}{2} \frac{y-\lambda}{h}} \right\} = -\frac{i}{2h} \tanh \frac{\pi}{2} \frac{y-\lambda}{h}$$

can be made which greatly simplifies the analysis. The restriction that the flow be broad is made so that integrals of the form

$$\frac{\partial}{\partial y} \int_{-\infty}^{\infty} \tanh \frac{\pi}{2} \frac{y-\lambda}{h} \bar{V}(\lambda) d\lambda$$

can be easily evaluated. The above expression is equal to

$$\frac{\pi}{2h} \int_{-\infty}^{\infty} \bar{V}(\lambda) \operatorname{sech}^2 \frac{\pi}{2} \frac{(y-\lambda)}{h} d\lambda$$

The function $\operatorname{sech}^2 \frac{\pi}{2} \frac{y-\lambda}{h}$ is sharply peaked at $\lambda = y$, being only about 1/7 of its peak value at $\lambda = y \pm h$. Provided V changes little over the range $y - h < \lambda < y + h$ the above integral simply is $2\bar{V}$. The slight averaging is

essentially a consequence of the expansion procedure used here. It can be shown that no such horizontal averaging occurs for barotropic flows.

The convolution of g and 1 is combined with the other terms from the expansion of the second term of equation 1 with the result that:

$$\phi(y,z) = F_y \left\{ \int_{-h}^{z} V(y,\xi)\,d\xi + \int_{-h}^{0} \frac{\xi}{h} V(y,\xi)\,d\xi + \frac{\rho_1}{\rho_2 h} \frac{d}{dy} \int_{-h}^{0} \xi V^*(y,\xi)\,d\xi \right\}$$

$$- F_z \left\{ \frac{1}{2} \int_{-\infty}^{\infty} \tanh \frac{\pi}{2} \frac{y-\lambda}{h} \bar{V}(\lambda)\,d\lambda - \frac{(z+h)^2}{2} \frac{d\bar{V}(y)}{dy} - \frac{1}{2h} \frac{d}{dy} \int_{-h}^{0} \xi^2 V(y,\xi)\,d\xi \right.$$

$$\left. - \frac{\rho_1}{\rho_2} (z+h) \bar{V}^*(y) - \frac{\partial}{\partial y} \int_{-h}^{z} (\xi - z) V(y,\xi)\,d\xi \right\}$$

$$\frac{\partial \phi(y,z)}{\partial y} = B_y \left\{ \frac{d}{dy} \int_{-h}^{z} V(y,\xi)\,d\xi + \frac{d}{dy} \int_{-h}^{0} \frac{\xi}{h} V(y,\xi)\,d\xi + \frac{\rho_1}{\rho_2} \frac{d^2}{dy^2} \int_{-h}^{0} \frac{\xi}{h} V^*(y,\xi)\,d\xi \right\}$$

$$- F_z \left\{ \bar{V}(y) - \frac{(z+h)^2}{2} \frac{d^2\bar{V}(y)}{dy^2} - \frac{1}{2h} \frac{d^2}{dy^2} \int_{-h}^{0} \xi^2 V\,d\xi \right.$$

$$\left. - \frac{\rho_1}{\rho_2} (z+h) \frac{d}{dy} \bar{V}^*(y) - \frac{\partial^2}{\partial y^2} \int_{-h}^{z} (\xi - z) V(y,\xi)\,d\xi \right\}$$

$$\frac{\partial \Phi(y,z)}{\partial z} = F_y V(y,z) + F_z \frac{\partial}{\partial y} \int_z^0 (V(y,\xi) - \bar{V}(y))\, d\xi$$

$$+ F_z \frac{\rho_1}{\rho_2} \bar{V}^*(y)$$

where $\bar{V}(y) = \frac{1}{h} \int_{-h}^{0} V(y,\xi)\, d\xi$ and

$$V^*(y,z) = \frac{i}{2\pi} \int_{-\infty}^{\infty} \operatorname{sgn}\beta\, \hat{V}(\beta,z)\, e^{-i\beta y}\, d\beta .$$

APPENDIX E
THE INFLUENCE OF SEA WATER RESISTIVITY VARIATIONS ON ELECTRIC CURRENTS

The spacial variation of sea water resistivity will produce slight distortions to the potential field as derived in Chapter 1. It has been shown (L-HSS) that the vertical variation of resistivity can affect the electric currents generated in a stream. This subject was reinvestigated because an analysis of previous GEK and submarine cable data seemed to indicate that the effect might have been underestimated. It was thought that horizontal variations in the resistivity, although much smaller than the vertical, would be important because the horizontal current density is much larger than the vertical current density.

Starting with the divergence of $\underline{J} = \sigma\{-\nabla\phi + \underline{v}\times\underline{F}\}$, assuming $\nabla\cdot\underline{J} = 0, \sigma = \frac{1}{\rho}$ and $\underline{F}$ uniform, we obtain

$$\nabla^2\phi = \underline{F}\cdot\nabla\times\underline{V} - \underline{J}\cdot\nabla\rho \qquad \text{E.1}$$

Since the term $\underline{J}\cdot\nabla\rho$ is small compared to the first term on the right hand side of equation E.1, (order h/L), it is sufficient to produce a perturbation solution. Hence, from equation 7 , we let

$$\underline{J}\cdot\nabla\rho = \frac{F_z}{\rho}\left\{\frac{\partial\rho}{\partial y}\frac{\partial}{\partial z} - \frac{\partial\rho}{\partial z}\frac{\partial}{\partial y}\right\}\int_z^0 (V(y,\xi) - \bar{V}(y))\,d\xi$$

$$= F_z\,\nabla \ln\frac{\rho}{\rho_0}\times\nabla T^*\cdot\underline{1}_z$$

where

$$T^* = \int_z^0 (V(y,\xi) - \bar{V}(y))\,d\xi \qquad \text{E.2}$$

and ρ_0 is an arbitrary constant. Equation E.1 is solved

by the method of Appendix D. Consistent with the approximations used to derive equation E.2 the solution is

$$\frac{\partial \phi(y,z)}{\partial y} = -F_z \bar{V}(y) - \frac{F_z}{h}\int_{-\infty}^{y}\int_{-h}^{0} \nabla \ln\frac{\rho}{\rho_0} \times \nabla T^* \cdot \underline{n}\, d\xi\, d\lambda$$

where $\underline{n}$ is the unit normal pointing in the positive x direction. Since $\nabla \ln\frac{\rho}{\rho_0} \times \nabla T^* \cdot \underline{n} = \nabla \times \ln\frac{\rho}{\rho_0} \nabla T^* \cdot \underline{n}$ Stokes's theorem can be used with the result

$$\frac{\partial \phi(y,z)}{\partial y} = -F_z \bar{V}(y) + \frac{F_z}{h}\oint \ln\frac{\rho}{\rho_0} \nabla T^* \cdot d\underline{l} \ .$$

The line integral can be readily evaluated since

$$T^*(y,0) = T^*(y,-h) = T^*(-\infty, z) = 0 \ .$$

Thus,

$$\frac{\partial \phi(y,z)}{\partial y} = -F_z \bar{V}(y) - \frac{F_z}{h}\int_{-h}^{0} \ln\left[\frac{\sigma}{\sigma_0}\right](V(y,\tau) - \bar{V}(y))\, d\xi \qquad \text{E.3}$$

where $\sigma = \rho^{-1}$. Expressed in terms of the surface electric current density:

$$\rho J_y = -F_z\,(V(y,z) - \bar{V}(y)) + \frac{F_z}{h}\int_{-h}^{0} \ln\frac{\sigma}{\sigma_0}\,(V(y,\xi) - \bar{V}(y))\, d\xi \qquad \text{E.4}$$

This result shows that only the vertical conductivity structure influences GEK readings. The conductivity is usually small but should be taken into consideration. Typically, this correction amounts to about 20% of $\bar{V}$, acting to increase its value, in the Gulf Stream.

In this connection it should be noted that fixed electrodes, according to equation E.3, would provide an indication of $\bar{V}$ which would be too large.

Equation E.4 takes on a simplier form if we assume $\sigma = \sigma(z)$

and that it varies slightly through the water column. Then letting $\ln \frac{\sigma}{\sigma_0} \doteq \left(\frac{\sigma}{\sigma_0} - 1\right)$ and $\sigma_0 = \bar{\sigma}$, the average conductivity, equation E.4 becomes

$$\rho J_y = -F_z V(y,z) + \frac{F_z}{h} \int_{-h}^{0} \frac{\sigma(\xi)}{\bar{\sigma}} V(y,\xi)\, d\xi . \qquad \text{E.5}$$

This result, first derived by L-HSS appears **adequate to** adjust the surface electric current density for the conductivity structure provided the conductivity **variations** are small.

APPENDIX F

THE INFLUENCE OF TEMPERATURE, SALINITY AND PRESSURE ON ELECTRODE SYSTEMS

The utility of the vertical GEK depends directly on our understanding of the electrochemistry of electrodes and non-uniform electrolytes. Although electrode difficulties are everpresent in the use of the horizontal GEK, the vertical gradients of temperature and salinity can produce comparatively large vertical potential gradients which are independent of the motion of the sea water. Preliminary experiments on concentration and thermal cells indicated that the estimates of salinity and temperature effects available in the literature were in error. A redetermination of these electrochemical effects in sea water was needed. The experimental technique and equipment were first tested on a pure sodium chloride solution of ionic strength near that of sea water before either temperature or concentration (salinity) measurements were made on sea water itself. The measured potentials of both the thermal and concentration cell were compared with either published determinations or theoretical predictions. Satisfactory agreement increased confidence in the equivalent measurements made on sea water.

The basic problem was to determine what the potential difference would be between two electrodes when their electrochemical environments differ. Considering the two variables, salinity and temperature, the potential difference is given, formally, by the equation

$$E(T_2, S_2) - E(T_1, S_1) = \int_{T_1, S_1}^{T_2, S_2} \mathcal{E}_S(T,S)\,dS + \mathcal{E}_T(T,S)\,dT \qquad \text{F.1}$$

The potential difference must be independent of the path in the TS plane followed in the evaluation of the integral. Hence, the substitutions

$$\mathcal{E}_S(T,S) = \frac{\partial E(T,S)}{\partial S} \quad \text{and} \quad \mathcal{E}_T(T,S) = \frac{\partial E(T,S)}{\partial T} \qquad \text{F.2}$$

can be made. Implicit in this substitution is the assumption that

$$\frac{\partial \mathcal{E}_S}{\partial T} = \frac{\partial \mathcal{E}_T}{\partial S} \qquad \text{F.3}$$

a requirement which has been confirmed experimentally. On the basis of the theoretical expression for E_S and the published determinations of E_T, equation **F.3** was found to be satisfied for a sodium chloride solution. It is assumed valid for sea water in the salinity and temperature range 33-38°/oo and 0-30°C. Therefore, equation **F.1** can be evaluated as simply the sum of two integrals representing, respectively, the potential of an isothermal concentration cell in series with a constant salinity thermal cell.

For practical purposes the expression

$$E(T_2,S_2) - E(T_1,S_1) = \mathcal{E}_S(T_1; S_1,S_2)\Delta S + \mathcal{E}_T(T_1,T_2; S)\Delta T \qquad \text{F.4}$$

will be used where E_S and E_T are defined as

$$\mathcal{E}_S(T; S_1,S_2) = \frac{E(T,S_2) - E(T,S_1)}{S_2 - S_1} \qquad \text{F.5}$$

$$\mathcal{E}_T(T_1,T_2; S) = \frac{E(T_2,S) - E(T_1,S)}{T_2 - T_1}$$

Thus, E_S and E_T are the average coefficients over the range ΔS and ΔT, respectively.

Sodium Chloride and Sea Water Concentration Cells

Consider the cell

$$Ag/\ AgCl/\ NaCl(m_1) \ \vdots \ NaCl(m_2)/\ AgCl/\ Ag$$

where the vertical dots indicate the presence of a liquid junction. The emf of this concentration cell is (Ives and Jantz, 1960):

$$\Delta E = -\frac{2RT}{F}\int_{m_1}^{m_2} t_{Na^+}\, d \ln \gamma_{\pm m} \qquad \text{F.7}$$

$$\frac{dE}{d\gamma_{\pm m}} = -\frac{2RT\, t_{Na^+}}{F\gamma_{\pm m}}$$

An experiment was performed to determine the concentration coefficient, E_S, of an NaCl solution for comparison with the value predicted by equation F.7 . Two 125 ml aspirator bottles were joined by one foot of 3/8 inch Tygon tubing. The system was filled with 250 ml of 1 molar NaCl. An aged silver-silver chloride electrode was inserted into each bottle. Before any voltage measurements were made the electrodes were allowed about a day to come to equilibrium with the solution and with each other. At the end of this time the intercomparison or bias potential was less than 0.025 mv. A clamp was used to close the tube isolating each bottle, then 25 ml of solution was removed from one bottle and replaced by an equal amount of distilled water. This

reduced the NaCl concentration in the bottle to .8 molar. In order to measure the potential difference between the electrodes, the clamp was opened, the voltage reading taken and the clamp reclosed. The source impedance of this cell was about two thousand ohms, principally due to the salt bridge. The cell voltage, E_s, was measured with a Keithly 148 high-impedance millivoltmeter with the results shown in Figure F.1. The expected potential difference of this cell was 4.1 mv, according to equation F.7. The transport number, t_{Na^+}, was computed according to equation 7.40 of Robinson and stokes (1959). It is particularly evident that electrodes of this design require a long time to equibriate. The positive electrode was that in the weaker salt solution.

The same experiment was repeated using sea water and a new pair of silver-silver chloride electrodes which had been aged in sea water for several days. The initial solution had a salinity of $36.98^o/oo$ which when diluted as before became $29.6^o/oo$. This concentration cell yielded -532 as a final value for E_s as shown in Figure F.2.

If we assume that sea water behaves as a sodium chloride solution of equal ionic strength, we can apply the simple theory of the previous section. Introducing the relation $\gamma \pm m = \alpha S$ where α is a constant and an apparent transport number t_{sw^+} we get from equation F.7

$$\mathcal{E}_s = -\frac{2RT}{FS} t_{sw^+}$$

Figure F.1 Potential of NaCl concentration cell versus time for m_1 = 1 molar and m_2 = .8 molar.

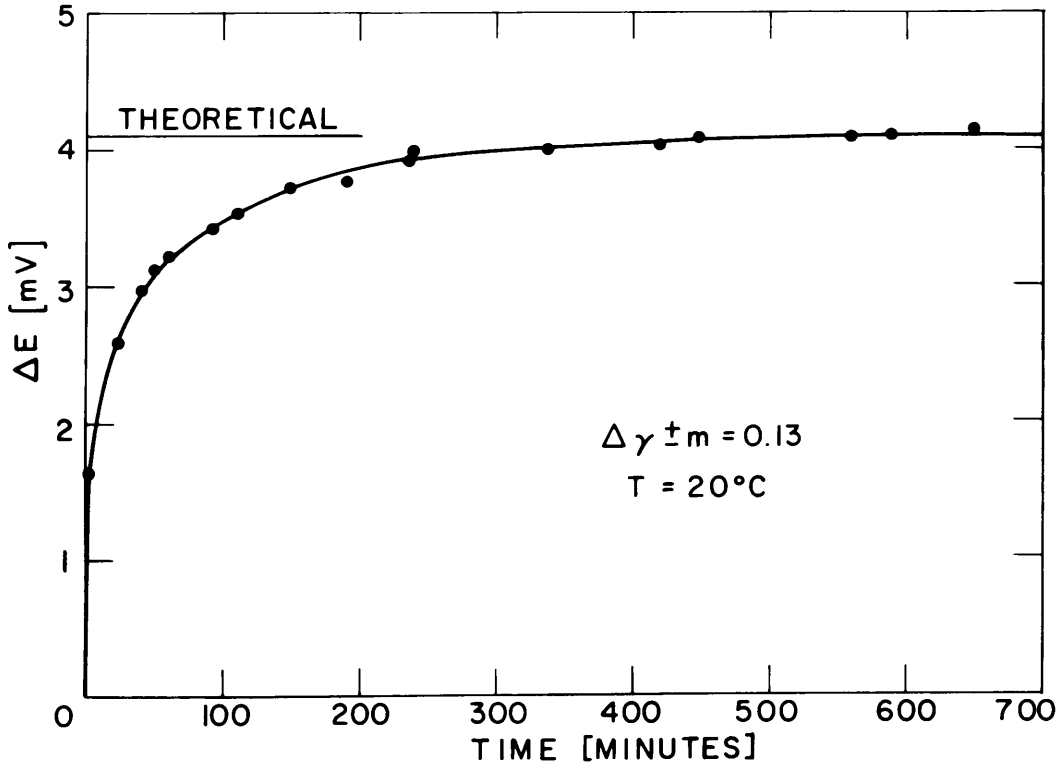
THEORETICAL
ΔE [mV]
Δγ ± m = 0.13
T = 20°C
TIME [MINUTES]
0
1
2
3
4
5
100
200
300
400
500
600
700

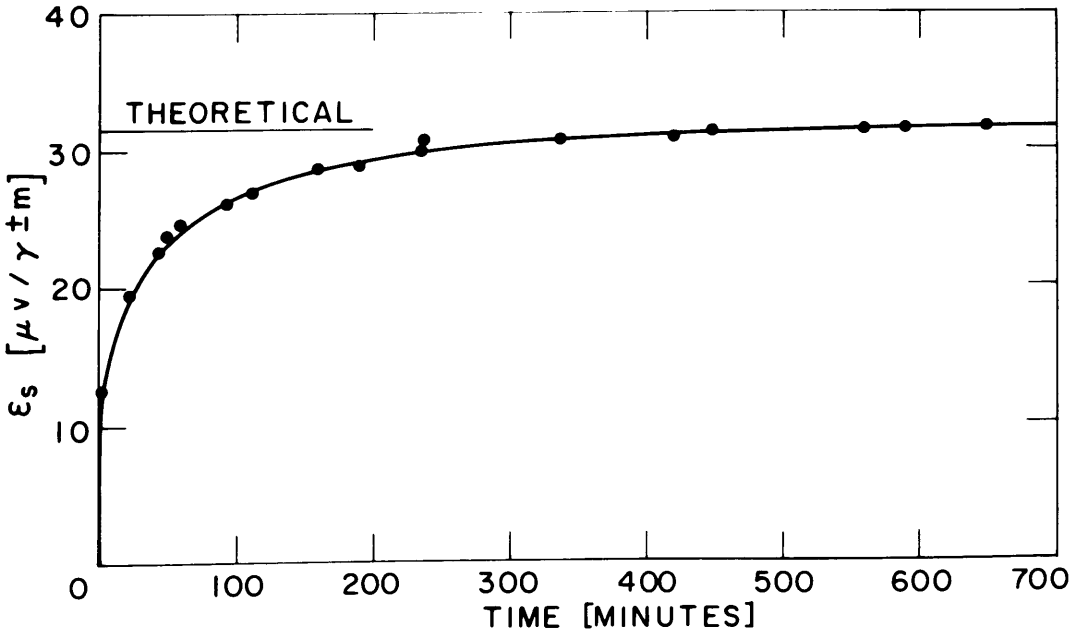
THEORETICAL
εs [μv / γ ± m]
TIME [MINUTES]
0
10
20
30
40
100
200
300
400
500
600
700

Figure F.2 Potential of sea water concentration cell versus time for s_1 = 37 $^{o}/oo$ and s_2 = 29.6$^{o}/oo$.

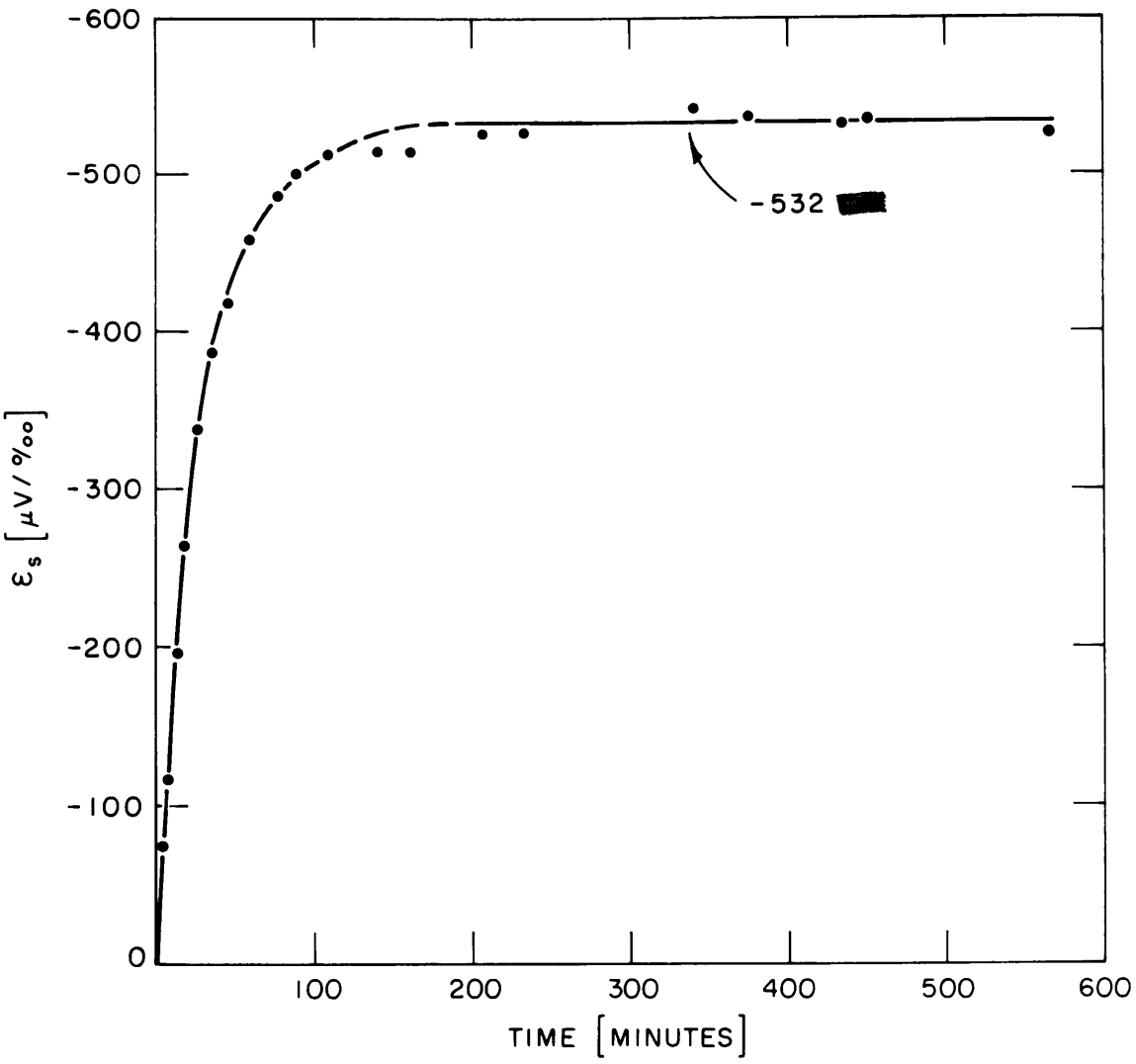
-600
-500
-400
-300
-200
-100
0
100
200
300
400
500
600
ε_s [μV/‰]
TIME [MINUTES]
-532

letting $t_{sw^+} = t_{Na^+}$ and T = 20° C we get

$$\mathcal{E}_s = \frac{\Delta E}{\Delta S} = \frac{-2RT}{F\Delta S} \ln\left[\frac{37.0}{29.6}\right] t_{Na^+} = -571\ \mu v/‰$$

Using the measured values of E_S for this salinity difference we can calculate the apparent transport number

$$t_{sw^+} = 0.355 \pm .001 \qquad (33-38‰)$$

The agreement between measurements and theory for aqueous sodium chloride solution is quite good. It seems that the concentration coefficient for sea water follows the same general theory. Using the apparent transport number for sea water the values of E_S can be found for various temperatures and salinities.

Since the salinity differences encountered in the ocean are usually small, the expression for ΔE due to concentration differences can be simplified:

$$\Delta E = \frac{-2RT}{FS_2}(S_1 - S_2) \qquad S_1 > S_2$$

$$= -\frac{61.18\,T}{S_2}\Delta S \ \mu v \qquad \text{F.8}$$

where T is in degrees Kelvin .

Hence,

$$\mathcal{E}_s = \frac{-61.18\,T}{S_2}\ \mu v/‰ \qquad \text{F.9}$$

with

$$\frac{\partial \mathcal{E}_s}{\partial T} = -2\ \mu v/‰/°C$$

for normal sea water.

Sodium Chloride and Sea Water Thermal Cells

A temperature gradient was established in a 1000 ml graduated cylinder by cooling the lower region and warming the upper portion. The warm electrode, at a temperature always near 22°C, was positive with respect to the cold one. The thermal coefficient is defined as

$$\mathcal{E}_o = \lim_{\Delta T \to 0} \frac{\Delta E}{\Delta T}$$

and is itself a function of temperature and concentration. For these experiments it was not possible to maintain or measure small temperature differences, so the thermal coefficient is defined

$$\mathcal{E}_T = \frac{E(T_2, S) - E(T_1, S)}{T_2 - T_1} \quad \text{with } T_2 - T_1 = \Delta T \geq 2^\circ C$$

In that the electrodes (constructed as in von Arx, 1950) had thermal inertia, it was decided to rely only on measurements made 15 minutes or more after any large temperature change.

First, measurements were made in a sodium chloride solution, and the results compared with the values reported by Haase and Schonert (1960). The values of E_T for a 0.75 molar sodium chloride soltuion over several values of ΔT ranging from 3-20°C was 277 $\pm$11 microvolts per °C. This value is marked on the NaCl curve of Figure F.3 .

Next, the same procedure was followed using sea water of salinity 36.98 °/oo. The measured potential difference,

Figure F.3 Thermal coefficients of NaCl, NaBr and NaI at 25°C versus molarity determined by Haase and Schonert (1960). The value found in this work for NaCl is indicated with bars.

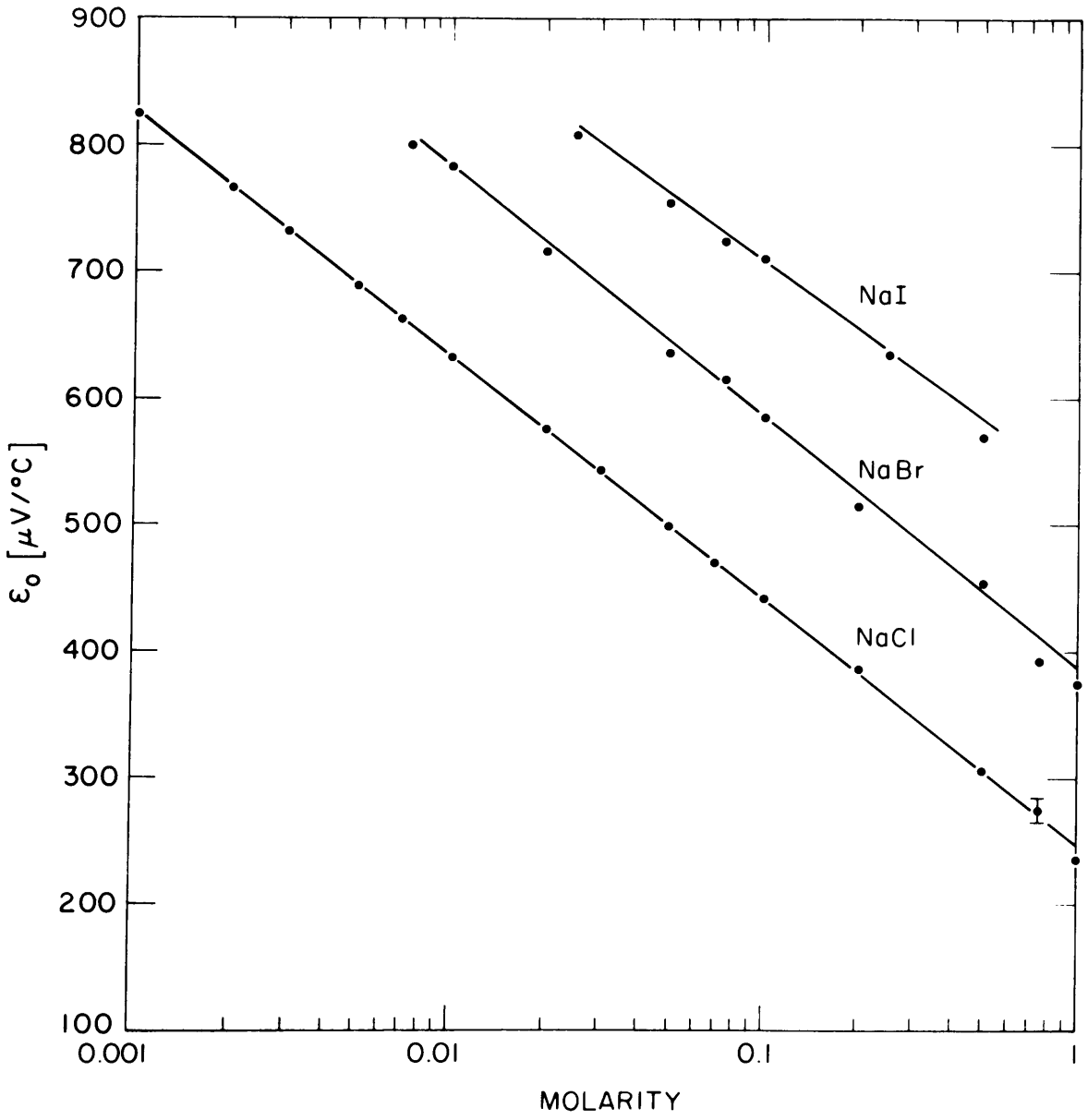
900
800
700
600
500
400
300
200
100
ε_o [μV/°C]
NaI
NaBr
NaCl
0.001
0.01
0.1
1
MOLARITY

ΔE , versus ΔT are presented in Figure F.4. The points fall along a line having a slope near .364 mv/°C. The data for E_o for KCl obtained by Haase and Schonert (1960), are thought to be similar to NaCl and sea water. These indicated that E_o increased as the temperature decreased. Since ΔT increases as the temperature of the cooled electrode decreases, it is expected that E_T (as defined here) should increase with ΔT . A closer examination of the data seems to support the latter behavior. Figure F.5 presents $\Delta E/\Delta T$ or E_T as a function of ΔT . The scatter in the values increases as ΔT decreases because smaller temperature differences were difficult to accurately measure. The data seem to follow the relationship

$$\mathcal{E}_T = 315 + 3.5\Delta T \quad \mu v/°c$$

The dependence of E_S on salinity can be estimated from the data of Haase and Schonert presented in Figure F.4 . As $\Delta T \to 0$, $\mathcal{E}_T(22°, 37‰) \to 315 \mu V/°C$ a value slightly larger than E_o for NaCl at the same ionic strength (.765 molal) but at a temperature of 25°C. Both NaCl and NaBr follow the approximate relationship

$$\mathcal{E}_o(25°, m) \doteq -200 \log m + F(T)$$

Measurements of E_T were not made at other salinities, but it seems likely that $E_T(T,S)$ follows the same relationship as E_o for NaCl and NaBr. Then the dependence of E_T on S can

Figure F.4 Potential of sea water (37°/oo) thermal cell versus half-cell temperature difference.

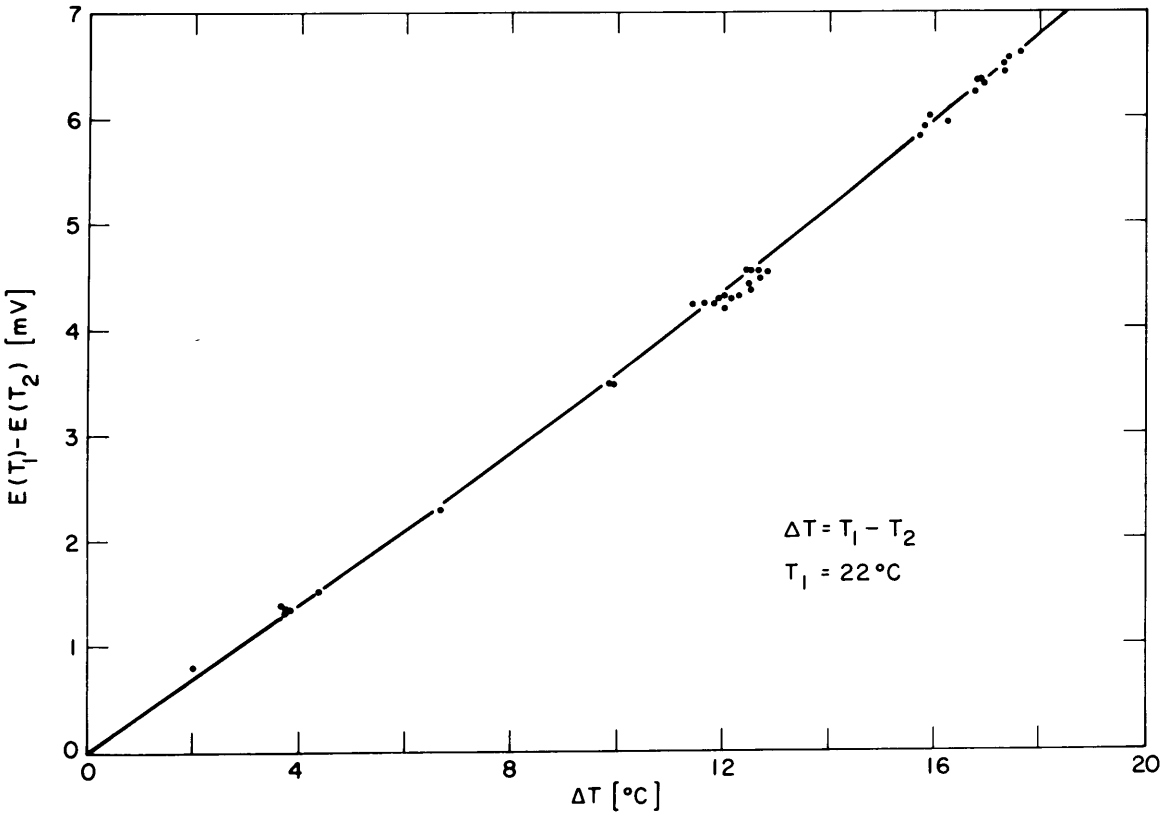
7
6
5
4
3
2
1
0
0
4
8
12
16
20
E(T1)-E(T2) [mV]
ΔT [°C]
ΔT = T1 - T2
T1 = 22°C

Figure F.5 Thermal coefficient of sea water ($37^{\circ}/oo$) versus half-cell temperature difference.

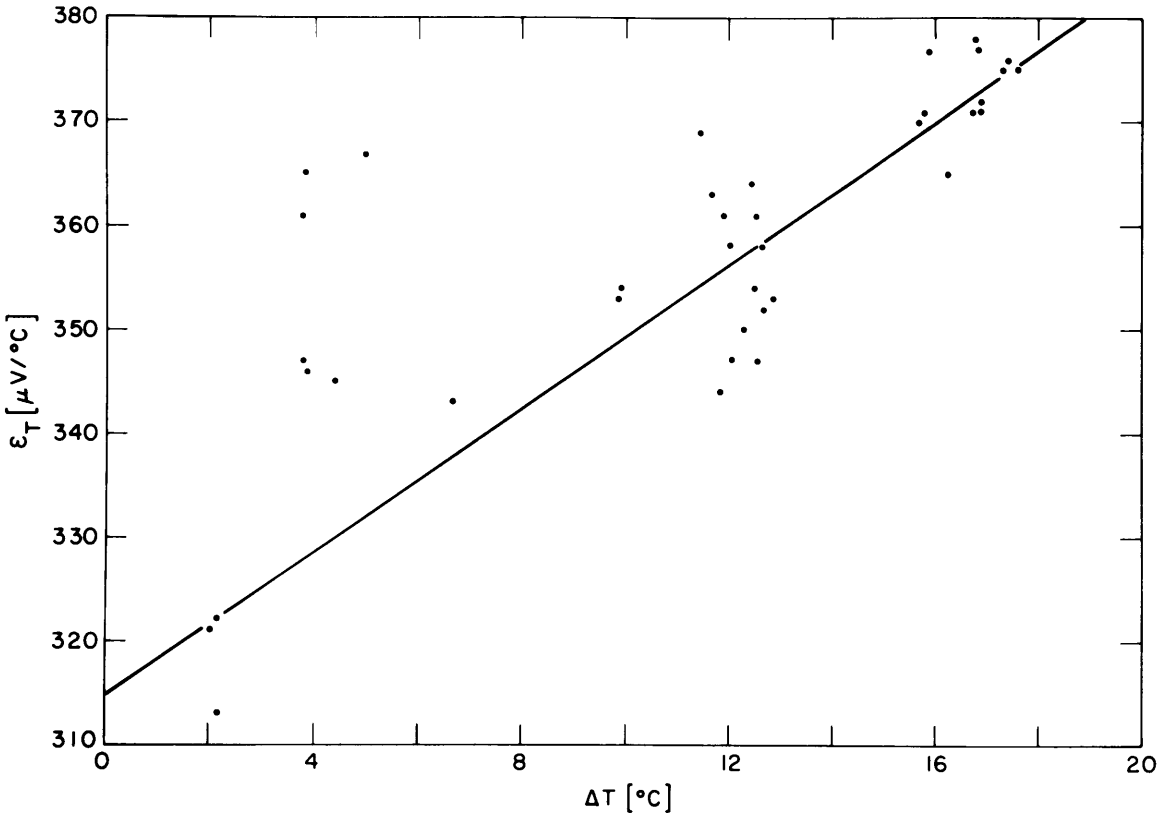
380
370
360
350
340
330
320
310
ε_T [μV/°C]
0
4
8
12
16
20
ΔT [°C]

be estimated to be

$$\frac{\partial \mathcal{E}_T}{\partial S} = \frac{-200}{2.3026 \times S} = -2.5 \mu v/^{\circ}c/‰ \text{ for } S = 35‰.$$

Oxygen and Pressure Effects on Electrode Systems

The effect of dissolved oxygen concentration on the potential of an electrode is discussed by Ives and Jantz (1960). It is thought that the oxidation reaction

$$2Ag + 2HCl + \tfrac{1}{2}O_2 \rightarrow 2AgCl + H_2O$$

occurs with silver-silver chloride electrodes in acid solution. This reaction can generate sizable voltages between electrodes surrounded by acid solutions differing in oxygen concentration, but does not occur at pH > 7. For this reason the oxygen effect is probably not important in sea water, which has a normal pH range between 7.5 and 8.4 (Sverdrup, et al, 1942).

The influence of pressure on electrodes can be considered a response to mechanical and thermodynamic effects. It seems possible that hydrostatic pressure might alter an electrode surface mechanically. Whether or not this actually occurs and what its magnitude might be is not known. Solov'yev (1961) reports that when two electrodes were at all times at the same pressure the potential difference between them did not depend on pressure changes of up to 30 atmospheres.

Assuming that the mechanical effect would be different on each electrode, it seems likely that influence of pressure is not significant.

An estimate of the upper bound on the thermodynamic pressure effect has been suggested by Horne (personal communication). In an isothermal cell where one electrode is at pressure, P_1 and the other is at P_2, the Nernst equation predicts the cell potential as

$$|\Delta E| = \frac{RT}{F} \ln \left[\frac{a_1}{a_2} \right]$$

where a is the activity of the sea water. Such a cell is different from a salinity cell in that salinity, by definition, is not a function of pressure while the activity depends on the compressibility of sea water. Assume for convenience that T = 0°C, S = 35°/oo; then

$$a(P) = \frac{\text{constant}}{\alpha_{35,0,P}}$$

In which case

$$|\Delta E| = \frac{RT}{F} \ln \left[\frac{\alpha_{35,0,P_2}}{\alpha_{35,0,P_1}} \right]$$

Tables of the specific volume, $\alpha_{35,0,P}$ as a function of pressure are available (see, for example, Sverdrup et al, 1942). Suppose P_1 = 1000 decibars and P_2 = 0, then

$$|\Delta E| \doteq 0.2 \text{ mV},$$

a voltage so small compared to those accompanying temperature and salinity contrasts that it may be neglected for practical purposes.

ADDITIONAL REFERENCES: APPENDIX F

Haase, R. and H. Schonert, Untersuchungen and thermoketten, IV. Messungen, Z. physik. Chem. Nev Folge 25, 194-204, 1960.

Ives, D. and G. Jantz, Reference Electrodes, Academic Press, New York, 1961.

Robinson, R. A. and R. H. Stokes, Electrolyte Solutions, Butterworths, London, 1959.

Solov'yev, L. G., Measurement of electric fields in the sea, Acad. of Sc. USSR, Doklady 138 (2), 32-34, 1961.

Sverdrup, H. V., M. W. Johnson and R. H. Fleming, The Oceans, Their Physics, Chemistry and General Biology, Prentice-Hall, Englewood Cliffs, 1942.

APPENDIX G

ELECTRIC DISTURBANCES DUE TO SURFACE WAVES

Surface waves induce rather large electrical signals in the ocean. The vertical measurements made both from moorings and vessels contain voltage fluctuations due to this source. An example of this is taken from a segment of the chart record obtained during the December 19th experiment in the Northwest Providence Channel. The deep electrode was at 330 meters. This record, consisting of a section of filtered data (-3 db at 0.1 cps; -40 db per decade rolloff), a short segment of unfiltered readings and then a return to filtered record is reproduced in Figure G.1. The voltage excursions are somewhat larger than predicted by L-HSS. The period, T, of the sea was about 5 seconds and the wave amplitude, a, was about 80 cm. According to L-HSS,

$$|\Delta\phi| = \frac{aT}{2\pi} g F_H = 0.13 \text{ mV}$$

From the unfiltered data the estimate is that

$$|\Delta\phi| = 0.8 \text{ mV}.$$

The reason that the measured value is larger than expected is not clear. It might be related to the motion of the surface electrode in the near field of the vessel's electrical disturbance.

The existence of this wave-induced field must be considered in the design of any measuring system. Severe aliasing could result if this contribution was not recognized and an inappropriate sampling scheme chosen.

Figure G.1 Wave induced voltage fluctuations: filtered (using an inverting filter) and unfiltered on zero center chart of range ±3 mv.

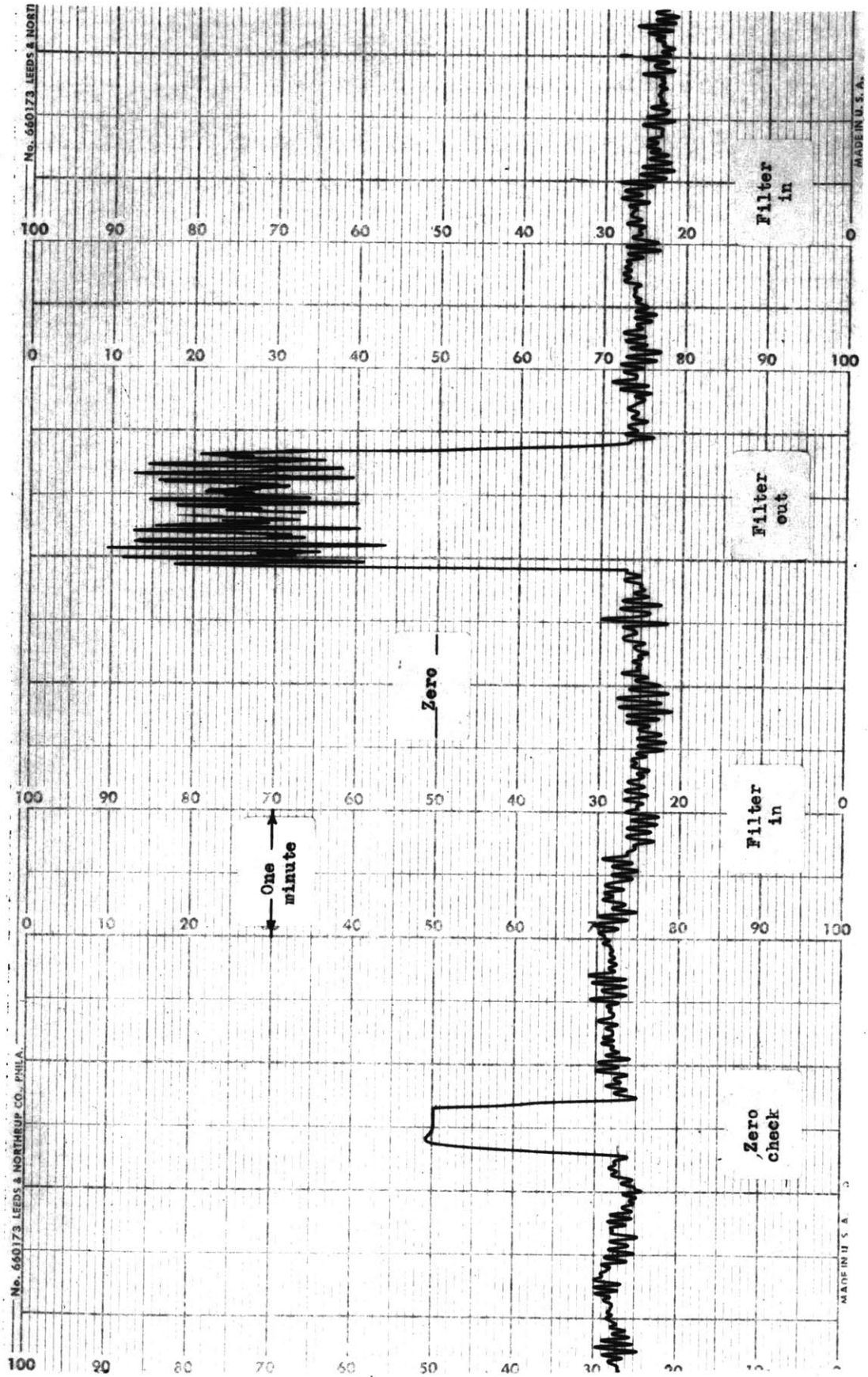
Filter in
Filter out
Zero
Filter in
One minute
Zero check
No. 660173 LEEDS & NORTHRUP CO., PHILA.
MADE IN U.S.A.

On the other hand, this signal might be useful in the study of surface waves. A measurement of the magnetic east-west transport of a wave might be a useful complement to the conventional studies of wave height.